Investigating Fusion Machinery in G Protein-Coupled Receptor Exocytosis

by

Hao Chen

A dissertation submitted in partial fulfillment
of the requirements for the degree of
Doctor of Philosophy
(Pharmacology)
in the University of Michigan
2024

Doctoral Committee:

Professor Manojkumar A. Puthenveedu, Chair
Associate Professor Paul M. Jenkins
Associate Professor Emily M. Jutkiewicz
Professor Lois S. Weisman

Hao Chen

tigerch@umich.edu

ORCID: 0000-0002-8369-1702

Dedication

To my mother, my father, and my love.

Acknowledgements

I have encountered many wonderful people over the past six years since I started my post-graduate study. To those who have encouraged, supported, and facilitated my pursuit of science in all aspects, either mentioned or not mentioned as follows, I am forever grateful to you.

First, I would like to thank all members of the Puthenveedu laboratory. My mentor, Manoj, your patience and encouragement lightened my path when nothing worked, your guidance put me on the right track when things started to work, and your inspiration led me to the confidence to believe everything should work. Zara, you enlightened me about the essence of science, everything about critical thinking, rigorous design, and rational interpretation. I cannot emphasize more that you made me the scientist I am now. Steph, Jenny, Josh, and Candy, I lost count of how many dumb and weird questions I had asked you, but you always answered and always helped. Loyda, Ian, and Caroline, I cannot imagine how life would be without your companionship and support. You are the peers and colleagues that all I could ask for. Adriana and Amanda, thank you for organizing our workplace and pardoning us from the endless trifles of maintenance. Kasun, I missed our random debates on out-of-nowhere subjects. Prahatha, your straightforwardness and outspokenness taught me to stand my ground. Swamy, I am glad to tell you that I am a master of maxi-prep now. Aditya, Dr. Kumar, D, I sincerely apologize for all the nicknames I bestowed on you, but please realize that it was an act of nothing but affection. You have always been an inspiration, and I appreciate all the support you provided me, scientifically and mentally. I would miss our lunch, our unnecessary argument about everything, and all the joy you brought me.

I would like to thank my thesis committee. Dr. Lois Weisman and Dr. Paul Jenkins, your consistent delivery of precise and constructive feedback to my research has largely improved my work and taught me to think more critically. Dr. Emily Jutkiewicz, you are the one that navigated me every step through the program, from prelim to graduation. Dr. Arun Anantharam and Dr. Shoji Maeda, your contribution to my research was also indispensable regardless of the limited period of time you were on my committee.

I would like to thank the Pharmacology Department. Dr. Lori Isom, you have been a wonderful and caring chair. It is my pleasure to witness your persistent effort to build a better department and your dedication to providing us with an inclusive and comfortable working environment. Dr. Stephen Fisher, you were the one that provided me the opportunity to join the department as a master's student and hand-to-hand guided me through the master's program. I still remember your consideration of sending us fellow Chinese students an email wishing us a happy lunar new year. It was a warm and welcoming gesture that made my first lunar new year in a foreign country not that nostalgic. I would also like to thank all the administrative staff of the department. Thanks to your efficiency and diligence, Ingrid, Sondra, Audrey, Dennis, Carol, Tom, Dar-Weia, Lisa, Liz, and all the others, that helped make my life much easier.

I would like to thank my friends. Jiayu, Wenhui, Yating, and Yang, my dear friends and colleagues, how fortunate am I to have met you here. You have brought me enormous happiness and comfort in the coldness of Ann Arbor, the tediousness of science, and the trivia of life.

Last, I would like to thank my family and my loved ones. My sincere gratefulness to my parents, who have raised me into an independent thinker, supported my every decision, and continuously encouraged me to face challenges. You are the bedrock of my foundation and the trampoline I know I will fall on. A special thanks to my love, Kaiyun. You have consoled me in

countless difficult situations, shared and eased my negative emotions, and celebrated my every insignificant achievement. I am wholeheartedly grateful to you for persistently standing by my side.

Table of Contents

List of Tables

List of Figures

List of Abbreviations

Abbreviation	Definition
AA	amino acid
AIC/ BIC	Akaike/ Bayesian information criterion
Alexa/ AF	Alexa Fluor
a.u.	arbitrary unit
B2AR	β2 adrenergic receptor
cAMP	cyclic adenosine monophosphate
CHX	cycloheximide
CI	confidence interval
CLEM	correlative light and electron microscopy
C-term/ Ct	carboxy-terminus
DAMGO	[D-Ala^2, *N*-Me-Phe^4, Gly^5-ol]-enkephalin
DAPI	4',6-diamidino-2-phenylindole
Dox	doxycycline
EEA1	early endosome antigen 1
EMCCD	electron multiplying charge-coupled device
EtOH	ethanol
FBS	fetal bovine serum
fluo.	fluorescence
fr	frame
GAPDH	glyceraldehyde 3-phosphate dehydrogenase
GFP/ RFP/ BFP	green/ red/ blue fluorescent protein
GM130	Golgi matrix protein 130
GPCR	G protein-coupled receptor
GRK	G protein-coupled receptor kinase
HEK293	human embryonic kidney 293 cells
HS	(donor) horse serum
IDoT	integrated density over threshold
IF	immunofluorescence
IgG	immunoglobulin G
Iso	isoproterenol
JMD	juxta-membrane domain
LP	longpass
MOR	μ opioid receptor

NA	numerical aperture
NGF	nerve growth factor
NSF	*N*-ethylmaleimide-sensitive factor
NT	non-treated
N-term/ Nt/ N	amino-terminus
ROI	region of interest
P	Pearson's coefficient
PBS	phosphate-buffered saline
PC12	(rat) pheochromocytoma 12 cells
PDL	poly-D-lysine
PDZ	PSD95/Dlg/ZO-1
Pen-Strep	penicillin and streptomycin
PKA/ PKC	protein kinase A/ C
PTM	post-translational modification
Scm	SNARE coiled-coil motif
SD	standard deviation
SEM	standard error of mean
shRNA	short hairpin RNA
SNAP	synaptosomal nerve-associated protein
SNARE	soluble *N*-ethylmaleimide-sensitive factor attachment receptor protein
SNX	sorting nexin
SpH	super ecliptic pHluorin
SRRF	super resolution radial fluctuation
TBST	tris-buffered saline Tween-20
TfR	transferrin receptor
TGN	trans-Golgi network
TIRF	total internal reflection fluorescence
TMD	transmembrane domain
t-SNARE	target-SNARE, or called Q-SNARE
v-SNARE	vesicle-SNARE, or called R-SNARE
VAMP	vesicle-associated membrane protein
WO	washout
WT	wildtype

Abstract

Vesicle fusion at the plasma membrane plays an essential role in the release of secretory molecules such as neurotransmitters and in the exocytosis of surface proteins such as GPCRs. For neurotransmitter release, vesicle fusion is mediated by a multi-protein machinery including the SNARE complex consisting of vesicle-localized v-SNAREs, called VAMPs, and their cognate t-SNAREs. Surprisingly, in contrast to the well-studied neurotransmitter release, it is largely unclear how fusion machinery is involved in GPCR exocytosis. GPCRs are signal-transducing receptors that sense and respond to extracellular stimuli. To allow for adaptive responses to the everchanging extracellular environment, the trafficking of GPCRs is strictly regulated. We sought to investigate the missing role fusion machinery plays in GPCR exocytosis by hypothesizing that there might be subtype-dependent specificity of v-SNAREs in the exocytosis of different GPCRs. In this dissertation, we focused on three receptors including two prototypical GPCRs, MOR and B2AR, and a non-GPCR trafficking model TfR. Evidence has shown that these receptors undergo distinct exocytic pathways.

First, we examined the specificity of VAMP2, a prototypical v-SNARE known to mediate exocytotic vesicle fusion, in GPCR recycling. Using high-speed multi-channel microscopy to visualize VAMP2 and receptors in fusion events simultaneously, we found that VAMP2 was preferentially enriched in vesicles that mediated MOR recycling but not B2AR and TfR. VAMP2 depletion significantly decreased the recycling capacity of MOR on both single cell and population levels and from a cell model where VAMP2 was expressed ectopically to neurons where VAMP2

was expressed endogenously. By contrast, the recycling of B2AR and TfR were not affected by VAMP2 depletion. Interestingly, VAMP2 showed similar subcellular localization on MOR- and B2AR-containing endosomes, suggesting that VAMP2 and MOR were co-packaged into vesicles from the same endosomes that also contained other receptors. These results indicated that VAMP2 was cargo-selective and GPCRs might utilize distinct SNARE assemblies for vesicle fusion.

Next, we sought to address whether B2AR depended on a v-SNARE other than VAMP2 for recycling. We examined B2AR recycling under the depletion of VAMP4 or VAMP7 and found neither of them was required. VAMP1 and VAMP3 were also excluded due to their lack of baseline expression. We concluded that there might not be an exclusive v-SNARE involved in B2AR recycling.

Finally, we investigated the underlying mechanism leading to VAMP2's cargo-selectivity by hypothesizing that VAMP2 might possess an unknown sorting sequence through which it was co-sorted to endosomal subdomains alongside MOR. Through a series of microscopy studies, we found VAMP2 showed a sub-endosomal localization distinct from VAMP7. To follow up on our results of VAMP2's MOR-selectivity, we generated VAMP2 truncation mutants and studied their involvement in MOR recycling. Interestingly, both the N-terminus (V2N) and SNARE motif (V2S) of VAMP2 were required for the MOR-selectivity. By studying chimeric VAMP7 transplanted with VAMP2's protein sequences, we found that although V2N alone was sufficient to transform VAMP7's sorting, full transformation only occurred when V2S was also transplanted. Moreover, V2S was required to maintain VAMP2's stable surface localization. These data indicated that V2N and V2S played critical but distinct roles in the sorting and trafficking of VAMP2.

Together, our results revealed a previously unclear mechanism in GPCR exocytosis and demonstrated another layer of regulation on GPCR trafficking. Moreover, our results provided

evidence to a novel mechanism of v-SNARE endosomal sorting and contributed to an improved understanding of cellular trafficking.

Chapter 1: Plasma Membrane Fusion in Surface Receptor Exocytosis

Abstract

Membrane fusion is essential to surface receptor trafficking. Fusion between plasma membrane and the membrane of vesicles that carry either recycled or newly synthesized surface receptors transfers the receptors onto cell surface. Recently, focus of studies on fusion machinery has been expanded from its prominent role in neurotransmitter release to its understudied role in receptor trafficking. In this Chapter, we summarize and discuss the current understanding of the molecular mechanism underlying membrane fusion and the evident function of fusion machinery in receptor exocytosis. Although mostly unclear, the involvement of fusion machinery in GPCR trafficking and the potential specificity is particularly discussed. Following endosomal sorting, different GPCRs can be trafficked through distinct pathways to allow for regulations tailored to their specific functions. The specificity of fusion machinery is likely developed to adapt to these distinct pathways. Factors including signaling-trafficking crosstalk, polymorphism, alternative splicing, and cell type-dependent heterogeneity might further complicate the relationship between fusion machinery and GPCR trafficking.

Introduction

Membrane fusion, a fundamental cellular process indispensable for various biological functions, has been a prevalent research topic for decades. Among the pioneers of the field, James Rothman, Randy Schekman, and Thomas Südhof were jointly awarded the 2013 Nobel Prize in

Physiology or Medicine for their discoveries and characterizations of the vesicular trafficking system and the vesicular fusion machinery (*1*). Through vesicular trafficking, the intracellular lipid-bilayer organelles are connected together, and the intracellular space and the extracellular space are bridged between. At the final step of vesicular trafficking, vesicles fuse with the targeted membrane to offload their carrying cargoes, which can range from secretory molecules to transmembrane receptors.

Regulated vesicular trafficking and fusion contributes to the normal functions of cells, particularly cells with secretory responsibilities such as neurons. Neurons communicate with each other through neuroendocrine molecules, including neurotransmitters such as glutamate and neuromodulators such as endogenous opioid peptides. In a classical view of synaptic transmission (*2*, *3*), neuroendocrine molecules are packaged in the lumen of vesicles and transported to the pre-synapses, where vesicular fusion releases the molecules to the extracellular space. After diffusing through the synaptic junction, these molecules bind to their cognate receptors on the post-synapses, therefore transferring the signal to the post-synaptic neurons. Activation of ionotropic receptors, such as the ligand-gated ion channels, causes either depolarization or hyperpolarization of the post-synaptic neurons. On the other hand, activation of metabotropic signal-transducing receptors such as the G protein-coupled receptors (GPCRs) fine-tune the response of the post-synaptic neurons via signaling of G proteins and second messengers (*4*–*6*).

Besides pre-synaptic neuroendocrine molecules, post-synaptic surface receptors, such as GPCRs, are also delivered to the plasma membrane through vesicular trafficking involving vesicular fusion machinery. GPCRs are the largest and most pharmacologically targeted receptor superfamily in the human body (*7*, *8*). Therefore, the surface levels of GPCRs can dictate the level of cellular response to not only endogenous neuroendocrine molecules but also exogenous drug

molecules. To precisely govern the level of cellular responses, GPCR trafficking is strictly regulated via a complex but organized trafficking network (*9*, *10*); however, we are yet to achieve a comprehensive understanding of the molecular mechanism underlying the vesicular delivery of GPCRs.

In this Chapter, we summarize the current understanding of the vesicular fusion machinery and discuss recent findings revealing its role in receptor exocytosis. Notably, we focus on the potential involvement of vesicular fusion machinery in the exocytosis of GPCRs, and how the highly regulated GPCR trafficking network might demand a differential requirement for fusion machinery.

Main

Molecular mechanism of vesicle fusion at the plasma membrane

Vesicle fusion at the plasma membrane is mediated by a collective effort of multiple proteins and protein complexes in sequential steps: tethering, docking, priming, fusion pore opening, and disassembly (*11–13*).

First, secretory vesicles derived from intracellular membrane compartments traffic along cytoskeletons and are tethered to the plasma membrane upon arrival by the exocyst complex (*14–19*). Tethering captures vesicles and restricts their departure from the plasma membrane. Next, vesicle docking is mediated by the soluble *N*-ethylmaleimide-sensitive factor (NSF) attachment receptor proteins (SNARE) complex, which is composed of vesicular membrane localized v/R-SNARE vesicle-associated membrane proteins (VAMPs), cytosolic t/Qbc-SNARE synaptosomal nerve-associated proteins (SNAPs) and plasma membrane localized t/Qa-SNARE syntaxins (*20–*

24). Interaction between VAMPs, SNAPs, and syntaxins forms a four-α-helix bundle anchoring the vesicular membrane to a close contact to the plasma membrane.

In reconstituted systems or spontaneous neurotransmitter release, the SNARE complex is considered the minimal machinery sufficient to mediate fusion (*25–27*). However, in stimulated neurotransmitter release, the function of calcium sensor synaptotagmins is normally required (*13*, *28–31*). The process of activating synaptotagmins while incorporating it with the SNARE complex to form a "matured" pre-fusion machinery is called priming and is mediated by complexins (*13*, *32–34*). Moreover, complexins can suppress spontaneous neurotransmitter release, thus allowing for the dominant presence of triggered release (*34*, *35*). The Ca^{2+}-binding C2 domains of activated synaptotagmins are inserted into the plasma membrane.

To provide a local concentrated field of Ca^{2+} influx, the active zone protein complex composed of scaffolding proteins such as RIM (Rab3 interacting molecules), RIM-BP (RIM-binding proteins), and Munc-13 is responsible for recruiting voltage-gated calcium channels to the assembled fusion machineries (*36*, *37*). Once the calcium channels are activated by excitatory membrane potential, the influxed Ca^{2+} ions bind to membrane embedded C2 domains causing disturbance to the local membrane. This disturbance will generate mechanical force to induce a trans-to-cis conformational change of the SNARE complex leading to a "zipping" movement, thus pulling vesicular and plasma membrane together, resulting in the opening of fusion pore (*27*, *38–40*). After fusion, NSF catalyzes the disassembly of the fusion machinery, and the disassembled components are cycled for the next fusion process (*13*, *20*, *41*).

Exocytosis of surface proteins utilizes divergent SNARE assemblies

Since the discovery and establishment of the molecular mechanism of fusion machinery in neurotransmitter release, the attempt to achieve a comprehensive understanding of the functions

of fusion machinery in all aspects of vesicular trafficking has been constantly pursued. One research aspect that has drawn quite of interest is to understand the role of the SNARE complex in surface protein exocytosis. However, in contrast to neurotransmitter release which utilizes a well-established universal SNARE assembly of VAMP2-SNAP25-syntaxin1 (reviewed in *13*), SNARE assemblies utilized for surface protein exocytosis seems to exhibit great divergency.

The SNARE proteins can have multiple subtypes. To date, eight v/R-SNAREs (VAMP1/ 2/ 3/ 4/ 5/ 7/ 8 and Vti1a), four Qbc-SNAREs/ SNAP-25-like proteins (SNAP-23/ 25/ 29/ 47), and fifteen Qa-SNAREs/ syntaxins (Stx1/ 2/ 3/ 4/ 5/ 6/ 7/ 8/ 10/ 11/ 12/ 16/ 17/ 18/ 19), are reported to function in mammalian cells (reviewed in *42*). It has long been proposed that the composition of the SNARE assemblies by different SNARE protein subtypes can encode specificities toward trafficking directionalities (exocytosis or endocytosis), trafficking origins (e.g., Golgi apparatus or endosomes), client cargoes, and the specific biological functions (*22*, *43–45*). In this Chapter, we focus on discussing the function of SNARE proteins from the perspective of exocytic vesicular trafficking (SNARE-mediated vesicle to plasma membrane fusion). From this perspective, the idea of cognate SNARE assemblies is elucidated by the specific requirement of SNARE assemblies in the exocytosis of surface proteins (e.g., receptors, ion channels, transporters, etc.), as accumulating evidence has shown that different surface proteins require distinct SNARE assemblies for their exocytosis (summarized in Table 1.1).

Table 1.1. Examples of reported SNARE assemblies in the exocytosis of surface receptors, ion channels, and transporters.

Receptor	R-SNARE	Qbc-SNARE	Qa-SNARE	Exocytic mode	Reference
Surface receptors					
TfR	VAMP2/ 3/ 4	SNAP-23/25	Non-tested	Constitutive & ligand (transferrin) present	(*46–48*)
TCR	TeNT-sensitive	SNAP-23	Syntaxin4	Stimulated by APC contact	(*49*, *50*)
MOR	VAMP2	Non-tested	Non-tested	Stimulated by agonist	*(*51*)
Surface ion channels					
AMPAR	VAMP2	SNAP-47	Syntaxin3	Stimulated during LTP	(*52*, *53*)
NMDAR	VAMP1	SNAP-25	Syntaxin4	Constitutive	(*54*)
TRPC3	TeNT-sensitive	Non-tested	Non-tested	Constitutive & stimulated	(*55*)
Surface transporters					
GLUT4	VAMP2	Non-tested	Syntaxin4	Stimulated by insulin	(*56–59*)
NKCC2	VAMP2	Non-tested	Non-tested	Stimulated by cAMP increase	(*60*)

Abbreviations in the table: TfR: transferrin receptor; TCR: T-cell receptor; MOR: μ opioid receptor; AMPAR: α-amino-3-hydroxy-5-methyl-4-isoxazolepropionic acid receptor; NMDAR: *N*-methyl-D-aspartate receptor; TRPC3: transient receptor potential channel 3; GLUT4: glucose transporter type 4; NKCC2: $Na^+/K^+/2Cl^-$ co-transporter 2; TeNT: tetanus toxin; APC: antigen-presenting cell; LTP: long-term potentiation. Note: TeNT-sensitive R-SNAREs include VAMP1/ 2/ 3. *: see Chapter 2 for details.

However, the molecular mechanism underlying SNARE assemblies' specificity is still largely debatable. Several mechanisms that have been proposed include cell type-dependent differential expression, sequence-dependent endosomal sorting, and tethering complex-mediated SNARE selection (*22*, *61–64*; the sequence-dependent sorting aspect is additionally discussed in a later section of "*The potential application and regulation of fusion machinery in GPCR exocytosis*").

In Chapter 2 of this dissertation, as an attempt to uncover the role of fusion machinery in GPCR exocytosis, we discuss our findings on VAMP2's preferential involvement in the stimulated exocytosis of the μ opioid receptor (MOR).

Heterogeneity in recycling pathways of different GPCRs

GPCRs are seven-transmembrane domain (7TM) receptors that transduce signals from a large variety of extracellular stimuli, ranging from endogenous hormones, neurotransmitters, chemokines, and pH to exogenous odorants, photons, and drug molecules, etc.

Because of the critical role GPCRs play in orchestrating a complex and diverse signal transduction system, both their surface levels and intracellular trafficking are strictly regulated. In a classical view of GPCR signaling, the surface levels of GPCRs directly dictate the intensity of cellular response (*10*, *65*). In general, cells utilize two major pathways to control the surface levels of GPCRs: biosynthesis and recycling (*9*, *10*, *66*). The biosynthetic pathway delivers newly synthesized GPCRs to the cell surface through vesicles derived from the trans-Golgi network. Once the GPCRs are on the cell surface, they can be activated by agonists which will cause an acute desensitization cascade to terminate their signaling through phosphorylation by kinases such as the GRKs (GPCR kinases) and the subsequent recruitment of β-arrestins (*67*, *68*). β-arrestin-bound GPCRs are then internalized to endosomes through clathrin-mediated endocytosis (*69*, *70*).

Endosomes are a collective of functionally and biochemically distinct endomembrane organelles serving as the transit centers of the cellular transport system. Although not fully understood, the current consensus on endosome biogenesis and development is that endosomes initiate as internalized vesicles. And through a series of biochemical modifications including but not limited to acidification, Rab GTPase (a family of small G proteins that regulate trafficking) conversion, protein recruitment, and fusion with other endomembrane compartments, the internalized vesicles gradually remodel and mature into distinct endosome subpopulations (*71*–*75*). Rab GTPases and their effectors are often used to define these subpopulations, e.g., early endosomes are defined by the presence of Rab5 and its effector EEA1 (early endosomal antigen

1) while recycling endosomes are defined by the presence of Rab11 (*76–78*). Endosome-anchored sorting machineries function to decide the destinies of the internalized GPCRs, which are either packaged into vesicles and recycled back to the cell surface or retained for degradation in the lysosomes (*9*, *10*, *66*).

The recycling of GPCRs is not regulated by a universal mechanism. Instead, different GPCRs utilize different mechanisms and undergo specific recycling pathways (Fig. 1.1 A). For instance, the β2 adrenergic receptor (B2AR) is reported to be primarily recycled from actin-dependent endosomal tubules after isoproterenol-induced internalization (*79–82*). Sorting of B2AR to these specialized tubules allows for regulated recycling. This sorting is mediated by a hierarchical mechanism composed of a protein kinase A (PKA)-mediated double phosphorylation (S345/346) at B2AR's carboxy-terminal (C-term) tail and a distal C-term PSD-95/Dlg/ZO-1 (PDZ) ligand, where the PKA-mediated double phosphorylation prevents B2AR from entering unregulated "bulk" recycling tubules on the endosomes (*81*), and the PDZ ligand mediates the association between B2AR and the actin-sorting nexin 27 (SNX27)-Retromer sorting machinery (*80*, *83*, *84*; the sorting aspect is additionally discussed in a later section "*The potential application and regulation of fusion machinery in GPCR exocytosis*"). Disruption of B2AR's PDZ ligand largely decreases its recycling capacity, while the introduction of phosphorylation-deficit mutation of S345/346 to PDZ-disrupted B2AR relieves it from restricted "bulk" recycling tubule entrance, thus increasing its recycling capacity (*81*).

Unlike B2AR, MOR is not yet identified to possess a PDZ ligand or interact with any PDZ proteins. Instead, evidence has been shown that the recycling of MOR requires a "bi-leucine" sequence of LENLEAE on its C-term tail, that either truncation of this sequence or mutation of the leucine residuals can largely decrease its recycling capacity (*85*, *86*). However, the exact

mechanism of how this sequence functions and whether it requires any interacting patterners to function is still unclear. On the other hand, the pathway selectivity of MOR recycling is proposed to be primarily regulated by post-translational modifications (PTMs), particularly through the phosphorylations of S363, T370, and S375 residues at its C-term tail (*87*, *88*). Activation of MOR by DAMGO ([D-Ala^2, *N*-Me-Phe^4, Gly^5-ol]-enkephalin), a full agonist, causes phosphorylation of all three sites (*89*). At this PTM state, MOR is recycled through a Rab5-dependent early endosome pathway (*86*). Interestingly, a MOR mutant with phosphorylation-deficits of all three sites can still recycle as long as the LENLEAE sequence is intact, though instead through a Rab11-dependent recycling endosome pathway (*86*), indicating the presence of a hierarchical regulatory mechanism. Moreover, T370 phosphorylation is suggested as DAMGO-specific, since morphine-activated MOR is not phosphorylated at this site (*89*). It is rational to speculate that the pathway selectivity of MOR recycling is agonist-dependent because of the differential PTM states agonists can lead to (Fig. 1.1 B). Nevertheless, there is still not enough evidence to make such conclusion.

Alternative splicing and polymorphism as other factors governing the recycling pathway selectivity of GPCRs

Although receptor-specific recycling sequences and agonist-dependent PTMs are already two powerful demonstrations of the complexity of GPCR trafficking, the story does not end here. To date, multiple GPCRs are reported to have genetic variants generated from alternative splicing or polymorphism, and the variants may not share the same trafficking patterns as the primary isoforms (*90*, *91*).

Besides MOR-1, the primary isoform, over twenty naturally occurring MOR isoforms are found either in mouse, rat, or human (*90*, *92*). Among them, the highly truncated single-TM MOR isoforms do not activate G protein signaling but instead act as chaperones to MOR-1 in the

endocytic reticulum to stabilize MOR-1 structure and facilitate its production (*93*). Amino-terminal (N-term) truncated 6TM MOR variants are mainly studied for their involvement in analgesia, with evidence showing that animals lacking all 7TM MOR variants are still responsive to certain opiates such as heroin and a novel opiate IBNtxA (*94*, *95*). In contrast, C-term MOR variants are 7TM receptors without apparent structural truncations but with varied C-term protein sequences: MOR-1B's 387-KIDLF, MOR-1D's 387-RNEEPSS, and MOR-1E's 387-KKKLDSQRGCVQHPV, all different from the 387-LENLEAE(TAPLP) of MOR-1 as mentioned above (*92*). However, lacking the bi-leucine sequence does not prevent these MOR variants from recycling in general since MOR-1B, 1D, and 1E still show recycling activities though seemingly of a lower degree compared to MOR-1 (*96*), indicating that MOR variants can utilize a diversified pool of sequences to recycle (Fig. 1.1 C). Whether the difference in recycling dynamics of these variants is due to differential recycling pathway selectivity is unclear but can be an exciting topic for future investigations.

GPCR variants resulting from polymorphisms can also display distinct trafficking patterns. The impact of polymorphisms on trafficking is often linked to the consequent alterations in PTMs (*88*, *97*). One interesting example is the *OPRM1* c.118A>G single nucleotide polymorphism (rs1799971) -correlated MOR variant p.N40D, which has been extensively linked to substance abuse disorders and addiction (*98–101*). Studies to gain mechanistic insights on this variant reveal that, compared to wildtype MOR-1, MOR p.N40D shows lower cell surface localization at steady state *in vitro* (*102*), decreased potency to a subset of opioid agonists without apparent binding affinity differences (*98*, *102*), and attenuated regulatory effects on synaptic transmission in neurons (*103*). Fundamentally, the MOR p.N40D variant loses a site for *N*-glycosylation, a critical PTM in receptor synthesis and trafficking shown by other GPCRs including α_{1D} adrenergic receptor (*104*)

and glucagon-like peptide 1 receptor (*105*). Therefore, the defective *N*-glycosylation may have also impaired the biosynthetic trafficking of MOR p.N40D, leading to the phenotypes of decreased cell surface localization and loss of function in response to agonists, at least to membrane-impermeant agonists such as DAMGO (Fig. 1.1 D). However, when MOR p.N40D is ectopically overexpressed in cells to a similar level as wildtype MOR-1, neither its function nor its intracellular trafficking shows noticeable differences (*106*). Nevertheless, the relationship between *N*-glycosylation and MOR's trafficking and signaling is not yet thoroughly investigated. Given now we realize from δ and κ opioid receptors that subtle differences in subcellular localization is enough to generate diversified signaling outputs (*107–109*), the impact of N40D on MOR should be more carefully looked at.

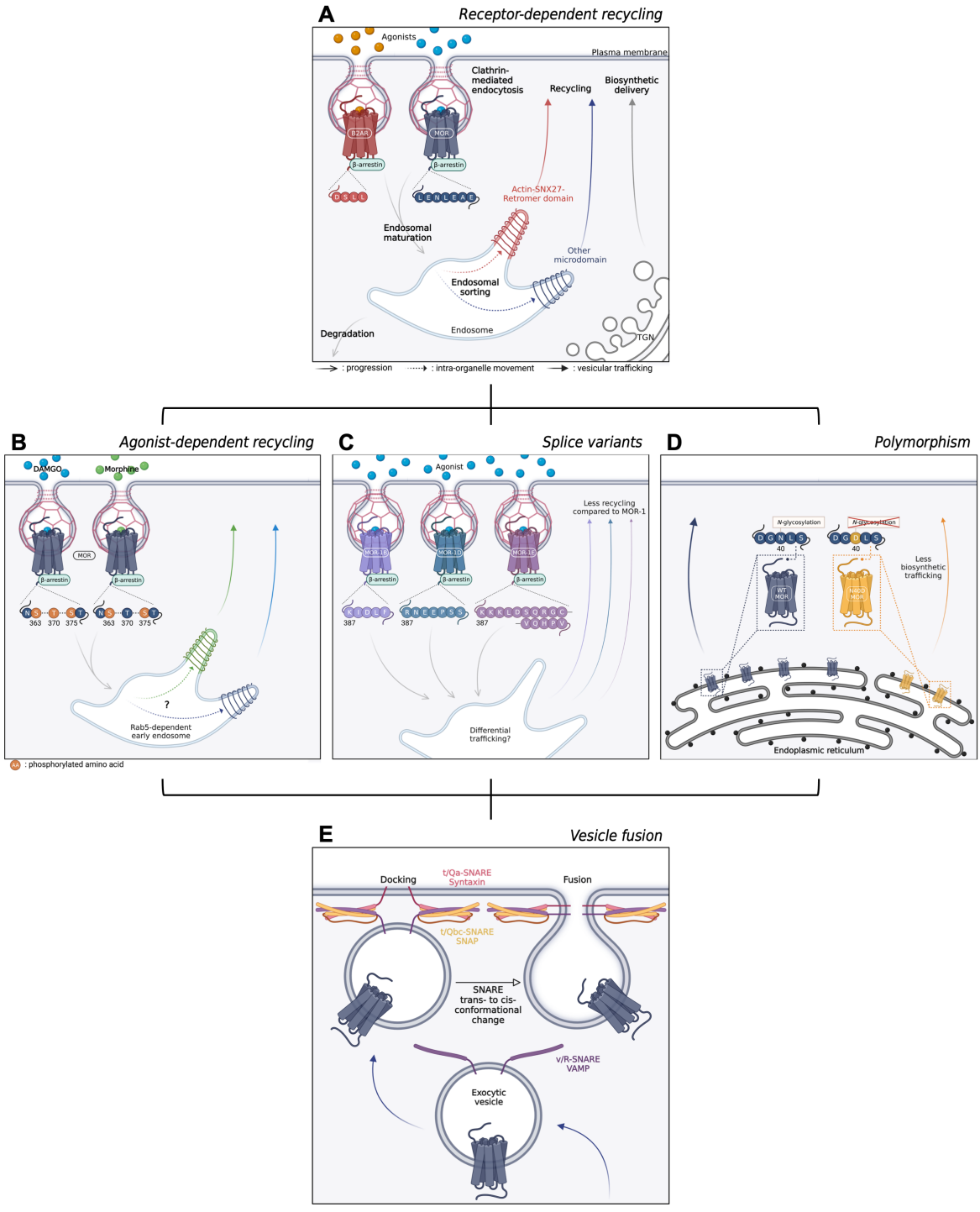

Figure 1.1. Schematics depicting GPCR's complex exocytic trafficking paradigm with multiple layers of regulations, and the relationship between trafficking and vesicle fusion.
A. Different GPCRs prefer different recycling pathways. The β2 adrenergic receptor (B2AR) is primarily recycled through the actin-SNX27-Retromer-tubular (ASRT) subdomains on the early endosomes. The sorting of B2AR to the specialized subdomains is mediated by its PDZ ligand, a distal C-terminal amino acid sequence of DSLL. On the other hand, the μ opioid receptor (MOR)

does not have an identified PDZ ligand. MOR is thought to be recycled via a different pathway or at least from a different kind of endosomal subdomains, through a mechanism depending on its C-terminal bi-leucine sequence of LENLEAE. Even for an individual GPCR the trafficking itinerary can still be diversified depending on the context. For examples: **B**. agonists-induced differential post-translational modifications of MOR may lead to diversified pathway selectivity; **C**. variants of MOR resulted from alternative splicing of exon 4 possessing different recycling sequences can exhibit different recycling dynamics; **D**. variants of MOR resulted from polymorphism such as the N40D variant that lacks an essential *N*-glycosylation site may have altered biosynthetic exocytosis. However, regardless of where the vesicles carrying exocytic GPCRs are originated from, (**E**.) they have to package v-SNARE(s) for the proper docking and fusion at the plasma membrane. Fusion machinery, especially the minimal machinery of SNARE complex, plays an indispensable role in the exocytosis of GPCRs as to mediate their plasma membrane insertion.

The potential application and regulation of fusion machinery in GPCR exocytosis

To summarize, GPCR trafficking is convoluted yet regulated. The choice of a trafficking pathway can be receptor-specific, agonist-specific, isoform-specific, or cellular context-specific. However, regardless of which endomembrane compartment the trafficking is originated from and which direction the trafficking is targeting to, fusion machinery will always be required to mediate the final step of vesicular fusion and subsequently the translocation of trafficked receptors onto the target membrane. Therefore, the vesicles are always packaged with some kind of v-SNARE(s) for proper docking (Fig. 1.1 E). The question is, does GPCR trafficking utilize the same sets of v/t-SNAREs as for neurotransmitter release, or is there specificity encoded in the convoluted GPCR trafficking network?

Although at current stage we have limited information to provide a comprehensive answer to this question, there are still several interesting aspects worth of discussion. The first aspect is the crosstalk between GPCR signaling and vesicle fusion. It is well-known that the Gβγ subunit of Gαi/o coupled GPCRs can activate pre-synaptic G protein-coupled inward rectifying potassium channels (*110–112*) and inhibit post-synaptic voltage-gated calcium channels (*113*, *114*) through direct interactions to decrease neuronal excitability and neurotransmitter release (reviewed in *115*). Interestingly, recent studies have identified that, both *in vitro* and *in vivo*, Gβγ can also compete

with synaptotagmin by directly interacting with SNAP-25 to suppress vesicle fusion, which is proposed to be an additional mechanism of Gβγ-mediated inhibition on neurotransmission (*116*, *117*). However, it has also been shown that DAMGO-activated MOR, a Gαi/o coupled GPCR, undergoes robust recycling and plasma membrane insertion under the requirement of S363 phosphorylation mediated by a Gβγ-phospholipase C-PKC mechanism (*118*). How does the activated Gβγ not inhibit the membrane insertion of MOR? One hypothesis of many to reconcile this contradiction is perhaps different sets of SNARE assemblies are utilized in the transport of MOR and neurotransmitters, and that Gβγ-mediated inhibition is specific to the SNARE assemblies for neurotransmitter release.

The second interesting aspect is the potential co-sorting of v-SNAREs and GPCRs. Similar to endosomal sorting leading to differential sub-endosomal localization of GPCRs, v-SNAREs or VAMP proteins may also undergo sorting alongside their client receptors, thus contributing to the receptor specificity of SNARE assemblies. Recent studies have identified two major endosomal sorting machineries, the Retromer (composed of Vps29, Vps35, and Vps26) and Retriever (composed of Vps29, Vps35L, and Vps26C) complexes, to be responsible for the sorting of cargoes targeting recycling pathways (reviewed in *119*). Both the Retromer and Retriever complexes function through their diversified interacting proteins, besides the common WASH (Wiskott-Aldrich syndrome protein and SCAR homolog) complex, including but not limited to cargo adaptor SNX27 for Retromer, or SNX17 and the CCC (COMMD/CCDC93/CCDC22) complex for Retriever (*119–121*). As mentioned above, the sorting of B2AR to actin-dependent tubules for recycling is mediated by the Retromer complex through the interaction between B2AR's PDZ ligand and SNX27, a PDZ protein (*83*, *84*). Whether these machineries also mediate the sorting of VAMP proteins and whether the sorting is mediated via direct protein-protein

interaction is currently unclear. However, evidence has shown that VAMP proteins do possess signal sequences for proper subcellular and vesicular targeting, where VAMP4's distant N-terminal (beyond the SNARE motif) is both required and sufficient for trans-Golgi network targeting (*62*), and VAMP2's amino acid sequence (AA) 41-50 of amphipathic nature is required for its vesicular targeting while its AA 61-70 can putatively autoinhibit this targeting process (*61*).

Currently, the understanding of v-SNARE sorting is still uncoupled from a meaningful impact on cellular functions, and the mechanistic detail of sorting is still not comparable to what has been resolved for receptor cargoes. In Chapter 3 of this dissertation, we discuss our attempt to use the known specificity of VAMP2 in MOR recycling (Chapter 2) to reveal the molecular basis of v-SNARE sorting.

Discussion

Fusion machinery is surprisingly understudied despite being a critical component for GPCR exocytosis. Studying fusion machinery involved in GPCR exocytosis is beneficial from both a basic biology and a translational standpoint.

From the basic biology standpoint, identifying the fusion machinery, particularly the SNARE assemblies, for different GPCRs at varied trafficking conditions can help characterize trafficking pathways systematically. Based on the assumption of SNARE proteins' pathway-selective assignment, the SNARE assemblies' identity can potentially serve as a pathway origin marker for each fusing vesicle. By simultaneously visualizing the exocytosis of GPCRs and v-SNAREs (ref. *80*, *81*, *108*, *118*, *122*, *123* for examples of GPCR exocytosis visualization, and ref. *48*, *124–126* for examples of v-SNARE exocytosis visualization), we can start answering long-standing questions on a whole new level. Such a method can be useful to characterize the overall exocytic profiles of GPCRs and detect the changes in exocytic pathways caused by certain

manipulations. In detail, instead of qualifying exocytic pathways through colocalization analysis of GPCRs and endosomal markers (*80*, *86*, *108*, *127*), we can use the presence or absence (or the level of enrichment) of a v-SNARE to analyze for real-time information of the involved pathways at a subendosomal resolution (due to v-SNARE endosomal sorting) on a scale of large fusion event populations. With this method we can achieve a precise characterization of the pathway and an accurate identification of the impact of the manipulations (ref. *48*, *51*, *128* as novel examples).

From the translational standpoint, fusion machinery may become a valuable drug target if we have gained a better understanding to its specificity (toward cargo, tissue, cellular context, etc.). Universally targeting fusion machinery, just as the mechanism of actions of tetanus and botulinum neurotoxins, leads to detrimental outputs (*129*). However, if we can modulate the function of the fusion machinery in a restricted manner (e.g., specifically inhibiting a syntaxin subtype that would function only for a subset of receptors or secretory molecules in a tissue-dependent manner), we might be able to modify the surface/release levels of this subset of receptors/molecules without causing severe side effects. These modifications can be useful in at least two clinical scenarios: (i). to decrease the surface localization of pathological receptors that are primarily activated by cell-impermeant ligands for the treatment of cancers, such as protease-activated receptors (PARs) and chemokine receptors that have been implicated for cancer cell proliferation (reviewed in *130*); (ii). to limit the abnormal release of neurotransmitters in specific brain regions for psychiatric disorders, such as the tonic dopamine release in the mesolimbic region in schizophrenia (reviewed in *131*).

In summary, fusion machinery in surface receptor exocytosis is an exciting perspective for future studies with many unknowns open for discoveries. As we gain more insights, we will not only have a better understanding of GPCR biology and protein trafficking, but it may also help to develop novel therapeutics for a better treatment of diseases.

References

1. I. Mellman, S. D. Emr, A Nobel Prize for membrane traffic: vesicles find their journey's end. *J. Cell Biol.* **203**, 559–561 (2013).

2. T. M. Jessell, E. R. Kandel, Synaptic transmission: a bidirectional and self-modifiable form of cell-cell communication. *Cell* **72**, 1–30 (1993).

3. T. C. Südhof, R. C. Malenka, Understanding synapses: past, present, and future. *Neuron* **60**, 469–476 (2008).

4. R. R. Gainetdinov, R. T. Premont, L. M. Bohn, R. J. Lefkowitz, M. G. Caron, Desensitization of G protein–coupled receptors and neuronal functions. *Annu. Rev. Neurosci.* **27**, 107–144 (2004).

5. K. J. Gerber, K. E. Squires, J. R. Hepler, Roles for regulator of G protein signaling proteins in synaptic signaling and plasticity. *Mol. Pharmacol.* **89**, 273–286 (2016).

6. G. A. Kumar, M. A. Puthenveedu, Diversity and specificity in location-based signaling outputs of neuronal GPCRs. *Curr. Opin. Neurobiol.* **76**, 102601 (2022).

7. R. Santos, O. Ursu, A. Gaulton, A. P. Bento, R. S. Donadi, C. G. Bologa, A. Karlsson, B. Al-Lazikani, A. Hersey, T. I. Oprea, J. P. Overington, A comprehensive map of molecular drug targets. *Nat. Rev. Drug Discov.* **16**, 19–34 (2017).

8. A. S. Hauser, M. M. Attwood, M. Rask-Andersen, H. B. Schiöth, D. E. Gloriam, Trends in GPCR drug discovery: new agents, targets and indications. *Nat. Rev. Drug Discov.* **16**, 829–842 (2017).

9. M. T. Drake, S. K. Shenoy, R. J. Lefkowitz, Trafficking of G protein–coupled receptors. *Circ. Res.* **99**, 570–582 (2006).

10. N. J. Pavlos, P. A. Friedman, GPCR signaling and trafficking: the long and short of it. *Trends Endocrinol. Metab.* **28**, 213–226 (2017).

11. W. Wickner, R. Schekman, Membrane fusion. *Nat. Struct. Mol. Biol.* **15**, 658–664 (2008).

12. S. Martens, H. T. McMahon, Mechanisms of membrane fusion: disparate players and common principles. *Nat. Rev. Mol. Cell Biol.* **9**, 543–556 (2008).

13. T. C. Südhof, Neurotransmitter release: the last millisecond in the life of a synaptic vesicle. *Neuron* **80**, 675–690 (2013).

14. D. Toomre, P. Keller, J. White, J. C. Olivo, K. Simons, Dual-color visualization of trans-Golgi network to plasma membrane traffic along microtubules in living cells. *J. Cell Sci.* **112 (Pt 1)**, 21–33 (1998).

15. E. Rodriguez-Boulan, G. Kreitzer, A. Müsch, Organization of vesicular trafficking in epithelia. *Nat. Rev. Mol. Cell Biol.* **6**, 233–247 (2005).

16. I. Verdeny-Vilanova, F. Wehnekamp, N. Mohan, Á. S. Álvarez, J. S. Borbely, J. J. Otterstrom, D. C. Lamb, M. Lakadamyali, 3D motion of vesicles along microtubules helps them to circumvent obstacles in cells. *J. Cell Sci.* **130**, 1904–1916 (2017).

17. S. M. Ahmed, H. Nishida-Fukuda, Y. Li, W. H. McDonald, C. C. Gradinaru, I. G. Macara, Exocyst dynamics during vesicle tethering and fusion. *Nat. Commun.* **9**, 5140 (2018).

18. B. Wu, W. Guo, The exocyst at a glance. *J. Cell Sci.* **128**, 2957–2964 (2015).

19. K. Mei, W. Guo, Exocytosis: a new exocyst movie. *Curr. Biol.* **29**, R30–R32 (2019).

20. T. Söllner, M. K. Bennett, S. W. Whiteheart, R. H. Scheller, J. E. Rothman, A protein assembly-disassembly pathway in vitro that may correspond to sequential steps of synaptic vesicle docking, activation, and fusion. *Cell* **75**, 409–418 (1993).

21. T. Söllner, S. W. Whiteheart, M. Brunner, H. Erdjument-Bromage, S. Geromanos, P. Tempst, J. E. Rothman, SNAP receptors implicated in vesicle targeting and fusion. *Nature* **362**, 318–324 (1993).

22. J. A. McNew, F. Parlati, R. Fukuda, R. J. Johnston, K. Paz, F. Paumet, T. H. Söllner, J. E. Rothman, Compartmental specificity of cellular membrane fusion encoded in SNARE proteins. *Nature* **407**, 153–159 (2000).

23. S. Schoch, F. Deák, A. Königstorfer, M. Mozhayeva, Y. Sara, T. C. Südhof, E. T. Kavalali, SNARE function analyzed in synaptobrevin/VAMP knockout mice. *Science* **294**, 1117–1122 (2001).

24. S. Koike, R. Jahn, SNAREs define targeting specificity of trafficking vesicles by combinatorial interaction with tethering factors. *Nat. Commun.* **10**, 1608 (2019).

25. T. Weber, B. V. Zemelman, J. A. McNew, B. Westermann, M. Gmachl, F. Parlati, T. H. Söllner, J. E. Rothman, SNAREpins: minimal machinery for membrane fusion. *Cell* **92**, 759–772 (1998).

26. F. Deák, O.-H. Shin, E. T. Kavalali, T. C. Südhof, Structural determinants of synaptobrevin 2 function in synaptic vesicle fusion. *J. Neurosci.* **26**, 6668–6676 (2006).

27. V. Kiessling, A. J. B. Kreutzberger, B. Liang, S. B. Nyenhuis, P. Seelheim, J. D. Castle, D. S. Cafiso, L. K. Tamm, A molecular mechanism for calcium-mediated synaptotagmin-triggered exocytosis. *Nat. Struct. Mol. Biol.* **25**, 911–917 (2018).

28. M. Geppert, Y. Goda, R. E. Hammer, C. Li, T. W. Rosahl, C. F. Stevens, T. C. Südhof, Synaptotagmin I: A major Ca2+ sensor for transmitter release at a central synapse. *Cell* **79**, 717–727 (1994).

29. C. Li, B. Ullrich, J. Z. Zhang, R. G. W. Anderson, N. Brose, T. C. Südhof, Ca2+-dependent and -independent activities of neural and non-neural synaptotagmins. *Nature* **375**, 375594a0 (1995).

30. T. Bacaj, D. Wu, X. Yang, W. Morishita, P. Zhou, W. Xu, R. C. Malenka, T. C. Südhof, Synaptotagmin-1 and synaptotagmin-7 trigger synchronous and asynchronous phases of neurotransmitter release. *Neuron* **80**, 947–959 (2013).

31. J. Wang, O. Bello, S. M. Auclair, J. Wang, J. Coleman, F. Pincet, S. S. Krishnakumar, C. V. Sindelar, J. E. Rothman, Calcium sensitive ring-like oligomers formed by synaptotagmin. *Proc. Natl. Acad. Sci.* **111**, 13966–13971 (2014).

32. H. T. McMahon, M. Missler, C. Li, T. C. Südhof, Complexins: cytosolic proteins that regulate SNAP receptor function. *Cell* **83**, 111–119 (1995).

33. H. Cai, K. Reim, F. Varoqueaux, S. Tapechum, K. Hill, J. B. Sørensen, N. Brose, R. H. Chow, Complexin II plays a positive role in Ca2+-triggered exocytosis by facilitating vesicle priming. *Proc. Natl. Acad. Sci.* **105**, 19538–19543 (2008).

34. A. Maximov, J. Tang, X. Yang, Z. P. Pang, T. C. Südhof, Complexin controls the force transfer from SNARE complexes to membranes in fusion. *Science* **323**, 516–521 (2009).

35. A. J. B. Kreutzberger, V. Kiessling, C. Stroupe, B. Liang, J. Preobraschenski, M. Ganzella, M. A. B. Kreutzberger, R. Nakamoto, R. Jahn, J. D. Castle, L. K. Tamm, In vitro fusion of single synaptic and dense core vesicles reproduces key physiological properties. *Nat. Commun.* **10**, 3904 (2019).

36. T. C. Südhof, The presynaptic active zone. *Neuron* **75**, 11–25 (2012).

37. J. Emperador-Melero, P. S. Kaeser, Assembly of the presynaptic active zone. *Curr. Opin. Neurobiol.* **63**, 95–103 (2020).

38. J. Kesavan, M. Borisovska, D. Bruns, v-SNARE actions during Ca2+-triggered exocytosis. *Cell* **131**, 351–363 (2007).

39. C. Wang, J. Tu, S. Zhang, B. Cai, Z. Liu, S. Hou, Q. Zhong, X. Hu, W. Liu, G. Li, Z. Liu, L. He, J. Diao, Z.-J. Zhu, D. Li, C. Liu, Different regions of synaptic vesicle membrane regulate VAMP2 conformation for the SNARE assembly. *Nat. Commun.* **11**, 1531 (2020).

40. Z. Wu, N. Dharan, Z. A. McDargh, S. Thiyagarajan, B. O'Shaughnessy, E. Karatekin, The neuronal calcium sensor Synaptotagmin-1 and SNARE proteins cooperate to dilate fusion pores. *eLife* **10**, e68215 (2021).

41. M. Zhao, S. Wu, Q. Zhou, S. Vivona, D. J. Cipriano, Y. Cheng, A. T. Brunger, Mechanistic insights into the recycling machine of the SNARE complex. *Nature* **518**, 61–67 (2015).

42. D. M. O. Ramirez, E. T. Kavalali, The role of non-canonical SNAREs in synaptic vesicle recycling. *Cell Logist.* **2**, 20–27 (2012).

43. F. Parlati, J. A. McNew, R. Fukuda, R. Miller, T. H. Söllner, J. E. Rothman, Topological restriction of SNARE-dependent membrane fusion. *Nature* **407**, 194–198 (2000).

44. R. Fukuda, J. A. McNew, T. Weber, F. Parlati, T. Engel, W. Nickel, J. E. Rothman, T. H. Söllner, Functional architecture of an intracellular membrane t-SNARE. *Nature* **407**, 198–202 (2000).

45. F. Parlati, O. Varlamov, K. Paz, J. A. McNew, D. Hurtado, T. H. Söllner, J. E. Rothman, Distinct SNARE complexes mediating membrane fusion in Golgi transport based on combinatorial specificity. *Proc. Natl. Acad. Sci.* **99**, 5424–5429 (2002).

46. T. Galli, T. Chilcote, O. Mundigl, T. Binz, H. Niemann, P. D. Camilli, Tetanus toxin-mediated cleavage of cellubrevin impairs exocytosis of transferrin receptor-containing vesicles in CHO cells. *J. Cell Biol.* **125**, 1015–1024 (1994).

47. K. Kubo, M. Kobayashi, S. Nozaki, C. Yagi, K. Hatsuzawa, Y. Katoh, H.-W. Shin, S. Takahashi, K. Nakayama, SNAP23/25 and VAMP2 mediate exocytic event of transferrin receptor-containing recycling vesicles. *Biol. Open* **4**, 910–920 (2015).

48. M. Bakr, D. Jullié, J. Krapivkina, V. Paget-Blanc, L. Bouit, J. D. Petersen, N. Retailleau, C. Breillat, E. Herzog, D. Choquet, D. Perrais, The vSNAREs VAMP2 and VAMP4 control

recycling and intracellular sorting of post-synaptic receptors in neuronal dendrites. *Cell Reports* **36**, 109678 (2021).

49. V. Das, B. Nal, A. Dujeancourt, M.-I. Thoulouze, T. Galli, P. Roux, A. Dautry-Varsat, A. Alcover, Activation-induced polarized recycling targets T cell antigen receptors to the immunological synapse. *Immunity* **20**, 577–588 (2004).
50. F. Finetti, L. Patrussi, D. Galgano, C. Cassioli, G. Perinetti, G. J. Pazour, C. T. Baldari, The small GTPase Rab8 interacts with VAMP-3 to regulate the delivery of recycling T-cell receptors to the immune synapse. *J. Cell Sci.* **128**, 2541–2552 (2015).
51. H. Chen, Z. Y. Weinberg, G. A. Kumar, M. A. Puthenveedu, Vesicle-associated membrane protein 2 is a cargo-selective v-SNARE for a subset of GPCRs. *J. Cell Biol.* **222**, e202207070 (2023).
52. S. Jurado, D. Goswami, Y. Zhang, A. J. M. Molina, T. C. Südhof, R. C. Malenka, LTP requires a unique postsynaptic SNARE fusion machinery. *Neuron* **77**, 542–558 (2013).
53. K. L. Arendt, Y. Zhang, S. Jurado, R. C. Malenka, T. C. Südhof, L. Chen, Retinoic acid and LTP recruit postsynaptic AMPA receptors using distinct SNARE-dependent mechanisms. *Neuron* **86**, 442–456 (2015).
54. Y. Gu, R. L. Huganir, Identification of the SNARE complex mediating the exocytosis of NMDA receptors. *Proc. Natl. Acad. Sci.* **113**, 12280–12285 (2016).
55. B. B. Singh, T. P. Lockwich, B. C. Bandyopadhyay, X. Liu, S. Bollimuntha, S. Brazer, C. Combs, S. Das, A. G. M. Leenders, Z.-H. Sheng, M. A. Knepper, S. V. Ambudkar, I. S. Ambudkar, VAMP2-dependent exocytosis regulates plasma membrane insertion of TRPC3 channels and contributes to agonist-stimulated Ca2+ influx. *Mol. Cell* **15**, 635–646 (2004).
56. B. Cheatham, A. Volchuk, C. R. Kahn, L. Wang, C. J. Rhodes, A. Klip, Insulin-stimulated translocation of GLUT4 glucose transporters requires SNARE-complex proteins. *Proc. Natl. Acad. Sci.* **93**, 15169–15173 (1996).
57. L. B. Martin, A. Shewan, C. A. Millar, G. W. Gould, D. E. James, Vesicle-associated membrane protein 2 plays a specific role in the insulin-dependent trafficking of the facilitative glucose transporter GLUT4 in 3T3-L1 adipocytes. *J. Biol. Chem.* **273**, 1444–1452 (1998).
58. V. K. Randhawa, P. J. Bilan, Z. A. Khayat, N. Daneman, Z. Liu, T. Ramlal, A. Volchuk, X.-R. Peng, T. Coppola, R. Regazzi, W. S. Trimble, A. Klip, VAMP2, but not VAMP3/cellubrevin, mediates insulin-dependent incorporation of GLUT4 into the plasma membrane of L6 myoblasts. *Mol. Biol. Cell* **11**, 2403–2417 (2000).
59. J. S. Bogan, Regulation of glucose transporter translocation in health and diabetes. *Annu. Rev. Biochem.* **81**, 507–532 (2012).
60. P. S. Caceres, M. Mendez, P. A. Ortiz, Vesicle-associated Membrane Protein 2 (VAMP2) but Not VAMP3 Mediates cAMP-stimulated Trafficking of the Renal Na+-K+-2Cl− Co-transporter NKCC2 in Thick Ascending Limbs. *J. Biol. Chem.* **289**, 23951–23962 (2014).
61. E. Grote, J. C. Hao, M. K. Bennett, R. B. Kelly, A targeting signal in VAMP regulating transport to synaptic vesicles. *Cell* **81**, 581–589 (1995).

62. Q. Zeng, T. T. H. Tran, H.-X. Tan, W. Hong, The cytoplasmic domain of Vamp4 and Vamp5 is responsible for their correct subcellular targeting. *J. Biol. Chem.* **278**, 23046–23054 (2003).

63. F. Paumet, V. Rahimian, J. E. Rothman, The specificity of SNARE-dependent fusion is encoded in the SNARE motif. *Proc. Natl. Acad. Sci.* **101**, 3376–3380 (2004).

64. R. Jahn, R. H. Scheller, SNAREs — engines for membrane fusion. *Nat. Rev. Mol. Cell Biol.* **7**, 631–643 (2006).

65. K. L. Pierce, R. T. Premont, R. J. Lefkowitz, Seven-transmembrane receptors. *Nat. Rev. Mol. Cell Biol.* **3**, 639–650 (2002).

66. F. Jean-Alphonse, A. C. Hanyaloglu, Regulation of GPCR signal networks via membrane trafficking. *Mol. Cell. Endocrinol.* **331**, 205–214 (2011).

67. M. Stoeber, D. Jullié, J. Li, S. Chakraborty, S. Majumdar, N. A. Lambert, A. Manglik, M. von Zastrow, Agonist-selective recruitment of engineered protein probes and of GRK2 by opioid receptors in living cells. *eLife* **9**, e54208 (2020).

68. J. Drube, R. S. Haider, E. S. F. Matthees, M. Reichel, J. Zeiner, S. Fritzwanker, C. Ziegler, S. Barz, L. Klement, J. Filor, V. Weitzel, A. Kliewer, E. Miess-Tanneberg, E. Kostenis, S. Schulz, C. Hoffmann, GPCR kinase knockout cells reveal the impact of individual GRKs on arrestin binding and GPCR regulation. *Nat. Commun.* **13**, 540 (2022).

69. Z. Y. Weinberg, M. A. Puthenveedu, Regulation of G protein-coupled receptor signaling by plasma membrane organization and endocytosis. *Traffic* **20**, 121–129 (2018).

70. M. Mettlen, P.-H. Chen, S. Srinivasan, G. Danuser, S. L. Schmid, Regulation of clathrin-mediated endocytosis. *Annu. Rev. Biochem.* **87**, 871–896 (2018).

71. A. Helenius, I. Mellman, D. Wall, A. Hubbard, Endosomes. *Trends Biochem. Sci.* **8**, 245–250 (1983).

72. J. Gruenberg, H. Stenmark, The biogenesis of multivesicular endosomes. *Nat. Rev. Mol. Cell Biol.* **5**, 317–323 (2004).

73. E. Perret, A. Lakkaraju, S. Deborde, R. Schreiner, E. Rodriguez-Boulan, Evolving endosomes: how many varieties and why? *Curr. Opin. Cell Biol.* **17**, 423–434 (2005).

74. B. D. Grant, J. G. Donaldson, Pathways and mechanisms of endocytic recycling. *Nat. Rev. Mol. Cell Biol.* **10**, nrm2755 (2009).

75. J. Huotari, A. Helenius, Endosome maturation. *EMBO J.* **30**, 3481–3500 (2011).

76. A. H. Hutagalung, P. J. Novick, Role of Rab GTPases in membrane traffic and cell physiology. *Physiol. Rev.* **91**, 119–49 (2011).

77. A. Wandinger-Ness, M. Zerial, Rab proteins and the compartmentalization of the endosomal system. *CSH Perspect. Biol.* **6**, a022616 (2014).

78. L. Langemeyer, F. Fröhlich, C. Ungermann, Rab GTPase function in endosome and lysosome biogenesis. *Trends Cell Biol.* **28**, 957–970 (2018).

79. T. T. Cao, H. W. Deacon, D. Reczek, A. Bretscher, M. von Zastrow, A kinase-regulated PDZ-domain interaction controls endocytic sorting of the beta2-adrenergic receptor. *Nature* **401**, 286–90 (1999).

80. M. A. Puthenveedu, B. Lauffer, P. Temkin, R. Vistein, P. Carlton, K. Thorn, J. Taunton, O. D. Weiner, R. G. Parton, M. von Zastrow, Sequence-dependent sorting of recycling proteins by actin-stabilized endosomal microdomains. *Cell* **143**, 761–773 (2010).

81. R. Vistein, M. A. Puthenveedu, Reprogramming of G protein-coupled receptor recycling and signaling by a kinase switch. *Proc. Natl. Acad. Sci.* **110**, 15289–15294 (2013).

82. S. L. Bowman, D. J. Shiwarski, M. A. Puthenveedu, Distinct G protein–coupled receptor recycling pathways allow spatial control of downstream G protein signaling. *J. Cell Biol.* **214**, 797–806 (2016).

83. B. E. L. Lauffer, C. Melero, P. Temkin, C. Lei, W. Hong, T. Kortemme, M. von Zastrow, SNX27 mediates PDZ-directed sorting from endosomes to the plasma membrane. *J. Cell Biol.* **190**, 565–574 (2010).

84. P. Temkin, B. Lauffer, S. Jäger, P. Cimermancic, N. J. Krogan, M. von Zastrow, SNX27 mediates retromer tubule entry and endosome-to-plasma membrane trafficking of signaling receptors. *Nat. Cell Biol.* **13**, 715–721 (2011).

85. M. Tanowitz, M. von Zastrow, A novel endocytic recycling signal that distinguishes the membrane trafficking of naturally occurring opioid receptors. *J. Biol. Chem.* **278**, 45978–45986 (2003).

86. F. Wang, X. Chen, X. Zhang, L. Ma, Phosphorylation state of mu-opioid receptor determines the alternative recycling of receptor via Rab4 or Rab11 pathway. *Mol. Endocrinol.* **22**, 1881–92 (2008).

87. M. L. Duarte, L. A. Devi, Post-translational modifications of opioid receptors. *Trends Neurosci.* **43**, 417–432 (2020).

88. A. Patwardhan, N. Cheng, J. Trejo, Post-translational modifications of G protein–coupled receptors control cellular signaling dynamics in space and time. *Pharmacol. Rev.* **73**, 120–151 (2021).

89. C. Doll, J. Konietzko, F. Pöll, T. Koch, V. Höllt, S. Schulz, Agonist-selective patterns of μ-opioid receptor phosphorylation revealed by phosphosite-specific antibodies. *BJP* **164**, 298–307 (2011).

90. F. A. Oladosu, W. Maixner, A. G. Nackley, Alternative splicing of G protein–coupled receptors: relevance to pain management. *Mayo Clin. Proc.* **90**, 1135–1151 (2015).

91. B. K. Rana, T. Shiina, P. A. Insel, Genetic variations and polymorphisms of G protein-coupled receptors: functional and therapeutic implications. *Annu. Rev. Pharmacol. Toxicol.* **41**, 593–624 (2001).

92. S. Liu, W.-J. Kang, A. Abrimian, J. Xu, L. Cartegni, S. Majumdar, P. Hesketh, A. Bekker, Y.-X. Pan, Alternative pre-mRNA splicing of the mu opioid receptor gene, OPRM1: insight into complex mu opioid actions. *Biomolecules* **11**, 1525 (2021).

93. J. Xu, M. Xu, T. Brown, G. C. Rossi, Y. L. Hurd, C. E. Inturrisi, G. W. Pasternak, Y.-X. Pan, Stabilization of the μ-opioid receptor by truncated single transmembrane splice variants through a chaperone-like action. *J. Biol. Chem.* **288**, 21211–21227 (2013).

94. A. G. P. Schuller, M. A. King, J. Zhang, E. Bolan, Y. Pan, D. J. Morgan, A. Chang, M. E. Czick, E. M. Unterwald, G. W. Pasternak, J. E. Pintar, Retention of heroin and morphine–6β–glucuronide analgesia in a new line of mice lacking exon 1 of MOR–1. *Nat. Neurosci.* **2**, 151–156 (1999).

95. S. Majumdar, S. Grinnell, V. L. Rouzic, M. Burgman, L. Polikar, M. Ansonoff, J. Pintar, Y.-X. Pan, G. W. Pasternak, Truncated G protein-coupled mu opioid receptor MOR-1 splice variants are targets for highly potent opioid analgesics lacking side effects. *Proc. Natl. Acad. Sci.* **108**, 19778–19783 (2011).

96. M. Tanowitz, J. N. Hislop, M. von Zastrow, Alternative splicing determines the post-endocytic sorting fate of G-protein-coupled receptors. *J. Biol. Chem.* **283**, 35614–35621 (2008).

97. T. Schöneberg, I. Liebscher, Mutations in G protein–coupled receptors: mechanisms, pathophysiology and potential therapeutic approaches. *Pharmacol. Rev.* **73**, 89–119 (2021).

98. C. Bond, K. S. LaForge, M. Tian, D. Melia, S. Zhang, L. Borg, J. Gong, J. Schluger, J. A. Strong, S. M. Leal, J. A. Tischfield, M. J. Kreek, L. Yu, Single-nucleotide polymorphism in the human mu opioid receptor gene alters β-endorphin binding and activity: possible implications for opiate addiction. *Proc. Natl. Acad. Sci.* **95**, 9608–9613 (1998).

99. N. M. Lee, A. P. Smith, Opioid receptor polymorphisms and opioid abuse. *Pharmacogenomics* **3**, 219–227 (2002).

100. J. Lötsch, G. Geisslinger, Are μ-opioid receptor polymorphisms important for clinical opioid therapy? *Trends Mol. Med.* **11**, 82–89 (2005).

101. B. S. Haerian, M. S. Haerian, OPRM1 rs1799971 polymorphism and opioid dependence: evidence from a meta-analysis. *Pharmacogenomics* **14**, 813–824 (2013).

102. T. Kroslak, K. S. LaForge, R. J. Gianotti, A. Ho, D. A. Nielsen, M. J. Kreek, The single nucleotide polymorphism A118G alters functional properties of the human mu opioid receptor. *J. Neurochem.* **103**, 77–87 (2007).

103. D. Popova, N. Desai, J. A. Blendy, Z. P. Pang, Synaptic regulation by OPRM1 variants in reward neurocircuitry. *J. Neurosci.* **39**, 5685–5696 (2019).

104. E. M. Janezic, S. M.-L. Lauer, R. G. Williams, M. Chungyoun, K.-S. Lee, E. Navaluna, H.-T. Lau, S.-E. Ong, C. Hague, N-glycosylation of α1D-adrenergic receptor N-terminal domain is required for correct trafficking, function, and biogenesis. *Sci. Rep.* **10**, 7209 (2020).

105. Q. Chen, L. J. Miller, M. Dong, Role of N-linked glycosylation in biosynthesis, trafficking, and function of the human glucagon-like peptide 1 receptor. *Am. J. Physiol. - Endocrinol.* **299**, E62–E68 (2010).

106. A. Beyer, T. Koch, H. Schröder, S. Schulz, V. Höllt, Effect of the A118G polymorphism on binding affinity, potency and agonist-mediated endocytosis, desensitization, and resensitization of the human mu-opioid receptor. *J. Neurochem.* **89**, 553–560 (2004).

107. N. N. Jimenez-Vargas, J. Gong, M. J. Wisdom, D. D. Jensen, R. Latorre, A. Hegron, S. Teng, J. J. DiCello, P. Rajasekhar, N. A. Veldhuis, S. E. Carbone, Y. Yu, C. Lopez-Lopez, J. Jaramillo-Polanco, M. Canals, D. E. Reed, A. E. Lomax, B. L. Schmidt, K. W. Leong, S. J. Vanner, M. L. Halls, N. W. Bunnett, D. P. Poole, Endosomal signaling of delta opioid receptors is an endogenous mechanism and therapeutic target for relief from inflammatory pain. *Proc. Natl. Acad. Sci.* **117**, 15281–15292 (2020).

108. J. M. Kunselman, A. Gupta, I. Gomes, L. A. Devi, M. A. Puthenveedu, Compartment-specific opioid receptor signaling is selectively modulated by different Dynorphin peptides. *eLife* **10**, e60270 (2021).

109. S. E. Crilly, W. Ko, Z. Y. Weinberg, M. A. Puthenveedu, Conformational specificity of opioid receptors is determined by subcellular location irrespective of agonist. *eLife* **10**, e67478 (2021).

110. C. L. Huang, P. A. Slesinger, P. J. Casey, Y. N. Jan, L. Y. Jan, Evidence that direct binding of G beta gamma to the GIRK1 G protein-gated inwardly rectifying K+ channel is important for channel activation. *Neuron* **15**, 1133–43 (1995).

111. Q. Lei, M. B. Jones, E. M. Talley, A. D. Schrier, W. E. McIntire, J. C. Garrison, D. A. Bayliss, Activation and inhibition of G protein-coupled inwardly rectifying potassium (Kir3) channels by G protein βγ subunits. *Proc. Natl. Acad. Sci.* **97**, 9771–9776 (2000).

112. K. K. Touhara, R. MacKinnon, Molecular basis of signaling specificity between GIRK channels and GPCRs. *eLife* **7**, e42908 (2018).

113. T. Takahashi, I. D. Forsythe, T. Tsujimoto, M. Barnes-Davies, K. Onodera, Presynaptic calcium current modulation by a metabotropic glutamate receptor. *Science* **274**, 594–597 (1996).

114. Y. Kajikawa, N. Saitoh, T. Takahashi, GTP-binding protein βγ subunits mediate presynaptic calcium current inhibition by GABAB receptor. *Proc. Natl. Acad. Sci.* **98**, 8054–8058 (2001).

115. K. Wickman, D. E. Clapham, Ion channel regulation by G proteins. *Physiol. Rev.* **75**, 865–885 (1995).

116. Z. Zurawski, B. Page, M. C. Chicka, R. L. Brindley, C. A. Wells, A. M. Preininger, K. Hyde, J. A. Gilbert, O. Cruz-Rodriguez, K. P. M. Currie, E. R. Chapman, S. Alford, H. E. Hamm, Gβγ directly modulates vesicle fusion by competing with synaptotagmin for binding to neuronal SNARE proteins embedded in membranes. *J. Biol. Chem.* **292**, 12165–12177 (2017).

117. Z. Zurawski, A. D. T. Gray, L. J. Brady, B. Page, E. Church, N. A. Harris, M. R. Dohn, Y. Y. Yim, K. Hyde, D. P. Mortlock, C. K. Jones, D. G. Winder, S. Alford, H. E. Hamm, Disabling the Gβγ-SNARE interaction disrupts GPCR-mediated presynaptic inhibition, leading to physiological and behavioral phenotypes. *Sci. Signal.* **12**, eaat8595 (2019).

118. J. M. Kunselman, A. S. Zajac, Z. Y. Weinberg, M. A. Puthenveedu, Homologous regulation of mu opioid receptor recycling by Gβγ, protein kinase C, and receptor phosphorylation. *Mol. Pharmacol.* **96**, 702–710 (2019).

119. K. Chen, M. D. Healy, B. M. Collins, Towards a molecular understanding of endosomal trafficking by Retromer and Retriever. *Traffic* **20**, 465–478 (2019).

120. C. Burd, P. J. Cullen, Retromer: a master conductor of endosome sorting. *CSH Perspect. Biol.* **6**, a016774 (2014).

121. K. E. McNally, R. Faulkner, F. Steinberg, M. Gallon, R. Ghai, D. Pim, P. Langton, N. Pearson, C. M. Danson, H. Nägele, L. L. Morris, A. Singla, B. L. Overlee, K. J. Heesom, R. Sessions, L. Banks, B. M. Collins, I. Berger, D. D. Billadeau, E. Burstein, P. J. Cullen, Retriever is a multiprotein complex for retromer-independent endosomal cargo recycling. *Nat. Cell Biol.* **19**, 1214–1225 (2017).

122. G. A. Yudowski, M. A. Puthenveedu, M. von Zastrow, Distinct modes of regulated receptor insertion to the somatodendritic plasma membrane. *Nat. Neurosci.* **9**, nn1679 (2006).

123. G. A. Yudowski, M. A. Puthenveedu, A. G. Henry, M. von Zastrow, Cargo-mediated regulation of a rapid Rab4-dependent recycling pathway. *Mol. Biol. Cell* **20**, 2774–2784 (2009).

124. J. Raingo, M. Khvotchev, P. Liu, F. Darios, Y. C. Li, D. M. O. Ramirez, M. Adachi, P. Lemieux, K. Toth, B. Davletov, E. T. Kavalali, VAMP4 directs synaptic vesicles to a pool that selectively maintains asynchronous neurotransmission. *Nat. Neurosci.* **15**, 738–745 (2012).

125. M. Martineau, A. Somasundaram, J. B. Grimm, T. D. Gruber, D. Choquet, J. W. Taraska, L. D. Lavis, D. Perrais, Semisynthetic fluorescent pH sensors for imaging exocytosis and endocytosis. *Nat. Commun.* **8**, 1412 (2017).

126. D. C. Stephens, N. Osunsanmi, K. A. Sochacki, T. W. Powell, J. W. Taraska, D. A. Harris, Spatiotemporal organization and protein dynamics involved in regulated exocytosis of MMP-9 in breast cancer cells. *J. Gen. Physiol.*, jgp.201812299 (2019).

127. E. Daro, P. van der Sluijs, T. Galli, I. Mellman, Rab4 and cellubrevin define different early endosome populations on the pathway of transferrin receptor recycling. *Proc. Natl. Acad. Sci.* **93**, 9559–9564 (1996).

128. F. Filippini, S. Nola, A. Zahraoui, K. Roger, M. Esmaili, J. Sun, J. Wojnacki, A. Vlieghe, P. Bun, S. Blanchon, J.-C. Rain, J.-M. Taymans, M.-C. Chartier-Harlin, C. Guerrera, T. Galli, Secretion of VGF relies on the interplay between LRRK2 and post-Golgi v-SNAREs. *Cell Reports* **42**, 112221 (2023).

129. C. Montecucco, G. Schiavo, Mechanism of action of tetanus and botulinum neurotoxins. *Mol. Microbiol.* **13**, 1–8 (1994).

130. R. T. Dorsam, J. S. Gutkind, G-protein-coupled receptors and cancer. *Nat. Rev. Cancer* **7**, 79–94 (2007).

131. M. Sarter, J. P. Bruno, V. Parikh, Abnormal neurotransmitter release underlying behavioral and cognitive disorders: toward concepts of dynamic and function-specific dysregulation. *Neuropsychopharmacology* **32**, 1452–1461 (2007).

Chapter 2: VAMP2 Is a Cargo-Selective v-SNARE for a Subset of GPCRs[1]

Abstract

Vesicle fusion at the plasma membrane is critical for releasing hormones and neurotransmitters and for delivering the cognate G protein-coupled receptors (GPCRs) to the cell surface. The SNARE fusion machinery that releases neurotransmitters has been well characterized. In contrast, the fusion machinery that delivers GPCRs is still unknown. Here, using high-speed multi-channel imaging to simultaneously visualize receptors and v-SNAREs in real time in individual fusion events, we identify VAMP2 as a selective v-SNARE for GPCR delivery. VAMP2 was preferentially enriched in vesicles that mediate the surface delivery of μ opioid receptor (MOR), but not other cargoes, and was required selectively for MOR recycling. Interestingly, VAMP2 did not show preferential localization on MOR-containing endosomes, suggesting that v-SNAREs are co-packaged with specific cargo into separate vesicles from the same endosomes. Together, our results identify VAMP2 as a cargo-selective v-SNARE and

[1] Besides the contents related to Fig. 2.10, this chapter is published as: H. Chen, Z. Y. Weinberg, G. A. Kumar, M. A. Puthenveedu. Vesicle-associated membrane protein 2 is a cargo-selective v-SNARE for a subset of GPCRs. *J. Cell Biol.* 222(7), e202207070 (2023).
Note: Fig. 2.2 E (as Fig. 2 E in the original publication) is modified from its original appearance, as part of the data are moved to Fig. 2.10 A to avoid duplication.
Statement of contribution: Computational analysis for Fig. 2.2 G and H is mainly contributed by Weinberg, Z. Y.; flow cytometry experiments for Fig. 2.5 I and J are mainly contributed by Kumar, G. A.; part of the immunoblot experiment for Fig. 2.10 C is contributed by Luo, Y.

suggest that surface delivery of specific GPCRs is mediated by distinct fusion events driven by distinct SNARE complexes.

Introduction

Membrane fusion at the plasma membrane is critical for many aspects of neuroendocrine physiology. Vesicle fusion releases neuroendocrine molecules such as hormones and neurotransmitters to the extracellular environment and delivers the receptors that recognize these molecules to the surface of cells (*1*, *2*). A large fraction of neuroendocrine molecules binds receptors of the G protein-coupled receptor (GPCR) family of signaling receptors (*3–5*). Delivery of GPCRs to the cell surface is therefore critical for determining the cellular responses to these signaling molecules (*6*, *7*).

The machinery that mediates the release of neuroendocrine molecules has been well studied. In neuronal cells, vesicles that carry secreted neuroendocrine molecules contain the v-SNARE vesicle-associated membrane protein 2 (VAMP2, also called synaptobrevin 2), which binds a t-SNARE complex on the target membrane (*8–14*). A subsequent conformational change in the SNARE complex provides the force to induce membrane fusion (*15*, *16*).

In contrast to the mechanisms mediating neuroendocrine molecules' release, the mechanisms mediating the delivery of GPCRs to the plasma membrane, including the identities of the SNARE proteins, are not well known. For many GPCRs, the primary mechanism of surface delivery is via the recycling pathway: after activation by their ligands, GPCRs are internalized into endosomes, from where many GPCRs are sorted into the recycling pathway and delivered back to the plasma membrane (*7*, *17*). Different GPCRs, however, can be sorted into different pathways with distinct molecular requirements and regulatory mechanisms (*18–21*). Which SNARE proteins

mediate delivery of GPCRs during recycling in neuroendocrine cells, and whether different GPCRs use different SNARE proteins, are fundamental questions that are still unanswered.

In this study, we addressed these questions by attempting to identify the v-SNARE that mediates GPCR recycling. We developed a high-resolution multi-channel total internal reflection fluorescence (TIRF) microscopy method to directly visualize individual plasma membrane fusion events of vesicles containing receptors and to simultaneously visualize the presence of VAMP2 at these fusion sites. We used two physiologically relevant GPCRs – the μ opioid receptor (MOR) and the β2 adrenergic receptor (B2AR) – as prototypes. We show that VAMP2 is enriched specifically in the vesicles that deliver MOR, but not B2AR or the nutrient receptor transferrin receptor (TfR), to the surface of HEK293 cells. Depletion of endogenous VAMP2 significantly reduced the rates of recycling of MOR in PC12 cells and rat striatal neurons. VAMP2 did not preferentially co-localize with MOR in specific endosomes, suggesting that VAMP2 was specifically packaged into recycling vesicles that preferentially contained MOR and not B2AR at the level of individual endosomes. Lastly, through a low-throughput screening, we did not find a VAMP subtype that was specific to B2AR recycling. Our results identify VAMP2 as the v-SNARE that mediates fusion specifically of recycling vesicles that contain MOR. Further, our results suggest that distinct v-SNAREs are co-packaged into vesicles with specific GPCRs from the same endosome.

Results

VAMP2 is detected preferentially in fusion events that mediate MOR recycling

We first asked whether VAMP2 was present in the cargo-containing vesicles that fuse to the plasma membrane, by designing a high-resolution imaging method to directly and simultaneously visualize VAMP2 and cargoes during individual fusion events at the plasma

membrane. We tagged a pH sensitive GFP mutant, called super ecliptic pHluorin (SpH; *22*), to the extracellular terminus of three different cargo molecules – MOR (SpH-MOR), B2AR (SpH-B2AR), and TfR (TfR-SpH). SpH fluorescence is quenched inside the acidic intracellular compartments (pH=4.5-6.5) but exerts high fluorescence once it is inserted into the plasma membrane and exposed to the neutral extracellular environment (pH=7.4; Fig. 2.1 A; *19*, *20*, *23*–*28*). This change in fluorescence can be visualized under TIRF microscopy where only fluorophores within 100 nm of the plasma membrane are excited (*29*).

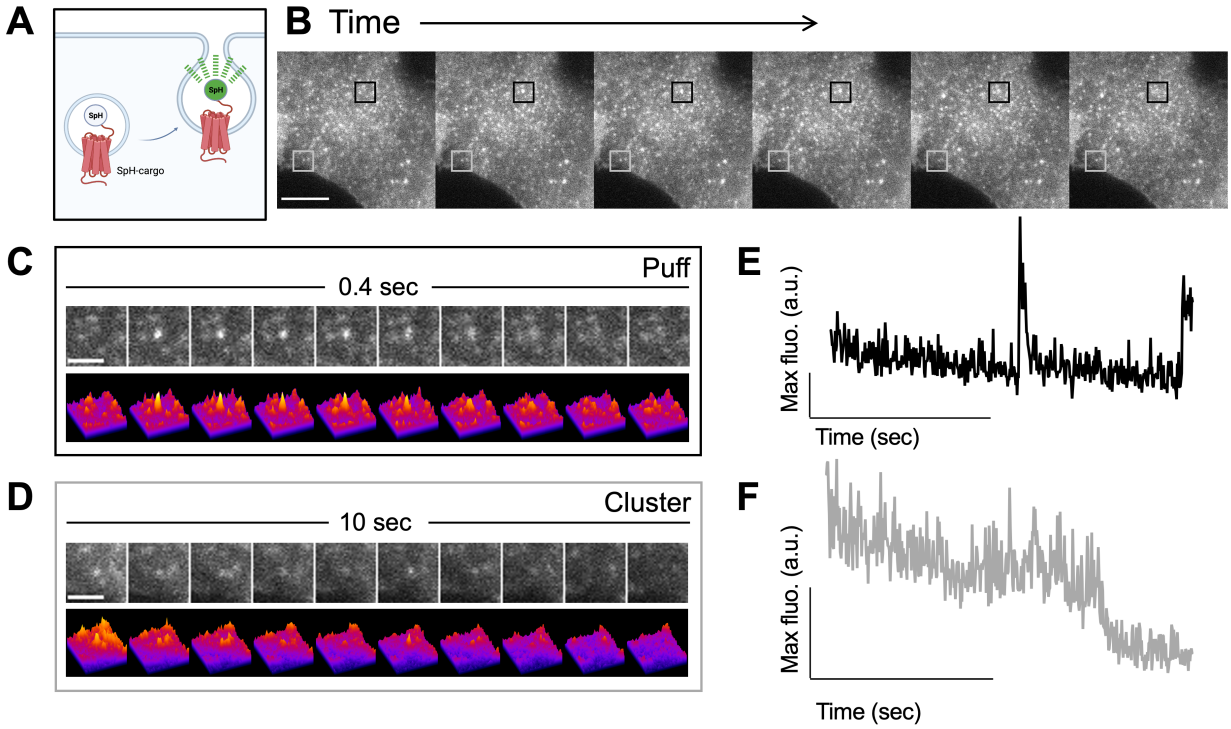

Figure 2.1. Individual vesicle fusion events delivering GPCRs to the cell surface can be resolved by TIRF microscopy.
A. Schematic of change in SpH fluorescence during a fusion event in SpH-cargo expressing cells. The fluorescence intensity of SpH-cargo increases upon exposure to the neutral extracellular environment. B. Montage of a SpH-MOR expressing cell showing a typical fusion event (black square) and an endocytic cluster event (gray square) post 5 min 12.5 µM DAMGO treatment at 37 ºC. Scale bar = 8 µm. **C** and **D.** Enlarged montages (top panels) of a fusion event (**C**) and an endocytic cluster event (**D**) shown in **B.** The fusion event showed an instantaneous increase in fluorescence intensity followed by a rapid (<0.4 sec) diffusion that was visualized as a "puff" of fluorescence. On the other hand, the endocytic cluster event showed sustained fluorescence (~8 sec) followed by an exponential decay. Surface plots of fluorescence are shown in the bottom

panels. Scale bar = 2 μm. **E** and **F.** Traces of changes in maximum fluorescence (Max fluo.) of the fusion event (**E**) and the endocytic cluster event (**F**) shown in **B**. Time 0 represents the onset of image acquisition. Horizontal scale bar = 5 sec and vertical scale bar = 2000 count of fluorescence intensity (arbitrary unit, a.u.).

To induce internalization and subsequent exocytic events for imaging, HEK293 cells stably expressing SpH-MOR or SpH-B2AR were treated with saturated concentration of agonists (12.5 μM), [D-Ala^2, *N*-Me-Phe^4, Gly^5-ol]-enkephalin (DAMGO) and isoproterenol (Iso), respectively. We chose DAMGO and Iso as standards, as these are the primary agonists that have been used to study MOR and B2AR trafficking characteristics, including using assays that resolve recycling at single-event resolution (*19*, *20*, *24–26*, *30–32*). HEK293 cells transiently expressing TfR-SpH were imaged at baseline since they exhibited constitutive exocytosis. When imaged at high speed under TIRF microscopy, individual exocytic fusion events that deliver SpH-cargo to the cell surface were observed as bursts or "puffs" of fluorescence. These events show an instantaneous increase in fluorescence intensity (Fig. 2.1 B, C and E), followed by a characteristic diffusion of fluorescence to the surrounding area (Fig. 2.1 B and C). These events (which we term "puffs" in this manuscript) were distinct from endocytic clusters based on their different time scales (milliseconds for puffs, and seconds to minutes for clusters), and on the characteristic diffusion of fluorescence that was not seen in endocytic clusters (Fig. 2.1 B, D and F). We and others have extensively characterized these puffs previously as individual vesicle fusion events mediating recycling of receptors from endosomes, by showing that GPCR puffs are rarely observed without prior agonist-mediated internalization of the receptors, that mutation of receptor sequences that are required for B2AR and MOR recycling abolishes the puffs, that pharmacological treatments that increase or decrease recycling causes a corresponding change in puffs, and that cycloheximide treatment does not significantly reduce the number of puffs (*19*, *20*, *24–27*, *33*).

To test whether the receptor cargoes and VAMP2 were present in the same vesicle fusion events, we co-expressed VAMP2 tagged with a pH-sensitive RFP pHuji to the extracellular terminus (VAMP2-pHuji; *34*, and SpH-tagged receptors in HEK293 cells (Fig. 2.2 A). We visualized vesicle fusion events using simultaneous rapid acquisition in two channels by TIRF microscopy to detect both SpH and pHuji. In a subset of fusion events, detected as puffs of SpH-cargo fluorescence, VAMP2-pHuji fluorescence showed similar characteristics as their corresponding SpH-cargo, i.e., a rapid increase in fluorescence and subsequent diffusion (Fig. 2.2 B and C). In another subset of fusion events detected as SpH-cargo puffs, VAMP2-pHuji fluorescence did not increase above baseline fluctuation (Fig. 2.2 D). To quantify the fraction of puffs with detectable changes of VAMP2-pHuji fluorescence, we developed a method to globally quantify VAMP2 enrichment in puffs based on the fold change of pHuji fluorescence over baseline standard deviation calculated as:

$$\text{VAMP2 enrichment} = \left(F'_p - F'_0\right) / SD_{baseline}$$

where, F'_p and F'_0 are the bleedthrough-corrected fluorescence in the VAMP2-pHuji channel at the peak of a puff and at the baseline, respectively, and $SD_{baseline}$ is the standard deviation of the baseline fluorescence fluctuation. As an initial parameter, we used 1x$SD_{baseline}$ as the cutoff to classify whether a puff had detectable VAMP2-pHuji. Puffs were classified as VAMP2-positive (VAMP2+) if the peak VAMP2-pHuji fluorescence difference was higher than 1x$SD_{baseline}$. Using this criterion, about 83% of SpH-MOR puffs were VAMP2+. SpH-MOR puffs showed a median VAMP2 enrichment of 5x$SD_{baseline}$ (Fig. 2.2 E). In contrast, TfR-SpH and SpH-B2AR showed no preference of VAMP2+ puffs, with median VAMP2 enrichments being within 1x$SD_{baseline}$ ($p<0.0001$; Fig. 2.2 E), indicating that VAMP2 was preferentially present in fusion vesicles containing SpH-MOR, but not the other two SpH-cargoes. Importantly, this conclusion

was valid regardless of the cutoffs (fold change over standard deviation) we used to define VAMP2+ puffs. When cutoffs of 1x$SD_{baseline}$ to 4x$SD_{baseline}$ were used to define VAMP2+ puffs with increasing confidence (~68% to >99%), VAMP2 was always enriched in puffs containing MOR compared to the other cargoes (Fig. 2.2 F).

As a control to test the specificity of VAMP2's presence in SpH-MOR puffs, we examined VAMP4, a related VAMP subtype that had been previously shown to mediate recycling of receptor cargoes (*35*). When VAMP4-pHuji was co-expressed and imaged with SpH-MOR using identical conditions, VAMP4 showed no preferential enrichment in SpH-MOR puffs, with a median enrichment smaller than 1x$SD_{baseline}$ (see below at Fig. 2.10 A). These results indicate that VAMP2, but not VAMP4, is specifically enriched in vesicles that recycle MOR.

Because the population of puffs showed a wide distribution of VAMP2 enrichment (Fig. 2.2 E), we next tested whether this population represented a single population or a mixture of multiple populations. We performed Gaussian mixture model fitting simulation with AIC/BIC loss metrics validation to identify the number of classes that best fit the distribution. The best fit model suggested that there were three classes of puffs based on VAMP2 enrichment – a "no VAMP2" class with mean = -0.24, a "VAMP2+" class with mean = 5.54, and a "high VAMP2" class with mean = 22.32 (Fig. 2.2 G). Importantly, when the fraction of puffs in each class was estimated for each SpH-cargo, SpH-MOR showed a noticeably larger fraction of VAMP2+ puffs (classes of "VAMP2+" and "high VAMP2") compared to SpH-B2AR, while TfR-SpH showed a distribution that was in between SpH-MOR and SpH-B2AR (Fig. 2.2 H).

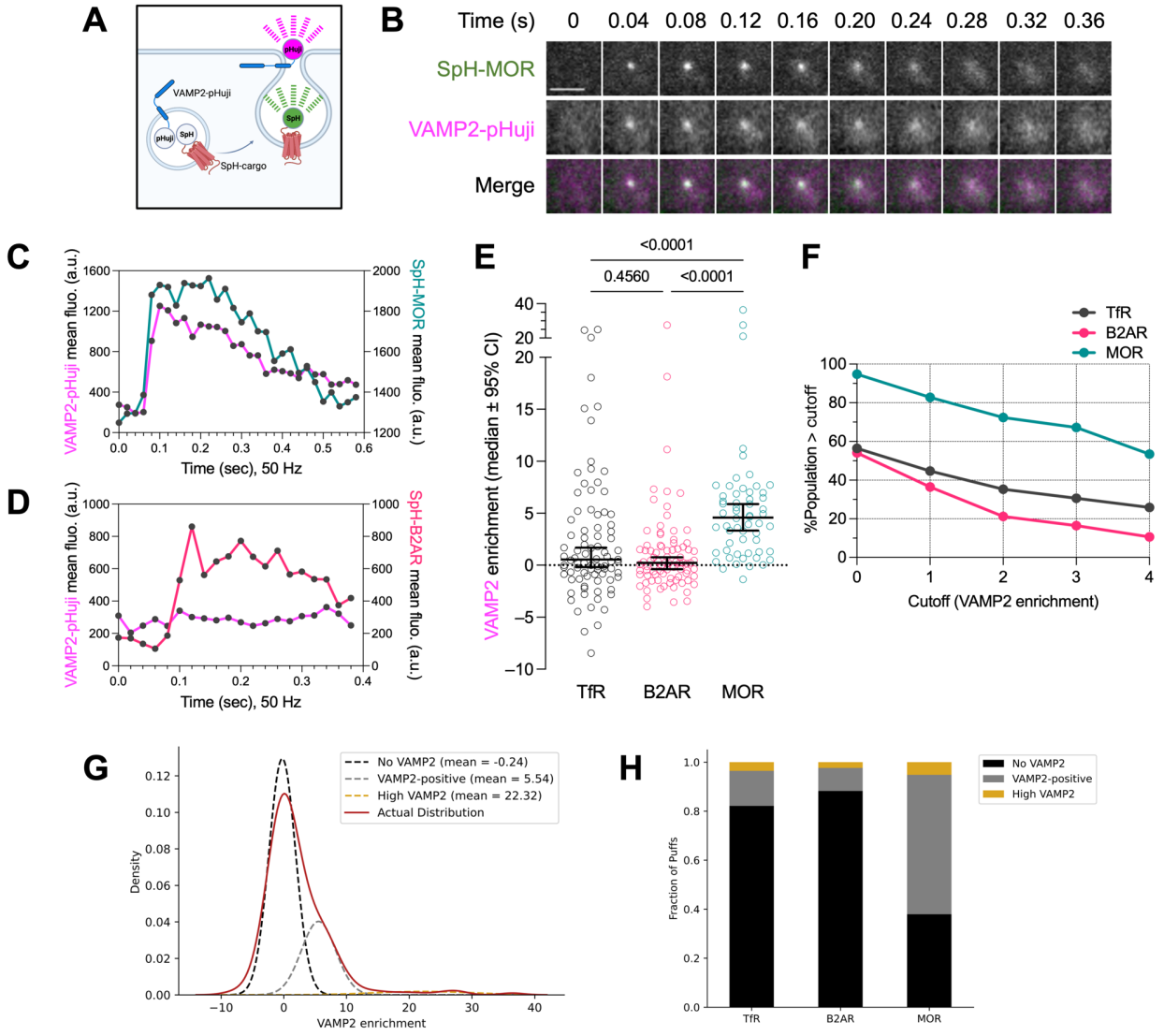

Figure 2.2. VAMP2 is detected preferentially in fusion events (puffs) delivering MOR to the surface.

A. Schematic of a VAMP2 positive (VAMP2+) puff in SpH-cargo and VAMP2-pHuji co-expressing cells. When a vesicle carrying both SpH-cargo and VAMP2-pHuji fuses to the plasma membrane, the fluorescence intensity increases in both the SpH channel and the pHuji channel. **B.** Montage of a SpH-MOR puff co-localizing with VAMP2-pHuji (SpH-MOR in green and VAMP2-pHuji in magenta) from a SpH-MOR and VAMP2-pHuji co-expressing cell 5 min after DAMGO treatment at 37 ºC. Scale bar = 2 µm. **C.** Representative time-course traces of mean SpH-MOR (cyan) and the corresponding mean VAMP2-pHuji fluorescence (magenta) from a VAMP2+ puff of the SpH-MOR expressing cells. **D.** Representative time-course traces of mean SpH-B2AR (red) and the corresponding mean VAMP2-pHuji fluorescence (magenta) from a VAMP2- puff of the SpH-B2AR expressing cells. **E.** Quantification of VAMP2 enrichment in the population of puffs for each SpH-cargo. VAMP2 enrichment of individual puff event was calculated as the fold change of VAMP2-pHuji fluorescence at the peak of the event over baseline standard deviation, as described in the text (median ± 95% CI; TfR-SpH: 2 cells, puff=85; SpH-B2AR: 3 cells,

puff=85; SpH-MOR: 3 cells, puff=59; all conditions from 2 independent experiments). SpH-MOR puffs showed significantly more enrichment of VAMP2 compared to other cargoes (One-way ANOVA, post-hoc Kruskal-Wallis test: TfR vs. B2AR: $p=0.4560$; TfR vs. MOR: $p<0.0001$; B2AR vs. MOR: $p<0.0001$). **F.** The fraction of VAMP2+ puffs (%population) as defined by different folds of VAMP2 enrichment over baseline standard deviation (cutoff) show a consistent enrichment of VAMP2 preferentially in MOR puffs across all cutoffs. **G.** Kernel density estimation of the pooled population of all puffs to estimate subclasses. The best fit predicted three subclasses based on VAMP2 enrichment. Three Gaussian mixture model of the actual distribution (solid line) and predicted subclasses (dashed lines) are shown. **H.** Fraction of puffs in each predicted subclass shows distinct population composition of different SpH-cargoes and a preferential enrichment of VAMP2+ subclasses in SpH-MOR puffs.

As mentioned above, overwhelming evidence points to puffs as being derived from the recycling pathway, especially for GPCRs. Consistent with this idea, we observed very few to no SpH-MOR or SpH-B2AR puffs in the absence of agonist-mediated internalization. However, because VAMP2+ TfR puffs were present at steady state, we tested whether this fraction of VAMP2+ puffs were predominantly derived from biosynthetic delivery. To do so, we blocked biosynthesis by 2 hr 10 μm cycloheximide (CHX) pre-treatment to cells prior to imaging, to clear biosynthetic TfR-SpH stores that might be delivered to the cell surface, and asked whether the fraction of VAMP2+ TfR-SpH puffs changed under this condition. The fraction of VAMP2+ TfR-SpH puffs of CHX-treated cells was almost identical to the fraction of VAMP2+ TfR-SpH puffs of the non-treated cells (Fig. 2.3 A and B), indicating that VAMP2+ puffs were not predominantly derived from the biosynthetic pathway. CHX blocked biosynthesis of proteins under these conditions, as it caused about 40% reduction in total levels of GRK3, a protein that turns over fast (Fig. 2.3 C and D; *36*, *37*). Consistent with the lack of a role for VAMP2 in the biosynthetic pathway, VAMP2 did not colocalize with canonical Golgi markers, including trans-Golgi network marker TGN38 and cis-Golgi marker GM130 (Fig. 2.3 E and F). These data indicated that VAMP2 is not enriched on the Golgi, unlike in endosomes (see Fig. 2.8 below). Taken together, our data show that, among the cargo group of MOR, B2AR and TfR, VAMP2 is enriched preferentially in vesicles that mediate surface delivery of MOR from the recycling pathway.

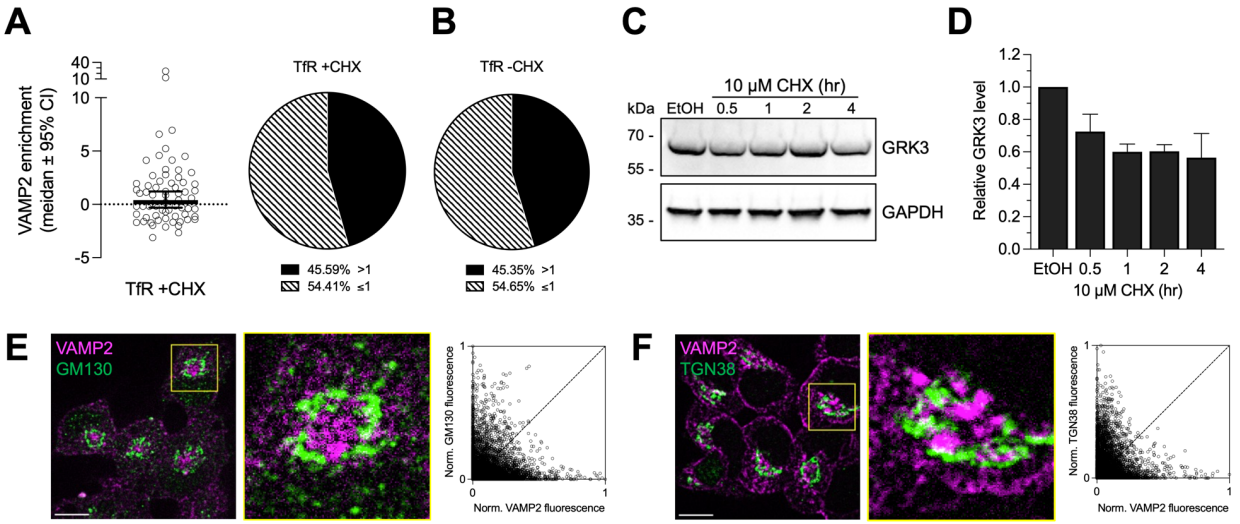

Figure 2.3. VAMP2 is not involved in delivery of receptors from the biosynthetic pathway. **A.** VAMP2 enrichment (left) in TfR puffs in cells co-expressing TfR-SpH and VAMP2-pHuji co-expressing cells pre-treated with 10 µM cycloheximide (CHX) for 2 hr before imaging (+CHX, median ± 95% CI, puff=67, 2 cells from 1 experiment). Proportion of puffs > or ≤ cutoff =1(x$SD_{baseline}$) is shown in the pie chart (right). **B.** Proportion of puffs from TfR-SpH and VAMP2-pHuji co-expressing cells non-treated with CHX (-CHX). Proportion > cutoff =1(x$SD_{baseline}$) is almost identical for cells treated or non-treated with CHX. **C.** Representative Western-blot probing a fast turnover protein GRK3 with GAPDH as internal control in whole cell lysates prepared from cells either treated with vehicle (EtOH) for 2 hr or 10 µM CHX for indicated time. **D.** Quantification of relative GRK3 levels by first normalizing to GAPDH levels then to vehicle control (±SD, n=3 independent experiments). **E and F.** Representative confocal slices of PC12 cells immunostained for endogenous VAMP2 and cis-Golgi marker GM130 (**E**) or tran-Golgi network marker TGN38 (**F**). Scale bar = 10 µm. Denoted sections (yellow squares and enlarged) were analyzed by pixel-by-pixel fluorescence correlation between the VAMP2 channel and the Golgi marker channels. Pixel fluorescence intensity was normalized to the maximum fluorescence and plotted in scatter plots on the right. The dashed diagonal line indicates perfect co-localization, and VAMP2 shows very little to no co-localization with GM130 or TGN38.

VAMP2 is specifically required for MOR recycling in PC12 cells and in primary neurons

To test whether VAMP2 was required for MOR recycling, we depleted VAMP2 and measured MOR recycling at the level of single recycling events and total surface levels. We used a doxycycline-inducible shRNA-tagBFP system to deplete VAMP2 first in PC12 cells, a rat neuroendocrine cell line that endogenously expressed high level of VAMP2 (Fig. 2.4 A and B). We chose PC12 cells because they are good models for studying opioid receptor trafficking, as the

mechanistic insights have held up previously in neurons and in animal models (*27*, *38–40*), and because rat VAMP2 shows close similarity to human VAMP2 isoform1 which is coded by the VAMP2-pHuji construct (Fig. 2.4 C).

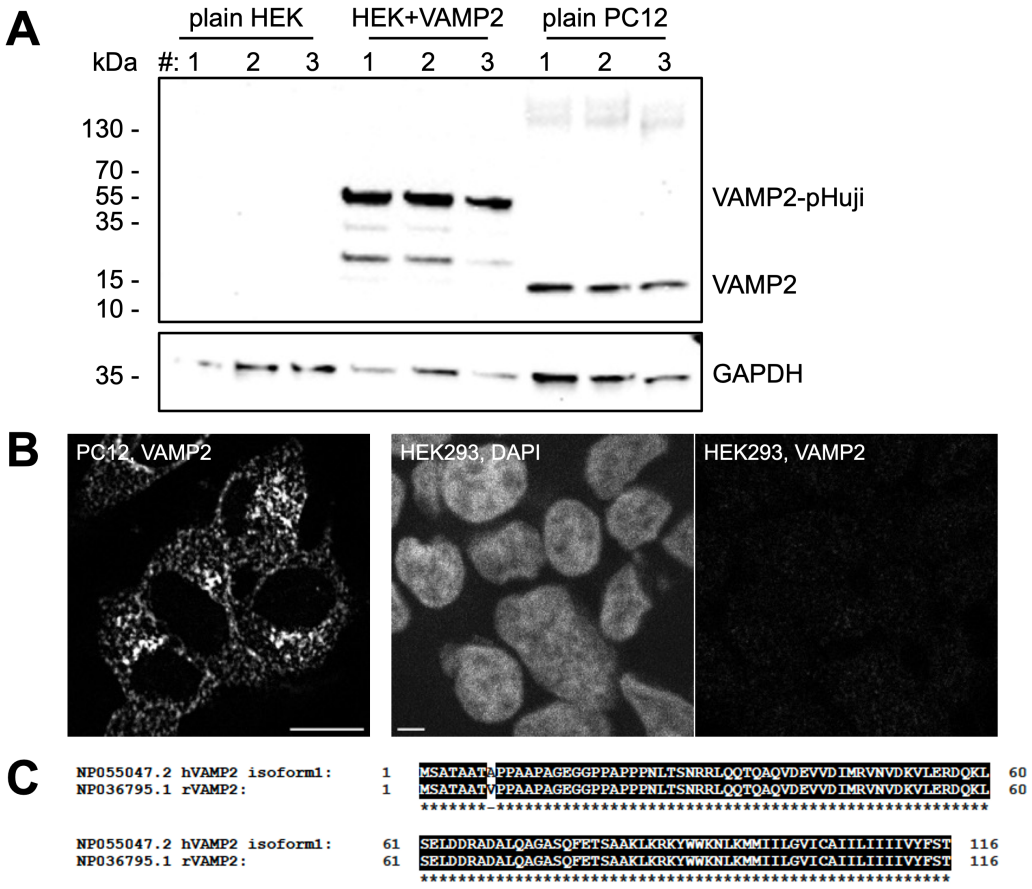

Figure 2.4. PC12 cells express detectable endogenous VAMP2, but (our) HEK293 cells do not. **A.** Immunoblot of VAMP2 from the whole cell lysates of un-transfected HEK293 cells (plain HEK), HEK293 cells transfected with VAMP2-pHuji (HEK+VAMP2), and un-transfected PC12 cells (plain PC12). Whole cell lysates were each prepared from one well of confluent 6-well plate. Three replicates of lysates preparation are shown. **B.** Representative confocal images showing that there is no VAMP2 immunostaining in plain HEK293 cells. The images in the VAMP2 channels of PC12 and HEK293 were acquired under similar conditions and were adjusted to the same levels. DAPI staining shows the nuclei to confirm that there are many cells in the field. Scale bar = 10 µm. **C.** Protein sequence alignment between human VAMP2 isoform1 (hVAMP2 isoform1) and rat VAMP2 (rVAMP2) shows close similarity.

Expression of shRNA against rat VAMP2 (shVAMP2) decreased VAMP2 protein level by ~66% compared to non-targeting shRNA construct generated using the same backbone

(shScramble), as observed by single-cell confocal imaging of VAMP2 immunostaining following 48 hr 200 ng/mL doxycycline (Dox) treatment ($p<0.0001$; Fig. 2.5 A-C). We then measured the rate of recycling of SpH-cargoes by quantifying the number of puffs per cell per minute, in cells expressing shVAMP2 or shScramble, or in Dox-treated control cells not expressing the shRNA constructs. We confirmed shRNA expression by tagBFP fluorescence in each cell using confocal microscopy before imaging puffs in TIRF microscopy. When the number of puffs per cell per min was counted across SpH-cargoes, shVAMP2 expression significantly decreased the number of SpH-MOR puffs ($p=0.0033$ compared to Dox alone and $p=0.0001$ compared to shScramble), but did not significantly decrease the number of TfR-SpH or SpH-B2AR fusion events (Fig. 2.5 D-F). Consistent with our results that VAMP4-pHuji was not enriched in SpH-MOR puffs (Fig. 2.5 E), depletion of VAMP4 using the same shRNA system (see Fig. 2.6 for knockdown verification) did not significantly decrease the number of SpH-MOR puffs per cell per min ($p=0.8898$ compared to shScramble; Fig. 2.5 G), indicating that VAMP2 but not VAMP4 was required for MOR recycling.

To test whether this decrease in the rate of individual fusion events decreased surface recycling of MOR at a whole-cell level, we measured MOR recycling using flow cytometry in PC12 cells co-expressing FLAG-tagged MOR (FLAG-MOR) and shVAMP2. We adapted an assay (Fig. 2.5 H) that we have used before to measure the amount of internalization and recycling of FLAG-MOR (*32*). Briefly, we compared three conditions: (i). non-treated cells (NT) representing baseline, (ii). agonist-treated cells (T, 20 min 10 μM DAMGO at 37 ºC) representing internalization, and (iii). cells in which agonist was washed out (WO, 20 min 10 μM DAMGO followed by 20 min 10 μM MOR antagonist Naltrexone at 37 ºC) representing recycling. After the treatments, cells were immediately transferred onto ice to terminate any residual trafficking activities and then labeled live with fluorescent anti-FLAG antibody (M1-Alexa-647) to label

surface MOR. Surface MOR levels were then measured using flow cytometry. Expression of shVAMP2 did not change MOR internalization, as FLAG-MOR cells co-expressing shVAMP2 showed similar decrease in surface fluorescence before and after 48 hr pre-treatment of 200 ng/mL Dox (Fig. 2.5 I and J). In contrast, expression of shVAMP2 significantly reduced MOR recycling, as FLAG-MOR cells co-expressing shVAMP2 showed a lower recovery of surface fluorescence after Dox treatment compared to before (p=0.0224; Fig. 2.5 I and J).

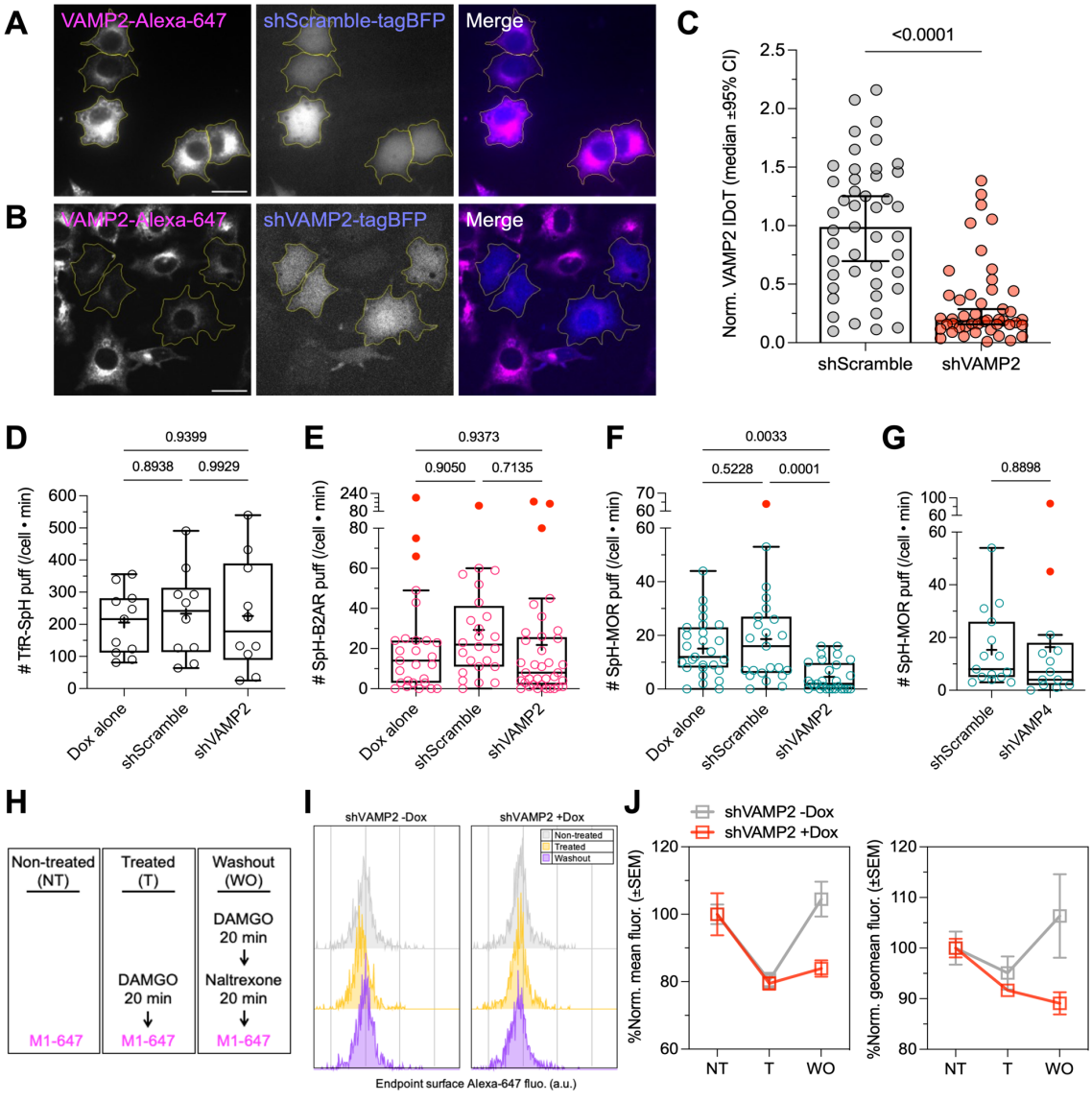

Figure 2.5. VAMP2 depletion inhibits the recycling of SpH-MOR but not that of SpH-B2AR and TfR-SpH.

A. Representative confocal image of PC12 cells expressing scrambled shRNA (shScramble-tagBFP, blue) immunostained for endogenous VAMP2 (magenta) after 48 hr of doxycycline (Dox) treatment. **B.** Representative confocal image of PC12 cells expressing VAMP2 shRNA (shVAMP2-tagBFP, blue) immunostained for endogenous VAMP2 (magenta) after 48 hr of Dox treatment, showing depletion of VAMP2. Scale bar = 20 μm. **C.** Scatter plots of normalized integrated density over threshold (IDoT) of VAMP2 immunostaining in shScramble-tagBFP (shScramble) or shVAMP2-tagBFP (shVAMP2) expressing cells (median ± 95% CI, n=45 or 46 cells, respectively, from 2 independent experiments), showing depletion of VAMP2 in the latter ($p<0.0001$, unpaired two-tailed t-test). **D.** The number of TfR-SpH puffs per cell per minute (/cell • min) in cells expressing either TfR-SpH alone (Dox alone), or in cells co-expressing shScramble or shVAMP2, treated with 48 hr of Dox, show no significant difference (Dox alone: n=11; shScramble: n=10; shVAMP2: n=10, from 2 independent experiments; One-way ANOVA, post-hoc Tukey test). **E.** A similar comparison shows no difference in the numbers of SpH-B2AR puffs across the three conditions (Dox alone: n=27; shScr+Dox: n=24; shVam+Dox: n=36, from 3 independent experiments, One-way ANOVA, post-hoc Tukey test). **F.** A similar comparison shows significant reduction in the number of SpH-MOR puffs in cells co-expressing shVAMP2 compared to the other two conditions (Dox alone: n=27; shScramble: n=23; shVAMP2: n=28, from 3 independent experiments, One-way ANOVA, post-hoc Tukey test). **G.** A similar comparison but in cells co-expressing SpH-MOR and shScramble or VAMP4 shRNA (shVAMP4), shows no difference in the numbers of SpH-MOR puffs (shScramble, n=15; shVAMP2, n=13, from 1 experiment, unpaired two-tailed t-test). Cells from **E-G** were treated with agonists 5 min at 37 ^{o}C before imaging. Filled dots in red from **E-G** represented outliers identified by the Tukey plot that were included in the statistical analysis. "+" in the Tukey plots from **D-G** represented mean. **H.** Schematic of the treatment and labeling conditions for the flow cytometry assay. Cells were labeled with M1-Alexa-647 (M1-647) antibody at the endpoint of treatment conditions to measure surface MOR levels: at baseline (Non-treated, NT), after DAMGO for 20 min at 37 ^{o}C (Treated, T), or after washing out DAMGO and incubating in Naltrexone for 20 min at 37 ^{o}C (Washout, WO). **I.** Representative histograms of PC12 cells co-expressing FLAG-MOR and shVAMP2, either without (shVAMP2 −Dox) or with (shVAMP2 +Dox) pre-treatment of Dox for 48 hr. **J.** Quantification of mean (left panel) and geometric mean (geomean, right panel) of surface MOR levels normalized to unlabeled baseline (±SEM, 3 samples each condition from 1 experiment).

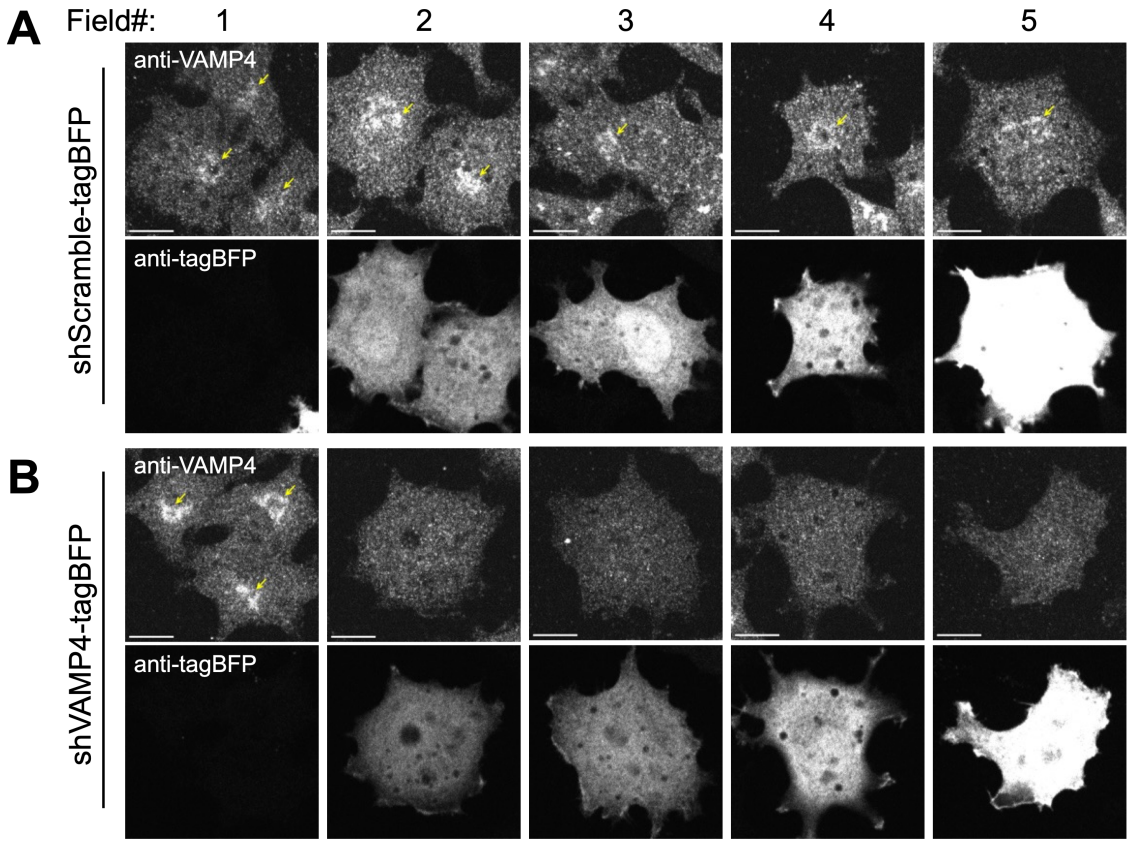

Figure 2.6. shVAMP4 knocks down VAMP4 expression in PC12 cells across varied tagBFP expression levels.
A. Representative confocal slices of PC12 cells expressing shScramble-tagBFP immunostained for endogenous VAMP4 (anti-VAMP4) and tag-BFP (anti-tagBFP) post 48 hr Dox treatment. Cells with different levels of tagBFP staining all show an intracellular pool of VAMP4 (yellow arrows). **B.** Representative confocal slices of PC12 cells expressing shVAMP4-tagBFP under similar experimental conditions as **A**. Compared to the cells with no anti-tagBFP staining (far-left panel), cells with varied levels of tagBFP staining all lose the VAMP4 pool. Corresponding channels of all images are contrasted to the same. Scale bar = 20 μm.

To directly measure the internalization and recycling of surface MOR without the potential confounding effects of newly synthesized receptors, we adapted a quantitative ratiometric fluorescence assay that followed the internalization and recycling of a pre-labeled pool of surface MOR (Fig. 2.7 A). Briefly, FLAG-MOR expressing cells were pre-labeled with M1-Alexa-647 to label the surface pool of MOR. Cells were exposed to the same treatment conditions as described in the flow cytometry assay and then labeled live with an Alexa Fluor 488-conjugated secondary antibody (Alexa-488 secondary), to label the M1-Alexa-647 selectively on the surface. The M1-

Alexa-647 primary labeling served as a control for total surface expression of FLAG-MOR at baseline, and the Alexa-488 secondary labeling indicated the post-treatment surface level of FLAG-MOR from the same pool of the primary labeling that either remained on the surface or being recycled (Fig. 2.7 B). The ratios of fluorescence intensity of Alexa-488 secondary labeling over M1-Alexa-647 primary labeling (488 / 647) in cells were calculated to measure the amount of pre-labeled surface receptors that were internalized at baseline (NT), after endocytosis (T), and after recycling (WO). This gave us a quantitative estimate of the amount of pre-existing surface receptors that were internalized in response to agonist, and the fraction of internalized receptors that recycled after washout, without the potential confounding effects of new receptor biosynthesis.

To optimize expression of the shRNA constructs and receptors, we generated lentiviruses for expression. PC12 cells infected with lentiviral particles of FLAG-MOR (Lenti-FLAG-MOR) and shVAMP2 (Lenti-shVAMP2) were either treated with 200 ng/mL 48 hr Dox (+Dox) or left untreated (−Dox). When the internalization and recycling of MOR was quantitatively measured, although baseline expression (NT) and the degree of internalization (T) of FLAG-MOR were similar for +Dox and −Dox cells, FLAG-MOR recycling was significantly lower in +Dox cells, as seen by lower 488 / 647 values compared to −Dox cells in the WO condition ($p=0.0073$; Fig. 2.7 C). These results further strengthen our conclusion that VAMP2 is required for MOR recycling.

To validate the requirement of VAMP2 in MOR recycling in a physiologically relevant system, we used an identical recycling assay in primary striatal neurons expressing MOR. Primary E18 rat striatal neurons infected with Lenti-FLAG-MOR and Lenti-shVAMP2. Lenti-shVAMP2 showed ~57% knockdown in neuronal cell bodies compared to Lenti-shScramble control (Fig. 2.7 D, E and F). When an identical paradigm as above was used to measure MOR recycling, +Dox

neurons showed significantly lower FLAG-MOR recycling compared to −Dox neurons, although both baseline expression and the degree of internalization of FLAG-MOR were similar ($p<0.0001$; Fig. 2.7 G and H). Together, our data strongly indicate that VAMP2 is required for MOR recycling in multiple cell models including physiologically relevant neurons.

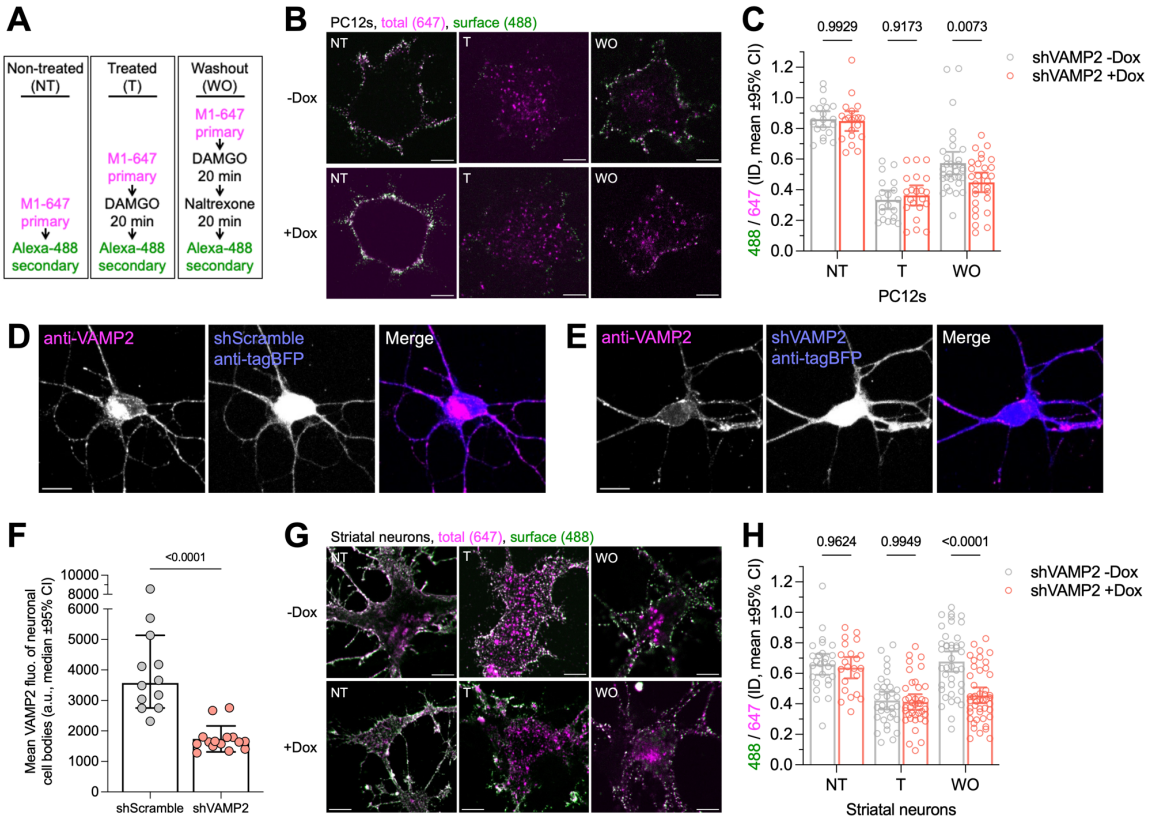

Figure 2.7. VAMP2 depletion in PC12 cells and striatal neurons decreased MOR recycling. **A.** Schematic of the treatment and labeling conditions for the ratiometric recycling assay, as described in the text. **B.** Representative confocal images of PC12 cells co-expressing FLAG-MOR and shVAMP2 either treated with (top panel, +Dox) or without (bottom panel, −Dox) 200 ng/mL Dox for 48 hr prior to the ratiometric recycling assay. Scale bar = 15 µm. **C.** Quantification of ratios between 488 nm fluorescence and 647 nm fluorescence (488 / 647) calculated using integrated density (ID) for PC12 cells of indicated conditions (NT, T, WO: −Dox: n=20, 20, 33 cells; +Dox: n=20, 21, 29 cells, from 2 independent coverslips). +Dox cells showed significantly lower MOR recycling compared to −Dox cells (Two-way ANOVA, post-hoc Šidák test, +Dox vs −Dox: NT: p=0.9929; T: p=0.9173; WO: p=0.0073). **D and E.** Representative confocal images of E18 rat striatal neurons expressing shScramble (**D**) or shVAMP2 (**E**) after 48 hr of Dox treatment, fixed and immunostained for endogenous VAMP2 (anti-VAMP2, magenta) and tagBFP (anti-tagBFP, blue). Scale bar = 20 µm. **F.** Scatter plots of mean fluorescence intensity of VAMP2 immunostaining in the cell bodies of shScramble or shVAMP2 expressing neurons (median ± 95% CI, n=12 or 15 cells, respectively, from 1 experiment), showing depletion of VAMP2 in the latter

($p<0.0001$, unpaired two-tailed t-test). **G.** Representative confocal images of rat striatal neurons co-expressing FLAG-MOR and shVAMP2 either treated with (top panel, +Dox) or without (bottom panel, −Dox) 48 hr Dox prior to the ratiometric recycling assay. Scale bar = 15 μm. **H.** Similar quantification of ratios as in **C** for rat striatal neurons of indicated conditions (NT, T, WO: −Dox: n=27, 33, 41 neurons; +Dox: n=22, 39, 46 neurons, from 2 independent neuronal cultures). +Dox neurons showed significantly lower MOR recycling compared to −Dox neurons (Two-way ANOVA, post-hoc Šídák test, +Dox vs −Dox: NT: $p=0.9624$; T: $p=0.9949$; WO: $p<0.0001$).

VAMP2 is not selectively enriched in MOR-containing endosomes

We next addressed whether the differential VAMP2 requirement reflected the segregation of MOR from other cargoes into specific endosomes that were competent to generate VAMP2+ vesicles. To test this question, we first addressed whether VAMP2 was preferentially localized in a subset of endosomes. For objective quantification, we developed and implemented an automated object-based method to analyze co-localization in immunofluorescence microscopy images. To standardize the co-localization method, we performed a positive control experiment in cells expressing MOR doubly tagged with FLAG and SpH (FLAG-SpH-MOR). FLAG-SpH-MOR expressing cells were treated with 12.5 μM DAMGO for 20 min to induce receptor internalization to endosomes, and then fixed and stained with M1-Alexa-647. This allowed us to compare FLAG staining with SpH fluorescence, and gave us an experimental measurement of co-localization from a system that should theoretically be fully co-localized. Confocal imaging revealed almost perfect co-localization between FLAG staining and SpH fluorescence (Fig. 2.8 A). Using the automated object-based analysis, we obtained average co-localizations of 77.49% when normalized to total FLAG spots, and 55.77% when normalized to total SpH spots (Fig. 2.8 E). This allowed us to calibrate our co-localization to account for limitations in antibody labeling and the algorithm used for analysis, and confirmed that automated analysis provided good dynamic range to analyze co-localization.

We next used immunofluorescence microscopy to study the co-localization between endogenous VAMP2 and early (EEA1), recycling (Rab11), and late (Rab7) endosomal markers (*41*) in PC12 cells. Objective automated analysis of the confocal images showed detectable co-localization between VAMP2 and all three endosomal markers (Fig. 2.8 B-D), although to varying degrees. VAMP2 co-localized with Rab11 and EEA1 to comparable amounts (36.34% and 35.25%, respectively) and less with Rab7 (21.03%; Fig. 2.8 F-H). This distribution is consistent with a role for VAMP2 primarily in recycling.

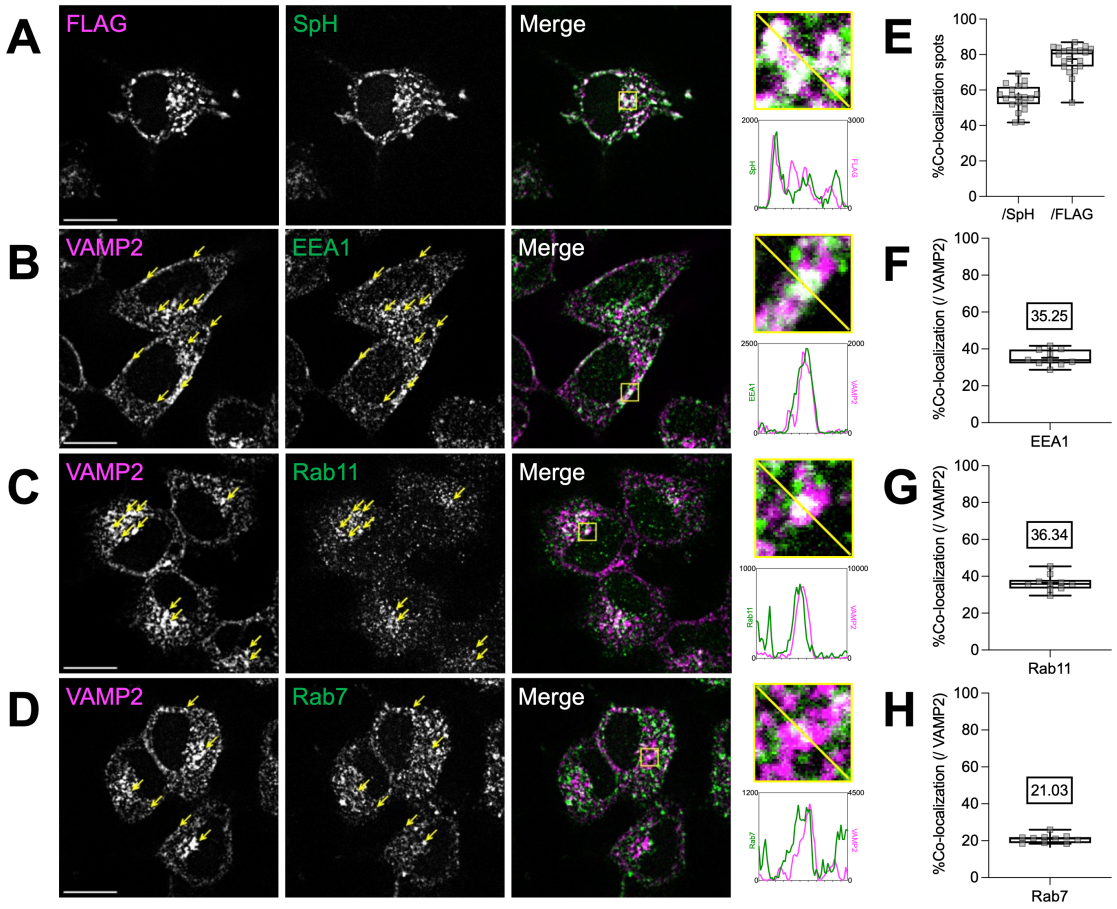

Figure 2.8. Endogenous VAMP2 localizes predominantly to EEA1 or Rab11 compartments. **A.** Representative confocal slice of a FLAG-SpH-MOR expressing cell showing co-localization of FLAG (magenta) and SpH (green) after 20 min 12.5 µM DAMGO treatment. Scale bar = 10 µm. And a line plot across a denoted section (yellow square and enlarged) of the representative slice. **B-D.** Representative confocal slices of PC12 cells immunostained for VAMP2 (magenta) and EEA1 (**B**), Rab11 (**C**) or Rab7 (**D**) (all in green). Example spots showing co-localization are marked with yellow arrows. Scale bar = 10 µm. Corresponding line plots across the denoted

sections (yellow squares and enlarged) of the representative slices are shown for each image. **E.** Percentage co-localization (%co-localization) calculated using an automated object-based method, shown as co-localized spots normalized to either total SpH spots (/SpH) or total FLAG spots (/FLAG) from multiple image stacks (±SD, n=20 from 2 independent coverslips). **F-H.** %Co-localization calculated as above for EEA1 (**F**), Rab11 (**G**) or Rab7 (**H**) are shown as co-localized spots normalized to total VAMP2 spots (/ VAMP2) from multiple image stacks (±SD, n=10 from 2 independent coverslips for each marker). "+" in the Tukey plots from **E-H** represented mean.

To test whether VAMP2 was enriched specifically in a subset of MOR-containing endosomes, we performed three-channel co-localization of VAMP2, SpH-cargoes, and endosomal markers. SpH-MOR and SpH-B2AR expressing PC12 cells were treated with agonist at identical conditions as used to image SpH-cargo fusion events as above. Confocal images showed partial co-localization of SpH-cargoes, VAMP2 and endosomal markers across all conditions (Fig. 2.9 A and B). To quantify co-localization, we first measured the co-localization between SpH-cargoes and endosomal markers (Fig. 2.9 C, outer columns and Fig. 2.9 D, circular pie charts). SpH-B2AR showed highest co-localization with EEA1 (22.73%), moderate level with Rab11 (17.44%), and least with Rab7 (11.68%). SpH-MOR showed higher levels of co-localization with EEA1 (24.15%) and Rab7 (22.50%), and lower co-localization with Rab11 (17.01%). Next, we measured what fraction of the cargo in each endosomal compartment also co-localized with VAMP2 (Fig. 2.9 C, inner columns and Fig. 2.9 D, stacked columns). As expected, we found the highest co-localization between VAMP2 and Rab11, and lowest with Rab7, consistent with our two-channel co-localization study (Fig. 2.8). Surprisingly, however, VAMP2 did not preferentially localize to Rab11 endosomes that co-localized with SpH-MOR, compared to the ones that co-localized with SpH-B2AR (VAMP2+Rab11+SpH-MOR: 6.32% of total SpH-MOR; VAMP2+Rab11+SpH-B2AR: 6.27% of total SpH-B2AR). Together, our data suggest that VAMP2 is co-packaged into recycling vesicles only with MOR, and not with B2AR, even though they might localize to the same endosomes.

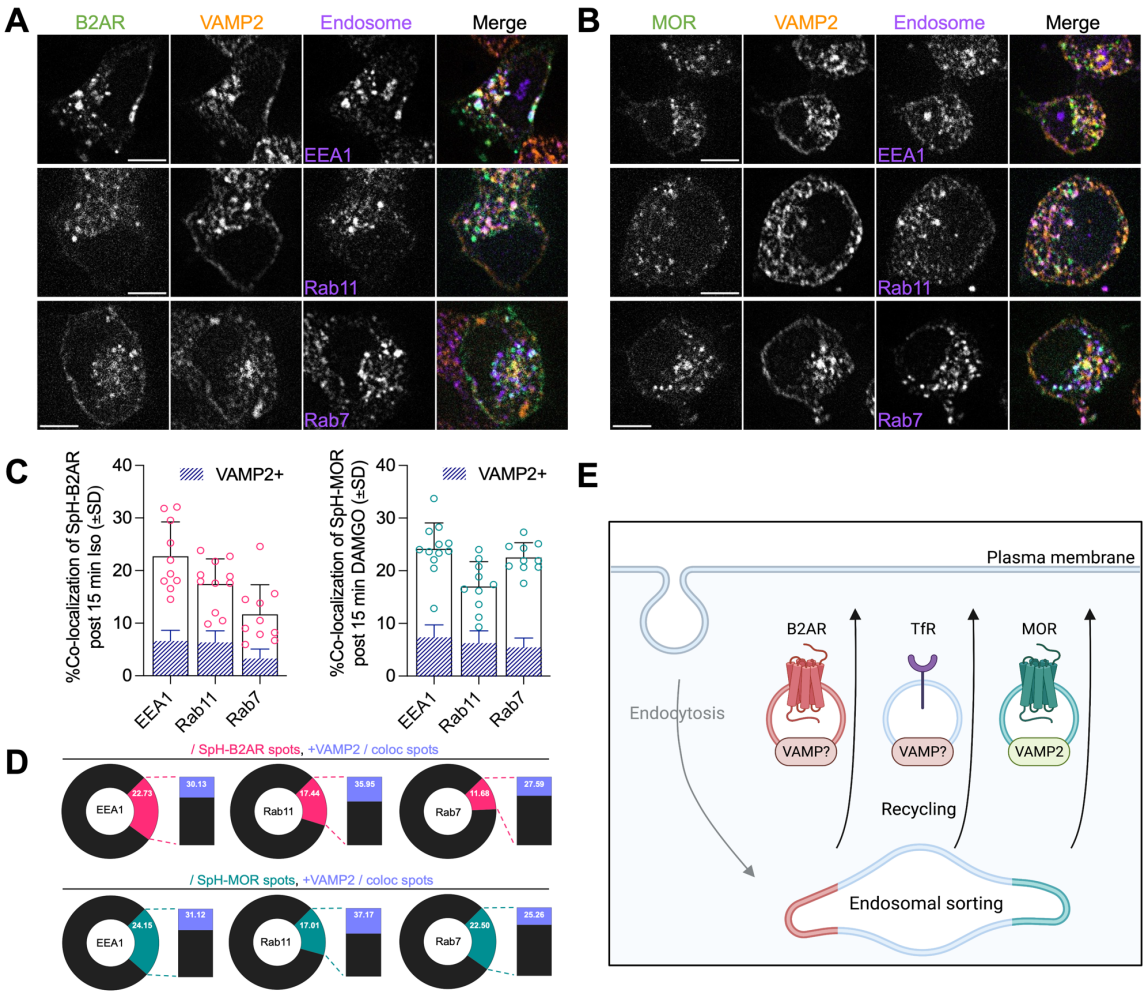

Figure 2.9. VAMP2 is not specifically co-localized with SpH-MOR-containing endosomes. **A.** Representative confocal slices of cells expressing SpH-B2AR (light green) immunostained for VAMP2 (orange) and EEA1, Rab11 or Rab7 (purple) after 15 min of agonist treatment. **B.** Representative confocal slices of cells expressing SpH-MOR (light green) immunostained for VAMP2 (orange) and EEA1, Rab11 or Rab7 (purple) after 15 min of agonist treatment. Scale bars = 6 µm. **C.** %Co-localization between the three labels calculated using an automated object-based method. %Co-localization was first analyzed between SpH-B2AR (left) or SpH-MOR (right) and the endosomal markers (outer columns, ±SD), then the co-localized spots were further analyzed for the presence of VAMP2 (VAMP2+, inner dashed columns, ±SD, SpH-B2AR: EEA1: n=10, Rab11: n=11, Rab7: n=10; SpH-MOR: EEA1: n=12, Rab11: n=10, Rab7: n=10, samples of all conditions were from 2 independent coverslips**). D.** Pie charts and stack columns showing the summary statistics of **C.** show no enrichment of VAMP2 in SpH-MOR-containing endosomes. **E.** Schematic of a proposed model of VAMP2's specificity in GPCR recycling. VAMP2 is preferentially co-packaged into vesicles from endosomal microdomains or tubules that contain a certain subset of GPCR cargoes, such as MOR but not B2AR, allowing it to mediate fusion in a cargo-selective manner. TfR on the other hand, can enter both microdomains or tubules (and other pathways if present), allowing redundant mechanisms of recycling.

The recycling of B2AR is not exclusively mediated by a singular VAMP subtype

Since VAMP2 showed cargo-selectivity to MOR, but not B2AR, we hypothesized that there might be a different VAMP subtype that was specific to B2AR's recycling. To find this VAMP subtype, we screened through all VAMPs other than VAMP2 that had been reported to function in exocytosis, namely VAMP1/ 3/ 4, and 7 (*35*, *42–44*).

Starting with VAMP4, we performed the two-channel TIRF microscopy assay in HEK293 cells co-expressing SpH-cargoes and VAMP4-pHuji to measure the levels of VAMP4 enrichment in puff events using the same method as described above. Interestingly, in comparison to SpH-MOR and SpH-B2AR, TfR-SpH puffs showed significantly lower levels of VAMP4 enrichment with a median score of $-1.43\text{x}SD_{baseline}$, indicating a depletion of pre-existing VAMP4-pHuji at the plasma membrane fusion sites from the TfR-SpH puffs (p=0.0002 vs SpH-B2AR and p=0.0003 vs SpH-MOR; Fig. 2.10 A). On the other hand, SpH-MOR and SpH-B2AR puffs showed neither enrichment nor depletion of VAMP4 with median scores both close to $0\text{x}SD_{baseline}$, indicating that these subsets of fusion vesicles were not carrying substantially different levels of VAMP4-pHuji as compared to the fusion sites' pre-existed levels (Fig. 2.10 A). Moreover, similar to MOR (Fig. 2.5 G), knockdown of VAMP4 using shVAMP4 did not significantly altered the frequency of Iso-induced SpH-B2AR puffs per unit time in PC12 cells (p=0.7234; Fig. 2.10 B). Together, we concluded that besides MOR, VAMP4 was also not mediating the recycling of B2AR.

Next, we tested the possibility of VAMP1 or VAMP3 being the specific VAMP subtype that mediates B2AR recycling. However, we found minimal protein expression of both VAMP1 and VAMP3 in baseline PC12 cells, in which we could robustly observe a plenty amount of B2AR recycling fusion events, either through immunoblots with PC12 cell whole cell lysates (Fig. 2.10 C) or with immunofluorescence staining (Fig. 2.10 D and E). Interestingly though, PC12 cells that

underwent nerve growth factor (NGF) -induced differentiation showed an apparent increase in the expression level of VAMP1 but not VAMP3 as detected using immunoblots (Fig. 2.10 C). We further confirmed this result using immunofluorescence staining and found that different from baseline PC12 cells, differentiated PC12 cells showed a higher fluorescence intensity of VAMP1 staining which appeared as intracellular puncta localized on compartmentalized organelles, while the staining of VAMP3 remained to be non-specific labeling across whole cell regions similar to we observed in baseline cells (Fig. 2.10 D, E, and F). These results suggested that at least in baseline PC12 cells, VAMP1 and VAMP3 were not involved in the recycling of B2AR.

Lastly, we tested whether VAMP7 was required for B2AR recycling. Immunofluorescence staining showed that VAMP7 was endogenously expressed at a high level in baseline PC12 cells with a similar endosomal localization as endogenous VAMP2 (Fig. 2.10 G; refer to Fig. 2.8 A-D for VAMP2 localization). We generated two shRNAs of different pairing sequences targeting rat VAMP7 using the same Dox-inducible shRNA-tagBFP system as described above, namely shVAMP7-1 and shVAMP7-2. We tested the shVAMP7s post varied amount of 200 ng/mL Dox treatment time and found that compared to shScramble, cells expressing shVAMP7-1 post 48 hr Dox treatment elicited the highest knockdown efficiency measured as ~49% reduction in VAMP7 immunostaining fluorescence intensity (Fig. 2.10 G and H). Under this knockdown condition, we tested the recycling capacity of B2AR using two different methods. VAMP7 depletion did not significantly alter SpH-B2AR's Iso-induced puff frequency, even though a trend was noticed ($p=0.1420$; Fig. 2.10 I). To verify if this trend was meaningful, we performed a ratiometric recycling assay in cells co-expressing FLAG-B2AR and shVAMP7-1 treated or non-treated with 48 hr Dox. In this assay, 10 μM Iso was used as agonist and 10 μm alprenolol was used as antagonist during washout. Consistent to the puff frequency data, the +Dox cells showed similar

levels of internalization and recycling as the −Dox cells (+ vs −Dox: internalization/ T: p=0.9372, recycling/ WO: p=0.9668; Fig. 2.10 J), confirming that VAMP7 was not required for the recycling of B2AR.

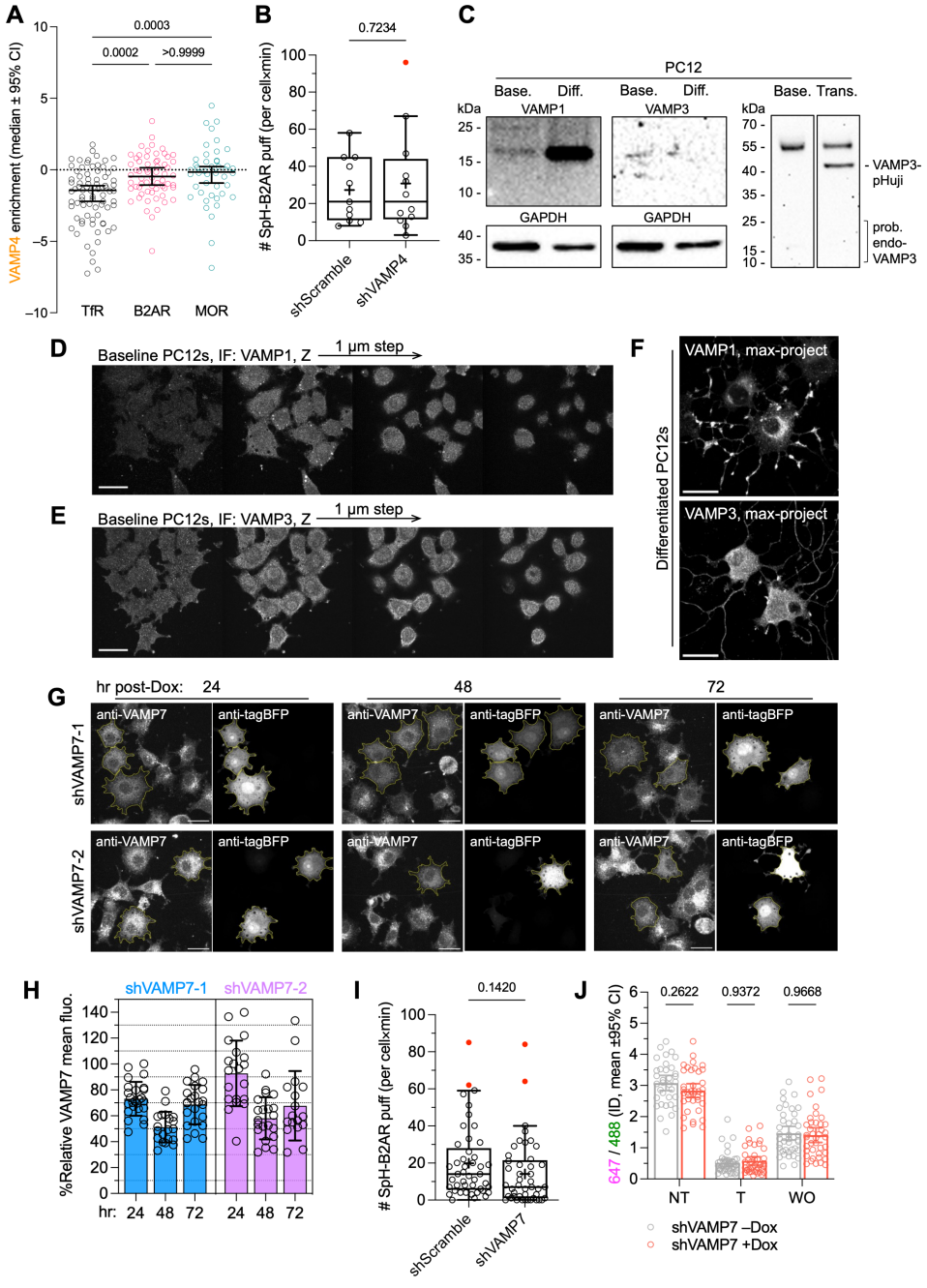

Figure 2.10. Besides VAMP2, neither VAMP1/ 3/ 4/ 7 is required for the recycling of B2AR.
A. VAMP4 enrichment in the population of puffs for each SpH-cargo measured and quantified using the same method as described above, except that all SpH-cargoes and VAMP4-pHuji were

transiently expressed in HEK293 cells (median ± 95% CI; TfR-SpH: 2 cells, puff=79; SpH-B2AR: 4 cells, puff=62; SpH-MOR: 4 cells, puff=44, from 2 coverslips, 1 experiment). Although none of the puff populations showed enrichment of VAMP4-pHuji, the TfR-SpH puff population showed significant deprivation of VAMP4-pHuji at the fusion sites (One-way ANOVA, post-hoc Kruskal-Wallis test: TfR vs. B2AR: p=0.0002; TfR vs. MOR: p=0.0003; B2AR vs. MOR: p>0.9999). **B.** The frequency of SpH-B2AR puffs per cell per minute (per cell×min) in PC12 cells co-expressing shScramble or shVAMP4, treated with 48 hr of 200 ng/mL Dox, showed no significant difference (shScramble and shVAMP2: 12 cells each, from 2 coverslips of 1 experiment; p=0.7234, unpaired two-tailed t-test). **C.** Representative immunoblot images showing the endogenous level of VAMP1 and VAMP3 in PC12 cell whole cell lysates at baseline (without any manipulation, Base.) or after NGF-induced differentiation (cells were treated with 100 ng/mL NGF for 9 days, Diff.) with GAPDH as an internal control. The activity of anti-VAMP3 antibody was confirmed using whole cell lysate of PC12 cells transiently expressing VAMP3-pHuji (Trans.). **D and E.** Representative confocal images of the vertical sections (left to right: 1 μm steps from cell bottom to top) of baseline PC12 cells immunostained for VAMP1 (**D**) or VAMP3 (**E**) showing only background fluorescence. Scale bars = 50 μm. **F.** Representative max-projected confocal images of differentiated PC12 cells immunostained for VAMP1 (top panel) or VAMP3 (bottom panel) with VAMP1 staining showing compartmentalized signal. Scale bars = 50 μm. **G.** Representative confocal slices of PC12 cells expressing shVAMP7-tagBFP with different pairing sequences (shVAMP7-1/ 2) immunostained for VAMP7 (anti-VAMP7) and tagBFP (anti-tagBFP) after 24, 48, or 72 hr of 200 ng/mL Dox treatment. Scale bars = 40 μm. **H.** Quantification of VAMP7 staining for images in **G** with whole cell mean fluorescence normalized to shScramble-expressing cells showing the knockdown efficiencies of shVAMP7s post varied amount of Dox treatment time (24, 48, 72 hr: shVAMP7-1: 25, 20, 23 cells; shVAMP7-2: 20, 21, 17 cells, from 2 coverslips of 1 experiment). shVAMP7-1 expression induced by 48 hr 200 ng/mL Dox treatment showed the highest VAMP7 knockdown level. **I.** The frequency of SpH-B2AR puffs (per cell×min) in cells co-expressing shScramble or shVAMP7-1, treated with 48 hr of 200 ng/mL Dox, showed no significant difference (shScramble and shVAMP7: 45 cells each, from 3 independent experiments; p=0.1420, unpaired two-tailed t-test). **J.** Similar ratiometric recycling assay as described above, but with 647 nm labeling surface FLAG-B2AR and 488 nm labeling total FLAG-B2AR, in cells co-expressing shVAMP7-1 +/− 48 hr 200 ng/mL Dox treatment. Ratios between surface and total fluorescence (647 / 488) were calculated using integrated density as described above (NT, T, WO: −Dox: 34, 41, 40 cells; +Dox: 38, 40, 40 cells, from 2 coverslips of 1 experiment). No significant difference in B2AR recycling capacity was noticed between + and −Dox cells (Two-way ANOVA, post-hoc Šídák test, +Dox vs −Dox: NT: p=0.2622; T: p=0.9372; WO: p=0.9668).

Discussion

In this study, we identify VAMP2 as a cargo-selective v-SNARE that is required for the fusion of recycling vesicles that contain MOR but not B2AR (Fig. 2.9 E). VAMP2 specificity is maintained across multiple different cell types, from HEK293 cells where both MOR and VAMP2 are ectopically expressed, to primary striatal neurons endogenously expressing MOR and VAMP2.

VAMP2 likely has broad but distinct roles in secretory vesicle release and in the delivery of signaling receptors. The canonical role of VAMP2 in mediating fusion of synaptic vesicles has been well studied (*8*, *13*, *14*, *45*, *46*). VAMP2 is also expressed in many secretory cells where it regulates the release of soluble hormones as well as GLUT4 from storage compartments (*47*, *48*). Given that neurotransmission and MOR membrane insertion both use VAMP2, specificity in fusion and regulation might be provided by the t-SNAREs. The best studied interactions of VAMP2 with t-SNAREs are for neurotransmitter release, where VAMP2 uses SNAP-25 and syntaxin1 as t-SNAREs to mediate fusion (*2*). However, during AMPA receptor membrane insertion in long term potentiation, VAMP2, interacts with SNAP-47 and syntaxin3 (*49*). It's unclear if VAMP2's role in GPCR delivery relies on either of these sets of t-SNAREs or an as yet unidentified set. As we continue to identify the components of specific fusion machinery that mediates the delivery of different GPCRs, we will be able to map specific SNARE complexes to specific pathways and cargo molecules.

In the broader context of trafficking, our data provide key evidence for the emerging idea that functionally distinct recycling pathways originate from the same endosomes, where each endosome is organized as a set of discrete microdomains from which biochemically distinct tubules extend to generate vesicles destined for the plasma membrane (*20*, *50*). B2AR is recycled via tubules from endosomal microdomains that are distinct from tubules that recycle TfR (*20*, *32*). Because we see little VAMP2 localization in B2AR or TfR fusion events, MOR is likely recycled via a third pathway distinct from these two. This idea is consistent with the different biochemical requirements that have been identified for the recycling of these different cargoes. B2AR uses a C-terminal PDZ ligand, which binds an actin-based machinery localized to a specific tubular microdomain on the endosome, to recycle (*20*, *51–54*). TfR, on the other hand, is sorted via

geometric sorting, seemingly independent of specific biochemical requirements (*55*). MOR does not have an identified PDZ ligand. Instead, it uses a bi-leucine sequence to recycle (*56*, *57*). The mechanism through which this motif acts has still not been identified. Importantly, the biochemical sequences on B2AR and MOR are transplantable, suggesting that the recycling characteristics are encoded in the sequences (*56*, *58*).

Our results support a model where specific components of the fusion machinery are selectively co-packaged into vesicles along with cargo at the endosomes. The specific enrichment and requirement of VAMP2 for MOR fusion could reflect two possibilities: (i). different GPCRs are localized to distinct endosomal compartments, with MOR specifically localized to endosomes containing VAMP2, or (ii). VAMP2 is co-packaged specifically into vesicles that contain specific cargoes even though VAMP2 and multiple cargoes are present on the same endosome. In our experiments, MOR and B2AR both co-localized with VAMP2 on early endosomes and recycling endosomes, from both of which cargo can be recycled to the surface (Fig. 2.8 and Fig. 2.9). MOR did not show preferential localization at an organellar level with VAMP2, suggesting that MOR and VAMP2 are sorted into vesicles at a sub-organellar level, supporting the second model that distinct v-SNAREs are co-packaged with specific GPCRs into distinct vesicles, all originating from the same set of endosomal compartments.

The exact mechanisms by which cargoes are sorted into these domains is an exciting area of future work, especially as these pathways could actively vary based on a variety of factors. Many cargo molecules themselves could be modified by alternative splicing, which could change functionally important sequences and alter sorting. For example, MOR is alternatively spliced, generating multiple isoforms expressed *in vivo*, including some that lack the canonical bi-leucine recycling sequence (*59*, *60*). We focused on the major isoform of MOR, which has been the

canonical version used to study the mechanisms and functional consequences of MOR trafficking and signaling. At present, how alternative splicing affects the trafficking of MOR, and whether and how all isoforms of MOR recycle, are not well studied. It is possible that different splice isoforms could engage different trafficking machinery, including SNAREs, based on the specific sequences that they use to recycle. In addition, different opioid agonists can drive differential sorting of opioid receptors in the endosome (*27*, *61*). In this context, one protein family that is of interest in mediating this process is the sorting nexin family (SNXs), which can interact with cargo molecules and drive localized membrane changes that allow vesicle formation from specific domains of endosomes. TfR recycling is mediated by SNX3 or SNX4 (*62*, *63*), while B2AR recycling requires SNX27 (*53*, *64*). A specific SNX protein required for MOR recycling has not been identified. How agonists can selectively drive different sorting fates is not known, but it is possible that specific agonist-bound conformations drive receptor interactions with specific sorting complexes that also co-package VAMPs and other fusion machineries.

Sorting of GPCRs into separate pathways that contain distinct fusion machineries could provide a mechanism for cells to selectively control the surface delivery of individual GPCRs, even though they all traverse the same endocytic pathways. The recycling of B2AR and MOR are regulated by distinct signaling pathways. B2AR recycling is inhibited by protein kinase A (PKA), via Gαs activation, providing a mechanism for feedback regulation (*25*). MOR recycling is independent of PKA but is increased by protein kinase C via activation of either Gβγ signaling downstream of MOR or Gα signaling downstream of co-expressed neurokinin-1 receptors (*26*, *32*). Importantly, these phosphorylation mechanisms modify sorting of the receptor cargo into recycling pathways, but should not regulate the pathway as a whole or the core components that mediate the fusion of these vesicles. The exact mechanism by which SNAREs are regulated

downstream of receptors is not clear, but this could involve direct regulation by G protein interactions. For example, Gβγ downstream of activated Gi/o coupled GPCRs can bind the SNARE complex, compete with synaptotagmin 1, and inhibit membrane fusion (*65*, *66*). Although MOR is a Gαi/o coupled GPCR, it does not autoinhibit its own membrane insertion. Therefore, it is possible that the modulation of SNAREs by Gβγ interaction follows a higher organizational principle, where specific VAMP/t-SNARE complexes are regulated differentially by G proteins derived from different receptor signaling pathways. Importantly, cargo molecules that mediate nutrient uptake, like TfR, typically can enter multiple trafficking pathways (*67–69*). The ability to enter multiple pathways allows TfR recycling to be mediated by multiple VAMP subtypes (*35*, *42*, *70*), making the v-SNARE requirements redundant. Consistent with this idea, although a subset of TfR fusion events were VAMP2-enriched (Fig. 2.2 H), depletion of VAMP2 did not cause a significant reduction in TfR delivery to the cell surface (Fig. 2.5 D). Such specificity and redundancy in the use of fusion machinery in surface delivery could allow cells to selectively control GPCR recycling, and therefore sensitivity to signaling, without affecting nutrient uptake or transport of other essential cargoes.

Nevertheless, we were unable to identify an exclusive v-SNARE that was specifically required for B2AR recycling (Fig. 2.2, 2.5, and 2.10). However, since we have not examined every v-SNAREs, possibility still remains for VAMP5, VAMP8, or Vti1a. One alternative model could be that the B2AR-containing vesicles were packaged with multiple functionally redundant v-SNAREs and the fusion of these vesicles did not depend on a singular v-SNARE. This hypothesis can be tested using multiple depletions. It is also possible that one of the tested v-SNAREs was actually specific to B2AR recycling, but a knockdown was insufficient to cause a detectable

inhibitory effect, as this v-SANRE could still function even at a low level. This hypothesis can be tested in v-SNARE knockout cells.

Materials and Methods

Plasmid cloning and lentivirus production

TfR-SpH plasmid was cloned by replacing mCherry on the mCherry-TfR-20 plasmid (a gift from Michael Davidson, Addgene, #55144) with a SpH-tag, using the AgeI and NotI sites. SpH-B2AR, SpH-MOR, FLAG-B2AR, and FLAG-MOR plasmids were all previously described (*24*, *57*, *71*). FLAG-SpH-MOR plasmid was cloned on a pcDNA3.1 backbone with FLAG sequence (GAC TAC AAG GAC GAT GAT GAC) inserted in between a signal sequence and an alanine spacer (GCC) followed by SpH-tag and MOR. All MOR-expressing constructs encode mouse MOR-1, the major MOR isoform. VAMP2-pHuji plasmid expressing human VAMP2 isoform1 was a gift from Justin Taraska (Addgene, #105289). VAMP4-pHuji plasmid expressing human VAMP4 was cloned by first replacing VAMP2 sequence of VAMP2-pHuji with a VAMP4 sequence from pEGFP-VAMP4 (a gift from Thierry Galli, Addgene, #42313), using XhoI and BamHI sites, then the stop codon and original linker were replaced by VAMP2-pHuji's linker. Lentivirus-compatible FLAG-MOR plasmid was cloned by recombing pENTR-FLAG-MOR with pLenti-CMV-Puro-DEST (a gift from Eric Campeau and Paul Kaufman, Addgene, #17452) through LR reaction following a published protocol (*72*).

The doxycycline-inducible shRNA backbone pLKO-tagBFP-TetOn was a gift from Paul Jenkins (*73*). shVAMP2 pairing sequence targeting rat VAMP2 was previously described (*43*), and the shVAMP2 sequence was designed as: 5'- CCG GAA CAA GTG CAG CCA AGC TCA ACT CGA GTT GAG CTT GGC TGC ACT TGT TTT TTT G -3'(sense) and 5'- AAT TCA AAA AAA CAA GTG CAG CCA AGC TCA ACT CGA GTT GAG CTT GGC TGC ACT TGT T -3'(antisense). shVAMP4 pairing sequence targeting rat VAMP4 was previously described (*35*), and the shVAMP4 sequence was designed as: 5'- CCG GGG ACC ATC TGG ACC AAG ATT CTC GAG AAT CTT GGT CCA GAT GGT CCT TTT TG -3' (sense) and 5'- AAT TCA AAA AGG ACC ATC TGG ACC AAG ATT CTC GAG AAT CTT GGT CCA GAT GGT CC -3' (anti-sense). shVAMP7 pairing sequences targeting rat VAMP7 were previously described (*74*). The shVAMP7-1 sequence was designed as: 5'- CCG GGA AGA GGT TCC AGA CCA CAC TCG

AGT GTG GTC TGG AAC CTC TTC TTT TTG -3'(sense) and 5'- AAT TCA AAA AGA AGA GGT TCC AGA CCA CAC TCG AGT GTG GTC TGG AAC CTC TTC -3'(antisense). The shVAMP7-2 sequence was designed as 5'- CCG GGT GGA GGA AAC TTC CTG GAG CTC GAG CTC CAG GAA GTT TCC TCC ACT TTT TG -3'(sense) and 5'- AAT TCA AAA AGT GGA GGA AAC TTC CTG GAG CTC GAG CTC CAG GAA GTT TCC TCC AC -3'(antisense). A universal non-targeting shScramble sequence was designed based on a published sequence (*75*): 5'- CCG GCC TAA GGT TAA GTC GCC CTC GCT CGA GCG AGG GCG ACT TAA CCT TAG GTT TTT G -3' (sense) and 5'- AAT TCA AAA ACC TAA GGT TAA GTC GCC CTC GCT CGA GCG AGG GCG ACT TAA CCT TAG G -3' (antisense). The shRNA sequences were cloned into the pLKO-tagBFP-TetOn backbone following a published protocol (*76*).

Lentiviral particles for FLAG-MOR (Lenti-FLAG-MOR), shVAMP2 (Lenti-shVAMP2), and shScramble (Lenti-shScramble) expression were produced following *The RNAi Consortium* protocol (Broad Institute). Briefly, LentiX-293 cells (gift from Adam Courtney) were transfected with plasmids of interest alongside psPAX2 (packaging) and pMD2.G (envelope) using TransIT-LT1 transfection reagent (MIR 2300, Mirus). Two batches of virus harvest were pooled together, and the pooled viral media were used for infection.

Cell culture and reagents

HEK293 and PC12 cells were purchased from American Type Culture Collection. SpH-B2AR and SpH-MOR stably expressing HEK293 cell lines were described previously (*24*, *57*). HEK293 cells were maintained in Dulbecco's modified eagle medium high glucose (SH3024301, Cytiva) supplemented with 10% fetal bovine serum (FBS, 26140079, Gibco) at 37 ^{o}C and 5% CO_2. VAMP2-pHuji was transiently transfected into the HEK293 stables or co-transfected with TfR-SpH into plain HEK293 cells using Effectene transfection reagent (301425, Qiagen) following the manufacturer's protocol. VAMP4-pHuji was transiently co-transfected with SpH-MOR into plain HEK293 cells using Effectene.

PC12 cells were maintained in Ham's F-12K (Kaighn's) medium supplemented with 10% horse serum (16050122, Gibco) and 5% FBS at 37 ^{o}C and 5% CO_2 in tissue culture flasks coated with Collagen IV (C5533, Sigma-Aldrich). Differentiation of PC12 cells was achieved by incubating the cells in 100 ng/mL nerve growth factor (NGF) added media for more than 8 days, with alternately media change or cell passing every two days depending on the cell confluency.

Plasmids were transiently transfected into PC12s using Lipofectamine 2000 transfection reagent (11668027, Invitrogen) following manufacturer's protocol.

Saturated concentrations (10/ 12.5 μM) of [D-Ala^2, *N*-Me-Phe^4, Gly^5-ol]-enkephalin (DAMGO; E7384, Sigma-Aldrich) were used to trigger the internalization and recycling of SpH-MOR, FLAG-MOR, and FLAG-SpH-MOR. 10/ 12.5 μM isoproterenol (Iso; I5627, Sigma-Aldrich) was used to trigger the internalization and recycling of SpH-B2AR and FLAG-B2AR. FLAG-tag was visualized using M1-Alexa-647 antibody (M1-647): anti-FLAG-M1 antibody (F3040, Sigma-Aldrich) conjugated with Alexa Fluor 647 (A20186, Invitrogen). In ratiometric recycling assays, 10 μM Naltrexone (N3136, Sigma-Aldrich) or Alprenolol (A0360000, Sigma-Aldrich) was used in medium to ensure sufficient washout of agonists and induce recovery of surface MOR or B2AR, respectively. All treatments intended to induce trafficking was done at 37 ^{o}C. Cycloheximide (CHX; C1988, Sigma-Aldrich) dissolved in ethanol (EtOH) was used to block biosynthesis. For live cell imaging, cells were pre-treated with 10 μM CHX for 2 hr at 37 ^{o}C and the same concentration of CHX was kept in the media during imaging to prevent effect turnover.

To induce shVAMP2, shVAMP4, shVAMP7, and shScramble expressions, cells were pre-treated with 200 ng/mL doxycycline (Dox, D43020, Research Products International) for 48 hr except otherwise stated before experiments. FLAG-MOR and shVAMP2 or shScramble co-expressing PC12 mixed population stable cell lines were generated with 10 days of 500 μg/mL G418 (10131035, Gibco) selection post transfection. After the selection the stable cells were cultured in PC12 cell maintenance media as described above.

Rat striatal neurons were dissociated from E-18 rat striatum obtained from TransnetYX Tissue using 2 mg/mL papain (NM100200, Genlantis), cultured on poly-D-lysine (PDL, P6407, Sigma-Aldrich) coated glass coverslips in Neurobasal media (21103049, Gibco) supplemented with B-27 (17504044, Gibco), 1% GlutaMAX (35050061, Gibco) and 1% Pen-Strep (15140122, Gibco) at 37 ^{o}C, 5% CO_2.

TIRF microscopy for fusion events imaging

All total internal reflection fluorescence (TIRF) microscopy was conducted using an Andor Dragonfly multimodal microscopy system (Andor) in TIRF mode. SpH-cargo expressing cells were passed to #1.5 25 mm glass coverslips (7222510, Electron Microscopy Sciences) one day post-transfection and imaged two days after the passing. Especially, SpH-cargo expressing PC12 cells were passed to PDL-coated glass coverslips. Coverslips were mounted in an imaging chamber

and imaged in CO_2-independent Leibovitz's L-15 medium (21803027, Gibco) with 1% FBS. The cells were visualized live using a 60X 1.49 NA Apochromat TIRF objective (Nikon Instruments) on a Nikon Eclipse Ti2 inverted microscope outfitted with a 37 ºC temperature controlling chamber. Movies of fusion events were taken after 5 min of agonist-induced internalization at 37 ºC for SpH-MOR and SpH-B2AR or immediately for TfR-SpH at 50 Hz (two-channel) or 10 Hz (single-channel) for 1 min. All recycling movies were collected within 20 min of agonist treatment.

Cells were excited using direct modulation lasers (Andor ILE) at the indicated wavelength passed through a 405/488/561/640 quad excitation dichroic. For two-channel simultaneous acquisition, SpH-cargoes and VAMP2-pHuji were simultaneously excited using 488 nm and 561 nm lasers, and the emission was split using a 565 longpass (LP) dichroic beamsplitter. SpH-cargo emission was collected through a 525/50 bandpass emission filter. VAMP-pHuji emission was collected through a 579/34 bandpass emission filter. For single channel imaging of fusion events, SpH-cargoes were excited using 488 nm light and collected through a 540/30 bandpass emission filter. All emission filters and dichroics were purchased from Semrock. All images were collected using iXon Life 888 electron-multiplying charge-coupled device (EMCCD) cameras (Andor) with one camera for each channel run simultaneously.

Immunoblots

For GRK3 CHX chase blot, whole cell lysates of plain HEK293 cells post 0.5 to 4 hr of 10 μM CHX treatment or post 4 hr of vehicle treatment were prepared from 90% confluent 6-well plates of cells. The cells were directly lysed and scraped in the plates with 2x diluted Laemmli Sample Buffer (1610747, Bio-Rad) supplemented with 10% β-mercaptoethanol (1610710, Bio-Rad), 50 mM dithiothreitol (1610611, Bio-Rad) and 10% protease inhibitor solution (1 tablet dissolved in 1 mL of water, A32965, Thermo Scientific). Lysates were then incubated at 95 ºC for 5 min. Right after sonication, the lysates were run on 10% polyacrylamide gel and then transferred to nitrocellulose membrane. Membranes were blocked with 5% milk Tris-buffered saline Tween-20 (TBST), then probed for GRK3 (1:1000; monoclonal mouse; sc-365197, Santa Cruz Biotechnology) and then developed using chemiluminescence. After imaging, the membranes were stripped for 20 min in stripping buffer (21059, Thermo Scientific), then reblocked in 5% milk TBST and probed for GAPDH (1:1000; monoclonal rabbit; 14C10, #2118, Cell Signaling Technology (CST) as an internal control. For VAMP2 blots, whole cell lysates were prepared from 90% confluent 6-well plates of HEK293 cells, VAMP2-pHuji expressing HEK293 cells and plain

PC12 cells. VAMP2-pHuji expressing HEK293 cells were lysed 48 hr post-transfection. All procedures of blotting were the same, except the samples were run on 4-20% gradient polyacrylamide gel and the membranes were first probed for VAMP2 (1:1000; monoclonal mouse; 104211, Synaptic Systems) before stripping and reprobing for GAPDH. For VAMP1 and VAMP3 blots, whole cell lysates were prepared from 90% confluent 6-well plates of plain PC12 cells or differentiated PC12 cells as described above. All procedures of blotting were the same as the VAMP2 blot, except the membrane was cut before antibody labeling to avoid cross-reaction of the secondary antibody. Anti-VAMP1 (polyclonal rabbit; 104022, Synaptic Systems) and anti-VAMP3 (polyclonal rabbit; 104103, Synaptic Systems) antibodies were used at 1:1000.

Sample preparation for immunofluorescence microscopy

To prepare samples for immunofluorescence microscopy, PC12 or HEK293 cells were passed to PDL-coated #1.5 12 mm glass coverslips (1254580P, Fisher Scientific). The cells were first fixed with 4% formaldehyde (FB002, Invitrogen) for 20 min at room temperature and then were permeabilized and blocked by incubating in phosphate-buffered saline (PBS) with 0.75% Triton-X-100, 5% FBS, 5% glycine, 1.25 mM magnesium chloride, and 1.25 mM calcium chloride (blocking buffer). Primary and secondary antibody labeling was performed in blocking buffer for 1 hr at room temperature. VAMP2 was stained by the same antibody as above at 1:1000. VAMP1 and VAMP3 were stained with the same antibodies as above at 1:500. For endosomal staining, anti-EEA1 (C45B10, #3288, CST), anti-Rab11 (D4F5, #5589, CST), and anti-Rab7 (D95F2, #9367, CST) monoclonal rabbit antibodies were used at 1:50. All fluorophore-conjugated secondary antibodies were used at 1:1000. For two-channel co-localization study, anti-VAMP2 was labeled with goat anti-mouse IgG (H+L)-Alexa Fluor 647 (A21235, Invitrogen) while anti-endosomal markers were labeled with goat anti-rabbit IgG (H+L)-Alexa Fluor 488 (A11008, Invitrogen). For three-channel co-localization study, anti-VAMP2 was labeled with goat anti-mouse IgG (H+L)-Alexa Fluor 568 (A11004, Invitrogen) while endosomal markers were labeled with goat anti-rabbit IgG (H+L)-Alexa Fluor 647 (A21244, Invitrogen). For shRNA knockdown verifications, anti-VAMP4 antibody (polyclonal rabbit; 136002, Synaptic Systems) was used at 1:500 and anti-VAMP7 antibody (monoclonal mouse; 232011, Synaptic Systems) was used at 1:250. For certain shRNA knockdown verifications, tagBFP signal was amplified using an anti-tagBFP nanobody conjugated to 2 × Alexa Fluor 647 at 1:500 (N0502-AF647, NanoTag Biotechnologies). After the labeling, coverslips were mounted on glass slides (12550123, Fisher

Scientific) using Prolong Diamond Antifade Mountant (P36961, Invitrogen). DAPI staining was introduced using Prolong Diamond Antifade Mountant with DAPI (P36962, Invitrogen).

Confocal microscopy

Confocal imaging of immunofluorescence microscopy samples was conducted using an Andor Revolution multimodal microscopy system in confocal mode. Glass slides with mounted coverslips were imaged using a 100X 1.49 NA Apochromat TIRF objective (Nikon Instruments) on a Nikon Eclipse Ti inverted microscope. Excitation was conducted using solid-state lasers (Andor ALC-500) at the indicated wavelength with light filtered through acousto-optic tunable filter. Alexa-488 was excited with 488 nm light and collected through a 525/50 bandpass emission filter. Alexa-568 was excited with 561 nm light and collected through a 620/60 bandpass emission filter. Alex-647 was excited with 640 nm light and collected through a 700/75 bandpass emission filter. All emission filters were from Chroma. Light of different wavelengths were collected using an iXon + 897 EMCCD camera (Andor) sequentially. Images were acquired in Z-stacks for 3D-quantification. For shRNA tagBFP confirmation before single channel puff imaging, cells were imaged live using the same Andor Dragonfly system as described in TIRF microscopy section but in confocal mode. tagBFP was excited using 405 nm light and collected through a 450/50 bandpass emission filter.

Flow cytometry

shVAMP2 and FLAG-MOR co-expressing PC12 cells (double-stables) were either treated with 200 ng/mL Dox for 48 hr (+Dox) or non-treated (−Dox) before experiments. Before flow cytometry analysis, the cells were either left untreated, treated with 10 μM DAMGO, or treated with 10 μM DAMGO and then 10 μM Naltrexone. All treatment conditions were 20 min at 37 ^{o}C to allow for trafficking. Next, the cells were immediately transferred onto ice (0 ^{o}C) to terminate trafficking and labeled with M1-647 antibody for 45 min. After labeling, the cells were scraped in the well and resuspended in 1% FBS supplemented Dulbecco's PBS (14040133, Gibco). Last, data from 1 x 10^5 cells for each sample were acquired using a BD LSRFortessa flow cytometer (BD Biosciences). Plain PC12 cells were used to gate for cell size, granularity, and background tagBFP fluorescence. Double-stables not labeled with M1-647 were used to gate for background Alexa-647 fluorescence. tagBFP was excited using 405 nm light and collected through a 450/50 bandpass emission filter. Events representing the top 10% of tagBFP fluorescence were gated to select for cells expressing shVAMP2. Relative changes in FLAG-MOR levels on the plasma membrane were

analyzed using mean fluorescence intensities of Alexa-647 excited by 640 nm light and collected through a 670/14 bandpass emission filter.

Ratiometric recycling assay

This assay was adapted from a published work by our group (*32*). To measure recycling of MOR, PC12 cells or neurons were infected with Lenti-FLAG-MOR and Lenti-shVAMP2 for 24 hr with 10 μg/mL polybrene. To measure recycling of B2AR, PC12 cells were transfected with FLAG-B2AR and shVAMP7 using Lipofectamine 2000. Cells were then either applied with 200 ng/mL Dox for 48 hr (+Dox) or not applied (−Dox). Particularly, neurons were infected on day 4 after plating and Dox was applied on day 7 after plating. During treatments, cells were first live labeled with M1-647 [M1-488 for FLAG-B2AR, following [] all indicate conditions for B2AR] for 10 min at 37 ºC, then either left untreated, treated with 10 μM DAMGO [Iso], or treated with 10 μM DAMGO [Iso] and then 10 μM Naltrexone [Alprenolol]. All treatment conditions were 20 min at 37 ºC to allow for trafficking. After, cells were second live labeled with goat anti-mouse IgG (H+L)-Alexa Fluor 488 (A11001, Invitrogen) [goat anti-mouse IgG (H+L)-Alexa Fluor 647] for 15 min at 4 ºC followed by 4% formaldehyde fixation for 20 min and 0.1 M glycine PBS blocking for 10 min, both at room temperature. Prepared samples were imaged with confocal microscopy as described above.

Image registration and data processing

All the images were processed with Fiji, ImageJ (*77*). Representative images and montages were made with ImageJ integrated functions and plugins.

Two-channel simultaneous acquisition images were processed with channel alignment using ImageJ plugin NanoJ-Core (*78*), global background subtraction using an ImageJ macro, and post-hoc bleedthrough correction. For channel alignment, fiducial images were taken by imaging TetraSpeck fluorescent microspheres slide (T14792, Invitrogen) with the same two-channel TIRF configurations as described above. For global background subtraction, mean fluorescence intensity within a cell region without either cluster or puff event was calculated and subtracted from each corresponding frame of the analyzed images. For bleedthrough correction, bleedthrough images were acquired using the same two-channel TIRF configurations as described above but with cells expressing SpH-cargo alone. Calculation of bleedthrough coefficient (k_{Bt}) and generation of related graphs were done by a pixel-by-pixel analysis macro in ImageJ. Bleedthrough correlation between SpH channel and pHuji channel was examined using all three SpH-cargoes and was found

linear with an average slope of 0.043 (Fig. 2.11). Given that bleedthrough was an intrinsic property decided solely by the fluorophore's spectrum, 0.043 was used as a uniform k_{Bl} across all analysis.

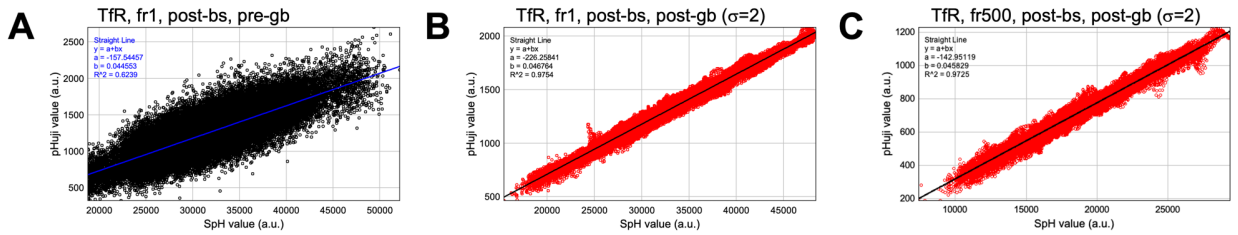

Figure 2.11. SpH bleedthrough into the pHuji channel is linearly correlated and therefore can be corrected.
A. Pixel-by-pixel fluorescence correlation plots between SpH and pHuji values fitted with simple linear regressions generated by analyzing TIR-FM images (256x256 pixels) of cells expressing SpH-cargoes alone, simultaneously acquired in both SpH and pHuji channels under identical conditions as in **Figure 2.2**. This panel shows the first frame (fr1) of a movie of TfR-SpH expressing cell post-background subtraction (post-bs) without Gaussian blur (pre-gb). **B.** Similar analysis post-Gaussian blur (post-gb, σ=2). **C.** Frame 500 (fr500) of the same movie as in **A** and **B** post-bs and post-gb (σ=2).

Population analysis of fusion events was performed using scikit-learn in Python (*79*, *80*). We established the number of components for the Gaussian mixture fitting via calculating AIC/BIC loss metrics for 1000 bootstrapped samples drawn all puff events from all SpH-cargoes. In the distributions from these samples, AIC minima were identified commonly at 3 and 9, and BIC minima were primarily seen at 3. Based on these metrics, we fit a Gaussian mixture model of 3 components to the pooled puff population. Using this model, we predicted component membership for the puff events for each SpH-cargo.

For VAMP2/ 7 knockdown efficiency analysis, we calculated integrated density of VAMP2/ 7 immunostaining over a uniform threshold (IDoT) established by averaging the auto-threshold values (method=default) of all cells. Particularly for shVAMP2, the shRNA expressing levels were approximated by calculating tagBFP IDoT using the same method. Then the shVAMP2-expressing cells were ranked by tagBFP IDoT and a hard cutoff (~50%) was applied to separate the cells into low-BFP and high-BFP groups. VAMP2 IDoT of high-BFP cells were first normalized to the mean of the low-BFP cells then double normalized to the mean of shScramble high-BFP cells to calculate the knockdown efficiency. For the shVAMP7-expressing cells, the IDoT of VAMP7 immunostaining were directly compared between conditions since the high-BFP cells were unambiguously marked out by the anti-tagBFP nanobody.

For ratiometric recycling assays, we first calculated the integrated density of the two channels in raw images within cell masks generated through automatically thresholding (method = triangle) the corresponding gaussian-blurred images (σ=2), then calculated the integrated density ratio of 488 nm over 647 nm [647 nm over 488 nm for B2AR], as the quantification of recycling.

Automated co-localization analysis was performed using Imaris software (Andor). Fluorescence-labeled endosomal compartments were automatically identified as 200 nm diameter spheres (spots) using the Imaris "Spots" function. Co-localization between two spots were calculated as proximity $\leq$ 200 nm using Imaris MATLAB-based extension "colocalize spots". %Co-localization was calculated per field.

Flow cytometry related histograms and statistics were generated using FlowJo (BD Biosciences). Raw data were processed using Excel (Microsoft) while statistical tests and graphs were generated using Prism 9 (GraphPad Software). All data distributions were assumed to be normal when subjected to parametric tests, although normality was not formally tested, except for the data of fusion events population which was established as a mixture of multiple Gaussian distributions as described above. Model schematics were made using BioRender.

References

1. W. Wickner, R. Schekman, Membrane fusion. *Nat. Struct. Mol. Biol.* **15**, 658–664 (2008).

2. T. C. Südhof, Neurotransmitter release: the last millisecond in the life of a synaptic vesicle. *Neuron*. **80**, 675–690 (2013).

3. K. L. Pierce, R. T. Premont, R. J. Lefkowitz, Seven-transmembrane receptors. *Nat. Rev. Mol. Cell Biol.* **3**, 639–650 (2002).

4. S. R. Foster, A. S. Hauser, L. Vedel, R. T. Strachan, X.-P. Huang, A. C. Gavin, S. D. Shah, A. P. Nayak, L. M. Haugaard-Kedström, R. B. Penn, B. L. Roth, H. Bräuner-Osborne, D. E. Gloriam, Discovery of human signaling systems: pairing peptides to G protein-coupled receptors. *Cell*. **179**, 895-908.e21 (2019).

5. G. Pándy-Szekeres, M. Esguerra, A. S. Hauser, J. Caroli, C. Munk, S. Pilger, G. M. Keserű, A. J. Kooistra, D. E. Gloriam, The G protein database, GproteinDb. *Nucleic Acids Res.* **50**, D518–D525 (2021).

6. M. T. Drake, S. K. Shenoy, R. J. Lefkowitz, Trafficking of G protein–coupled receptors. *Circ. Res.* **99**, 570–582 (2006).

7. N. J. Pavlos, P. A. Friedman, GPCR signaling and trafficking: the long and short of it. *Trends Endocrinol. Metab.* **28**, 213–226 (2017).

8. G. G. Schiavo, F. Benfenati, B. Poulain, O. Rossetto, P. P. de Laureto, B. R. DasGupta, C. Montecucco, Tetanus and botulinum-B neurotoxins block neurotransmitter release by proteolytic cleavage of synaptobrevin. *Nature*. **359**, 832–835 (1992).

9. T. Söllner, M. K. Bennett, S. W. Whiteheart, R. H. Scheller, J. E. Rothman, A protein assembly-disassembly pathway in vitro that may correspond to sequential steps of synaptic vesicle docking, activation, and fusion. *Cell*. **75**, 409–418 (1993).

10. T. Söllner, S. W. Whiteheart, M. Brunner, H. Erdjument-Bromage, S. Geromanos, P. Tempst, J. E. Rothman, SNAP receptors implicated in vesicle targeting and fusion. *Nature*. **362**, 318–324 (1993).

11. T. Weber, B. V. Zemelman, J. A. McNew, B. Westermann, M. Gmachl, F. Parlati, T. H. Söllner, J. E. Rothman, SNAREpins: minimal machinery for membrane fusion. *Cell*. **92**, 759–772 (1998).

12. J. A. McNew, F. Parlati, R. Fukuda, R. J. Johnston, K. Paz, F. Paumet, T. H. Söllner, J. E. Rothman, Compartmental specificity of cellular membrane fusion encoded in SNARE proteins. *Nature*. **407**, 153–159 (2000).

13. S. Schoch, F. Deák, A. Königstorfer, M. Mozhayeva, Y. Sara, T. C. Südhof, E. T. Kavalali, SNARE function analyzed in synaptobrevin/VAMP knockout mice. *Science*. **294**, 1117–1122 (2001).

14. F. Deak, O.-H. Shin, E. T. Kavalali, T. C. Sudhof, Structural determinants of synaptobrevin 2 function in synaptic vesicle fusion. *J. Neurosci.* **26**, 6668–6676 (2006).

15. V. Kiessling, A. J. B. Kreutzberger, B. Liang, S. B. Nyenhuis, P. Seelheim, J. D. Castle, D. S. Cafiso, L. K. Tamm, A molecular mechanism for calcium-mediated synaptotagmin-triggered exocytosis. *Nat. Struct. Mol. Biol.* **25**, 911–917 (2018).

16. C. Wang, J. Tu, S. Zhang, B. Cai, Z. Liu, S. Hou, Q. Zhong, X. Hu, W. Liu, G. Li, Z. Liu, L. He, J. Diao, Z.-J. Zhu, D. Li, C. Liu, Different regions of synaptic vesicle membrane regulate VAMP2 conformation for the SNARE assembly. *Nat. Commun.* **11**, 1531 (2020).

17. A. C. Hanyaloglu, M. von Zastrow, Regulation of GPCRs by endocytic membrane trafficking and its potential implications. *Annu. Rev. Pharmacol. Toxicol.* **48**, 537–568 (2008).

18. F. Wang, X. Chen, X. Zhang, L. Ma, Phosphorylation state of mu-opioid receptor determines the alternative recycling of receptor via Rab4 or Rab11 pathway. *Mol. Endocrinol.* **22**, 1881–92 (2008).

19. G. A. Yudowski, M. A. Puthenveedu, A. G. Henry, M. von Zastrow, Cargo-mediated regulation of a rapid Rab4-dependent recycling pathway. *Mol. Biol. Cell*. **20**, 2774–2784 (2009).

20. M. A. Puthenveedu, B. Lauffer, P. Temkin, R. Vistein, P. Carlton, K. Thorn, J. Taunton, O. D. Weiner, R. G. Parton, M. von Zastrow, Sequence-dependent sorting of recycling proteins by actin-stabilized endosomal microdomains. *Cell*. **143**, 761–773 (2010).

21. J. M. Kunselman, J. Lott, M. A. Puthenveedu, Mechanisms of selective G protein–coupled receptor localization and trafficking. *Curr. Opin. Cell Biol.* **71**, 158–165 (2021).

22. G. Miesenböck, D. A. D. Angelis, J. E. Rothman, Visualizing secretion and synaptic transmission with pH-sensitive green fluorescent proteins. *Nature*. **394**, 192–195 (1998).

23. S. M. Voglmaier, K. Kam, H. Yang, D. L. Fortin, Z. Hua, R. A. Nicoll, R. H. Edwards, Distinct endocytic pathways control the rate and extent of synaptic vesicle protein recycling. *Neuron*. **51**, 71–84 (2006).

24. G. A. Yudowski, M. A. Puthenveedu, M. von Zastrow, Distinct modes of regulated receptor insertion to the somatodendritic plasma membrane. *Nat. Neurosci.* **9**, nn1679 (2006).

25. R. Vistein, M. A. Puthenveedu, Reprogramming of G protein-coupled receptor recycling and signaling by a kinase switch. *Proc. Natl. Acad. Sci.* **110**, 15289–15294 (2013).

26. J. M. Kunselman, A. S. Zajac, Z. Y. Weinberg, M. A. Puthenveedu, Homologous regulation of mu opioid receptor recycling by Gβγ, protein kinase C, and receptor phosphorylation. *Mol. Pharmacol.* **96**, 702–710 (2019).

27. J. M. Kunselman, A. Gupta, I. Gomes, L. A. Devi, M. A. Puthenveedu, Compartment-specific opioid receptor signaling is selectively modulated by different Dynorphin peptides. *eLife*. **10**, e60270 (2021).

28. N. L. Chanaday, E. T. Kavalali, *Mol. Biol. Cell*, in press, doi:10.1091/mbc.e21-04-0213.

29. D. Axelrod, Total internal reflection fluorescence microscopy in cell biology. *Traffic*. **2**, 764–774 (2001).

30. M. von Zastrow, B. K. Kobilka, Ligand-regulated internalization and recycling of human beta 2-adrenergic receptors between the plasma membrane and endosomes containing transferrin receptors. *J. Biol. Chem.* **267**, 3530–3538 (1992).

31. J. T. Williams, S. L. Ingram, G. Henderson, C. Chavkin, M. von Zastrow, S. Schulz, T. Koch, C. J. Evans, M. J. Christie, Regulation of μ-opioid receptors: desensitization, phosphorylation, internalization, and tolerance. *Pharmacol. Rev.* **65**, 223–254 (2013).

32. S. L. Bowman, A. L. Soohoo, D. J. Shiwarski, S. Schulz, A. A. Pradhan, M. A. Puthenveedu, Cell-autonomous regulation of mu-Opioid receptor recycling by substance P. *Cell Reports*. **10**, 1925–1936 (2015).

33. S. Sposini, F. G. Jean-Alphonse, M. A. Ayoub, A. Oqua, C. West, S. Lavery, J. J. Brosens, E. Reiter, A. C. Hanyaloglu, Integration of GPCR signaling and sorting from very early endosomes via opposing APPL1 mechanisms. *Cell Reports*. **21**, 2855–2867 (2017).

34. M. Martineau, A. Somasundaram, J. B. Grimm, T. D. Gruber, D. Choquet, J. W. Taraska, L. D. Lavis, D. Perrais, Semisynthetic fluorescent pH sensors for imaging exocytosis and endocytosis. *Nat. Commun.* **8**, 1412 (2017).

35. M. Bakr, D. Jullié, J. Krapivkina, V. Paget-Blanc, L. Bouit, J. D. Petersen, N. Retailleau, C. Breillat, E. Herzog, D. Choquet, D. Perrais, The vSNAREs VAMP2 and VAMP4 control recycling and intracellular sorting of post-synaptic receptors in neuronal dendrites. *Cell Reports*. **36**, 109678 (2021).

36. K. Balabanian, A. Levoye, L. Klemm, B. Lagane, O. Hermine, J. Harriague, F. Baleux, F. Arenzana-Seisdedos, F. Bachelerie, Leukocyte analysis from WHIM syndrome patients reveals a pivotal role for GRK3 in CXCR4 signaling. *J. Clin. Invest.* **118**, 1074–1084 (2008).

37. P. Y. Sato, J. K. Chuprun, M. Schwartz, W. J. Koch, The evolving impact of G protein-coupled receptor kinases in cardiac health and disease. *Physiol. Rev.* **95**, 377–404 (2015).

38. D. J. Shiwarski, A. Tipton, M. D. Giraldo, B. F. Schmidt, M. S. Gold, A. A. Pradhan, M. A. Puthenveedu, A PTEN-regulated checkpoint controls surface delivery of δ opioid receptors. *J. Neurosci.* **37**, 3741–3752 (2017).

39. D. J. Shiwarski, S. E. Crilly, A. Dates, M. A. Puthenveedu, Dual RXR motifs regulate nerve growth factor-mediated intracellular retention of the delta opioid receptor. *Mol. Biol. Cell*. **30**, 680–690 (2019).

40. S. E. Crilly, W. Ko, Z. Y. Weinberg, M. A. Puthenveedu, Conformational specificity of opioid receptors is determined by subcellular location irrespective of agonist. *eLife*. **10**, e67478 (2021).

41. A. H. Hutagalung, P. J. Novick, Role of Rab GTPases in membrane traffic and cell physiology. *Physiol. Rev.* **91**, 119–49 (2011).

42. T. Galli, T. Chilcote, O. Mundigl, T. Binz, H. Niemann, P. D. Camilli, Tetanus toxin-mediated cleavage of cellubrevin impairs exocytosis of transferrin receptor-containing vesicles in CHO cells. *J. Cell Biol.* **125**, 1015–1024 (1994).

43. Y. Gu, R. L. Huganir, Identification of the SNARE complex mediating the exocytosis of NMDA receptors. *Proc. Natl. Acad. Sci.* **113**, 12280–12285 (2016).

44. F. Filippini, S. Nola, A. Zahraoui, K. Roger, M. Esmaili, J. Sun, J. Wojnacki, A. Vlieghe, P. Bun, S. Blanchon, J.-C. Rain, J.-M. Taymans, M.-C. Chartier-Harlin, C. Guerrera, T. Galli, Secretion of VGF relies on the interplay between LRRK2 and post-Golgi v-SNAREs. *Cell Reports*. **42**, 112221 (2023).

45. T. Galli, P. S. McPherson, P. D. Camilli, The V0 sector of the V-ATPase, synaptobrevin, and synaptophysin are associated on synaptic vesicles in a Triton X-100-resistant, freeze-thawing sensitive, complex. *J. Biol. Chem.* **271**, 2193–8 (1996).

46. M. A. Cousin, Synaptophysin-dependent synaptobrevin-2 trafficking at the presynapse-mechanism and function. *J. Neurochem.* **159**, 78–89 (2021).

47. B. Cheatham, A. Volchuk, C. R. Kahn, L. Wang, C. J. Rhodes, A. Klip, Insulin-stimulated translocation of GLUT4 glucose transporters requires SNARE-complex proteins. *Proc. Natl. Acad. Sci.* **93**, 15169–15173 (1996).

48. J. S. Bogan, Regulation of glucose transporter translocation in health and diabetes. *Annu. Rev. Biochem.* **81**, 507–532 (2012).

49. S. Jurado, D. Goswami, Y. Zhang, A. J. M. Molina, T. C. Südhof, R. C. Malenka, LTP requires a unique postsynaptic SNARE fusion machinery. *Neuron*. **77**, 542–558 (2013).

50. B. Simonetti, P. J. Cullen, Actin-dependent endosomal receptor recycling. *Curr. Opin. Cell Biol.* **56**, 22–33 (2019).

51. T. T. Cao, H. W. Deacon, D. Reczek, A. Bretscher, M. von Zastrow, A kinase-regulated PDZ-domain interaction controls endocytic sorting of the beta2-adrenergic receptor. *Nature*. **401**, 286–90 (1999).

52. B. E. L. Lauffer, S. Chen, C. Melero, T. Kortemme, M. von Zastrow, G. A. Vargas, Engineered protein connectivity to actin mimics PDZ-dependent recycling of G protein-coupled receptors but not its regulation by Hrs. *J. Biol. Chem.* **284**, 2448–2458 (2009).

53. B. E. L. Lauffer, C. Melero, P. Temkin, C. Lei, W. Hong, T. Kortemme, M. von Zastrow, SNX27 mediates PDZ-directed sorting from endosomes to the plasma membrane. *J. Cell Biol.* **190**, 565–574 (2010).

54. G. Romero, M. von Zastrow, P. A. Friedman, Role of PDZ proteins in regulating trafficking, signaling, and function of GPCRs: means, motif, and opportunity. *Adv. Pharmacol.* **62**, 279–314 (2011).

55. F. R. Maxfield, T. E. McGraw, Endocytic recycling. *Nat. Rev. Mol. Cell Biol.* **5**, 121–132 (2004).

56. M. Tanowitz, M. von Zastrow, A novel endocytic recycling signal that distinguishes the membrane trafficking of naturally occurring opioid receptors. *J. Biol. Chem.* **278**, 45978–45986 (2003).

57. A. L. Soohoo, M. A. Puthenveedu, Divergent modes for cargo-mediated control of clathrin-coated pit dynamics. *Mol. Biol. Cell*. **24**, 1725–1734 (2013).

58. R. M. Gage, K.-A. Kim, T. T. Cao, M. von Zastrow, A transplantable sorting signal that is sufficient to mediate rapid recycling of G protein-coupled receptors. *J. Biol. Chem.* **276**, 44712–44720 (2001).

59. M. Tanowitz, J. N. Hislop, M. von Zastrow, Alternative splicing determines the post-endocytic sorting fate of G-protein-coupled receptors. *J. Biol. Chem.* **283**, 35614–35621 (2008).

60. S. Liu, W.-J. Kang, A. Abrimian, J. Xu, L. Cartegni, S. Majumdar, P. Hesketh, A. Bekker, Y.-X. Pan, Alternative pre-mRNA splicing of the mu opioid receptor gene, OPRM1: insight into complex mu opioid actions. *Biomolecules*. **11**, 1525 (2021).

61. N. Marie, I. Lecoq, P. Jauzac, S. Allouche, Differential sorting of human δ-opioid receptors after internalization by peptide and alkaloid agonists. *J. Biol. Chem.* **278**, 22795–22804 (2003).

62. C. J. Traer, A. C. Rutherford, K. J. Palmer, T. Wassmer, J. Oakley, N. Attar, J. G. Carlton, J. Kremerskothen, D. J. Stephens, P. J. Cullen, SNX4 coordinates endosomal sorting of TfnR with dynein-mediated transport into the endocytic recycling compartment. *Nat. Cell Biol.* **9**, 1370–1380 (2007).

63. C. Chen, D. Garcia-Santos, Y. Ishikawa, A. Seguin, L. Li, K. H. Fegan, G. J. Hildick-Smith, D. I. Shah, J. D. Cooney, W. Chen, M. J. King, Y. Y. Yien, I. J. Schultz, H. Anderson, A. J. Dalton, M. L. Freedman, P. D. Kingsley, J. Palis, S. M. Hattangadi, H. F. Lodish, D. M. Ward, J. Kaplan, T. Maeda, P. Ponka, B. H. Paw, Snx3 regulates recycling of the transferrin receptor and iron assimilation. *Cell Metab.* **17**, 343–52 (2012).

64. P. Temkin, B. Lauffer, S. Jäger, P. Cimermancic, N. J. Krogan, M. von Zastrow, SNX27 mediates retromer tubule entry and endosome-to-plasma membrane trafficking of signaling receptors. *Nat. Cell Biol.* **13**, 715–721 (2011).

65. Z. Zurawski, B. Page, M. C. Chicka, R. L. Brindley, C. A. Wells, A. M. Preininger, K. Hyde, J. A. Gilbert, O. Cruz-Rodriguez, K. P. M. Currie, E. R. Chapman, S. Alford, H. E. Hamm, Gβγ directly modulates vesicle fusion by competing with synaptotagmin for binding to neuronal SNARE proteins embedded in membranes. *J. Biol. Chem.* **292**, 12165–12177 (2017).

66. Z. Zurawski, A. D. T. Gray, L. J. Brady, B. Page, E. Church, N. A. Harris, M. R. Dohn, Y. Y. Yim, K. Hyde, D. P. Mortlock, C. K. Jones, D. G. Winder, S. Alford, H. E. Hamm, Disabling the Gβγ-SNARE interaction disrupts GPCR-mediated presynaptic inhibition, leading to physiological and behavioral phenotypes. *Sci. Signal.* **12**, eaat8595 (2019).

67. E. Daro, P. van der Sluijs, T. Galli, I. Mellman, Rab4 and cellubrevin define different early endosome populations on the pathway of transferrin receptor recycling. *Proc. Natl. Acad. Sci.* **93**, 9559–9564 (1996).

68. D. Sheff, L. Pelletier, C. B. O'Connell, G. Warren, I. Mellman, Transferrin receptor recycling in the absence of perinuclear recycling endosomes. *J. Cell Biol.* **156**, 797–804 (2002).

69. J. W. Woods, M. Doriaux, M. G. Farquhar, Transferrin receptors recycle to cis and middle as well as trans Golgi cisternae in Ig-secreting myeloma cells. *J. Cell Biol.* **103**, 277–286 (1986).

70. K. Kubo, M. Kobayashi, S. Nozaki, C. Yagi, K. Hatsuzawa, Y. Katoh, H.-W. Shin, S. Takahashi, K. Nakayama, SNAP23/25 and VAMP2 mediate exocytic event of transferrin receptor-containing recycling vesicles. *Biol. Open*. **4**, 910–920 (2015).

71. X. M. Guan, T. S. Kobilka, B. K. Kobilka, Enhancement of membrane insertion and function in a type IIIb membrane protein following introduction of a cleavable signal peptide. *J. Biol. Chem.* **267**, 21995–21998 (1992).

72. E. Campeau, V. E. Ruhl, F. Rodier, C. L. Smith, B. L. Rahmberg, J. O. Fuss, J. Campisi, P. Yaswen, P. K. Cooper, P. D. Kaufman, A versatile viral system for expression and depletion of proteins in mammalian cells. *PLoS One*. **4**, e6529 (2009).

73. M. He, P. Jenkins, V. Bennett, Cysteine 70 of ankyrin-G is S-palmitoylated and is required for function of ankyrin-G in membrane domain assembly. *J. Biol. Chem.* **287**, 43995–44005 (2012).

74. C. M. Szalinski, A. Labilloy, J. R. Bruns, O. A. Weisz, VAMP7 modulates ciliary biogenesis in kidney cells. *PLoS One*. **9**, e86425 (2014).

75. D. D. Sarbassov, D. A. Guertin, S. M. Ali, D. M. Sabatini, Phosphorylation and regulation of Akt/PKB by the rictor-mTOR complex. *Science*. **307**, 1098–1101 (2005).

76. J. Moffat, D. A. Grueneberg, X. Yang, S. Y. Kim, A. M. Kloepfer, G. Hinkle, B. Piqani, T. M. Eisenhaure, B. Luo, J. K. Grenier, A. E. Carpenter, S. Y. Foo, S. A. Stewart, B. R. Stockwell, N. Hacohen, W. C. Hahn, E. S. Lander, D. M. Sabatini, D. E. Root, A lentiviral RNAi library for human and mouse genes applied to an arrayed viral high-content screen. *Cell*. **124**, 1283–1298 (2006).

77. J. Schindelin, I. Arganda-Carreras, E. Frise, V. Kaynig, M. Longair, T. Pietzsch, S. Preibisch, C. Rueden, S. Saalfeld, B. Schmid, J.-Y. Tinevez, D. J. White, V. Hartenstein, K. Eliceiri, P. Tomancak, A. Cardona, Fiji: an open-source platform for biological-image analysis. *Nat. Methods*. **9**, 676 (2012).

78. R. F. Laine, K. L. Tosheva, N. Gustafsson, R. D. M. Gray, P. Almada, D. Albrecht, G. T. Risa, F. Hurtig, A.-C. Lindås, B. Baum, J. Mercer, C. Leterrier, P. M. Pereira, S. Culley, R. Henriques, NanoJ: a high-performance open-source super-resolution microscopy toolbox. *J. Phys. D*. **52**, 163001 (2019).

79. F. Pedregosa, G. Varoquaux, A. Gramfort, V. Michel, B. Thirion, O. Grisel, M. Blondel, P. Prettenhofer, R. Weiss, V. Dubourg, J. Vanderplas, A. Passos, D. Cournapeau, M. Brucher, M. P. and É. Duchesnay, Scikit-learn: machine learning in Python. *JMLR*, 2825–2830 (2011).

80. Z. Weinberg, Mixed pop: public release. doi:10.5281/zenodo.6626090 (2022).

Chapter 3: Molecular Basis of VAMP2's Cargo-Selectivity

Abstract

In the previous Chapter, we discussed that the finding of VAMP2's specificity towards MOR recycling was likely resulted from co-sorting of MOR and VAMP2 on the endosomes. However, whether and how v-SNAREs are sorted is still mostly unknown. Here, by performing a series of high- to super-resolution microscopy assays, we provide evidence for the existence of sub-endosomal sorting of v-SNAREs and propose a sequence-directed sorting mechanism of VAMP2. First, using SRRF-deconvolved confocal imaging reaching super-resolution, we showed that VAMP2 and VAMP7 exhibited sub-endosomal segregation on distinct tubular structures. Next, through monitoring the colocalization between sequence-truncated VAMP2 mutants and MOR in fusion events in real-time, we found that VAMP2's endosomal sorting required both its distant N-terminal sequence as well as its SNARE coiled-coil motif. Finally, by transplanting VAMP2's N-terminus and SNARE motif to VAMP7, we showed that these two sequences were sufficient to restore VAMP2's sorting itinerary in a hierarchical manner. These results reveal novel mechanistic insights on v-SNAREs' sorting and trafficking.

Introduction

Endosomal sorting plays a crucial role in cellar trafficking by determining the destiny of in-traffic cargo molecules. Plasma membrane proteins internalized to the endosomes through the endocytic pathways are sorted to be either retained for degradation later in the lysosomes, further

trafficked to other intracellular compartments such as the Golgi apparatus, or recycled back to the plasma membrane (*1–3*). For plasma membrane-resident G protein-coupled receptors (GPCRs), endosomal sorting enables spatiotemporal regulation of their trafficking and signaling (*4–7*).

Canonical GPCRs such as the β2 adrenergic receptor (B2AR) and the μ opioid receptor (MOR) are recycled following sorting onto specific sub-endosomal microdomains. Recycling of B2AR is regulated by a hierarchical mechanism. Once on the endosomes, protein kinase A-mediated phosphorylation of serine-345 and -346 of B2AR's C-terminal tail prevents it from entering the "fast" recycling pathway (*8*, *9*). Next, the interaction between B2AR's distal C-terminal PSD95-Dlg-ZO-1 (PDZ) ligand and endosomal PDZ protein sorting nexin 27 (SNX27) sorts B2AR to actin-rich, retromer-presented tubules called the ASRT (actin-SNX27-retromer tubular) domains (*10–13*). And from the ASRT domains B2AR is packaged into vesicles and trafficked back to the plasma membrane. On the other hand, MOR does not possess a PDZ ligand but instead depends on a C-terminal bi-leucine sequence (Leu-Glu-Asn-Leu-Glu-Ala-Glu) for its recycling (*14*). Although both B2AR and MOR are recycled from Rab4-dependent early endosomes (*13*, *15*, *16*), presumably MOR is recycled from a different subset of microdomains other than ASRT due to its lack of PDZ ligand. In contrast to the GPCR cargoes undergoing strictly-regulated sorting and trafficking, the single-pass nutrient receptor transferrin receptor (TfR) is well-established to be recycled from multiple pathways including the "fast" recycling pathway of early endosomes and the "slow" recycling pathway of Rab11-dependent recycling endosomes (*9*, *11*, *17–19*).

To allow for proper fusion with the targeted membrane, vesicles must be packaged with fusion proteins from the endosomes. And the vesicular fusion proteins might have also undergone sorting just as the cargo molecules. One group of fusion proteins that have vesicular localization

are the v-SNAREs, or vesicular- soluble *N*-ethylmaleimide-sensitive factor (NSF)-attachment receptor proteins, which in the human body include eight members with seven from the vesicle-associated membrane protein (VAMP) family (*20*, *21*). Through a strong interaction with the other two counterparts of the SNARE complex, synaptosome nerve associated proteins and syntaxins, v-SNAREs serve as the vesicular-side anchor that dock the vesicles in close contact (<1 nm) to the plasma membrane (*22*, *23*). Interestingly, multiple v-SNAREs including canonical VAMP2 and uncanonical VAMP1/ 3/ 4/ 7 and Vti1a have all been reported to function in exocytic vesicular trafficking, while showing subtype-dependent specificity for different cargo molecules in distinct biological settings (*19*, *24–30*). The molecular mechanism underlying this cargo-oriented subtype specificity of v-SNAREs, or in general, SNARE assemblies, is still largely unknown. However, one mechanism can potentially be attributed to the endosomal sorting of v-SNAREs, particularly the co-sorting of v-SNAREs and cargo molecules, consequently allowing the cells to assign specific v-SNAREs for specific trafficking pathways.

In the previous Chapter, we showed that VAMP2 was preferentially associated with the vesicular fusion of recycling MOR in HEK293 cells and was required for a full recycling capacity of MOR in PC12 cells and in rat striatal neurons, but was neither associated with nor required for the recycling of B2AR and TfR (*30*). In this Chapter, we performed a series of high- to super-resolution microscopy assays on multiple VAMP2 truncation and chimeric mutants to test both the requirement and the sufficiency of various VAMP2 protein sequences for this cargo-selectivity and found evidence of a sequence-directed endosomal sorting mechanism of VAMP2.

Results

Subcellular localization of v-SNAREs varies on both organellar and sub-organellar levels

We first sought to verify if different v-SNARE subtypes have different subcellular, and more importantly, sub-organellar localization in our cell systems. In HEK293 cells, we found both endogenous VAMP4 (Fig. 3.1 A) and transiently expressed pHuji (a pH-sensitive red fluorescent protein/ RFP mutant with pKa of ~7.6) -tagged VAMP4 (VAMP4-pHuji; Fig. 3.1 B) showed colocalization with the trans-Golgi network (TGN) marker TGN38. On the other hand, in PC12 cells, both endogenous VAMP2 and VAMP7, particularly VAMP7, showed subcellular localization patterns that were distinct from VAMP4 (Fig. 3.1 C and D). To quantify the level of colocalization, we calculated Pearson's coefficient (P) between corresponding channels from auto-thresholded confocal images (Fig. 3.1 F). Images of cells expressing doubly tagged MOR (FLAG-SpH-MOR; SpH: super ecliptic pHluorin, a pH-sensitive green FP/ GFP mutant with pKa of ~7.1) post-agonist induced internalization (20 min treatment of 10 μM [D-Ala^2, *N*-Me-Phe^4, Gly^5-ol]-enkephalin, DAMGO, a full agonist of MOR, at 37 ℃; Fig. 3.1 E) was introduced as a positive control to test the upper limit of this quantification metrics, resulted in an average P ($\bar{P}$)= 0.671 between anti-FLAG antibody labeling and SpH fluorescence (Fig. 3.1 F). The $\bar{P}$ between transiently expressed VAMP4-pHuji and TGN38 appeared to be higher than the $\bar{P}$ between antibody-labelled VAMP4 and TGN38 ($\bar{P}$= 0.327 vs 0.167; Fig. 3.1 F), which can be due to an enhanced colocalization caused by VAMP4 overexpression or a dilution of colocalization caused by background signal from unspecific VAMP4 antibody labeling, or both. Interestingly, compared with the lack of co-localization between endogenous VAMP7 and VAMP4 ($\bar{P}$= 0.050), a moderate co-localization level of $\bar{P}$= 0.115 was observed between endogenous VAMP2 and VAMP4. These results indicate a differential subcellular distribution of v-SNAREs and are in consistent with previous reports, that VAMP2 and VAMP7 are endosomal/ vesicular-localized v-SNAREs (*28*, *30*, *31*), and VAMP4 primarily functions in TGN-to-endosome trafficking (*32*, *33*).

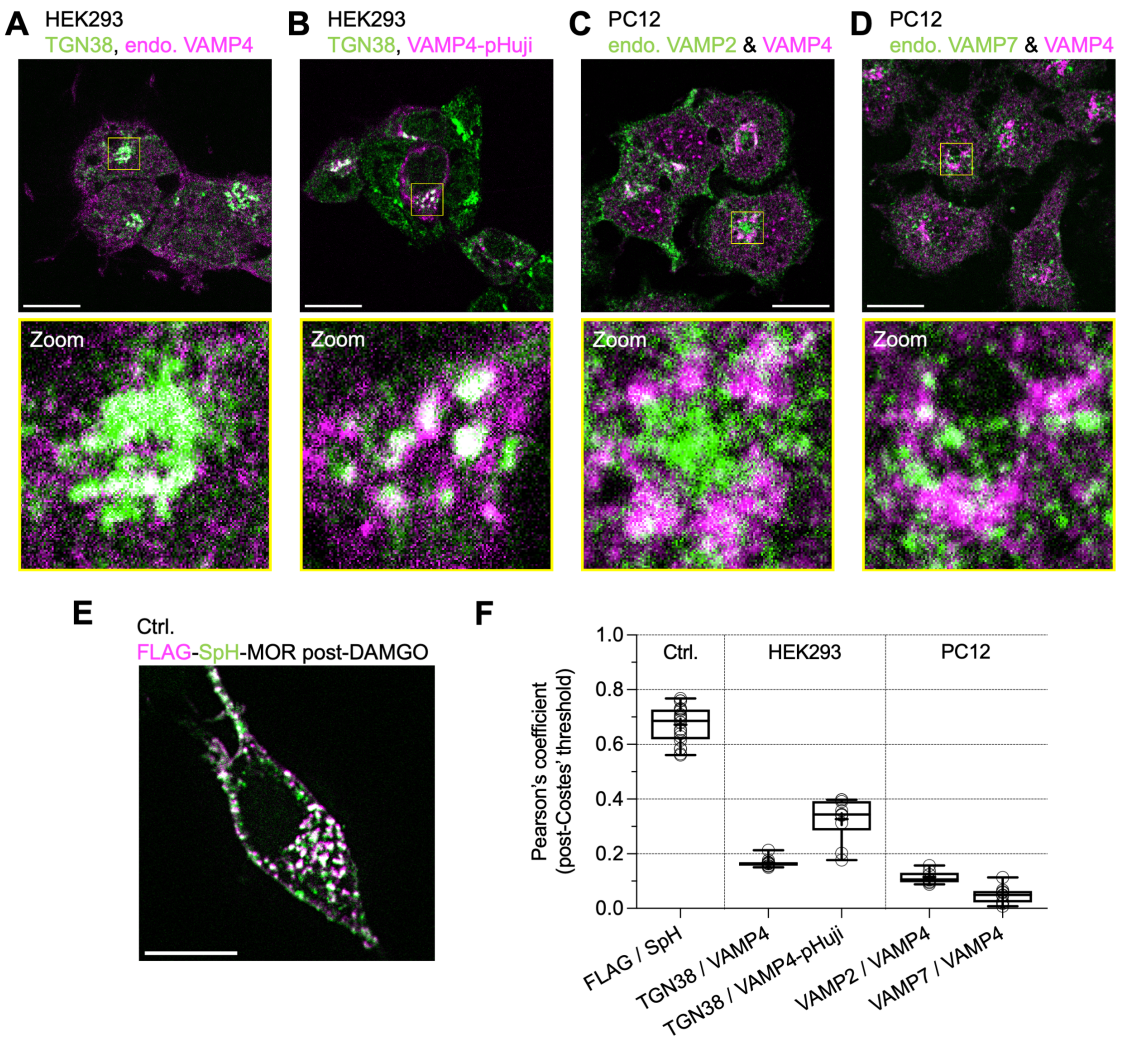

Figure 3.1. The subcellular localization of VAMP4 is different from VAMP2 and VAMP7s'. Representative confocal images showing immunostaining of **A.** TGN38 (green; marking trans-Golgi network) and endogenous, endo., VAMP4 (magenta) in HEK293 cells; **B.** TGN38 (green) in HEK293 cells transiently expressing VAMP4-pHuji (magenta); **C.** endo. VAMP2 (green) and endo. VAMP4 (magenta) in PC12 cells; **D.** endo. VAMP7 (green) and endo. VAMP4 (magenta) in PC12 cells. Enlarged views of the regions highlighted by yellow squares are shown in the bottom "Zoom" panels. Scale bars = 30 µm. **E.** Representative confocal image of a PC12 cell expressing doubly-tagged MOR, FLAG-SpH-MOR, post-20 min 10 µM DAMGO treatment at 37 °C with SpH fluorescence shown in green and anti-FLAG labeling shown in magenta, as a positive control condition for quantifying colocalization. Scale bar = 15 µm. **F.** Colocalization between channels from **A-E** (conditions indicated on the x-axis) quantified as Pearson's coefficient post-Costes' auto-threshold per field (FLAG / SpH control: 20 fields; TGN38 / VAMP4 in HEK293 cells: 11 fields; TGN38 / VAMP4-pHuji in HEK293 cells: 10 fields, VAMP4-pHuji non-expressing cells were excluded from quantification; VAMP2 / VAMP4 in PC12 cells: 9 fields; VAMP7 / VAMP4 in PC12 cells: 9 fields; from 1 experiment). "+" symbols indicate mean.

Given that VAMP2 and VAMP7 showed similar endosomal localization, we then tested whether they would have different localization on a sub-endosomal level. To visualize the sub-diffraction-limit endosomal microdomains, we implemented a microscopy method called super resolution radial fluctuations (SRRF) and acquired real-time deconvolved confocal images with a theoretical resolution of ~90 nm in fixed cell samples (*34*, *35*). SRRF imaging of HEK293 cells transiently expressing EGFP-VAMP7 and VAMP2-pHuji revealed a unique distribution pattern of partially colocalizing on ring-like intracellular compartments (Fig. 3.2 A, left panel). This distribution pattern was not observed in SRRF images of HEK293 cells either expressed of EGFP-VAMP7 and labeled by anti-VAMP7 antibody or expressed of VAMP2-pHuji and labeled by anti-VAMP2 antibody, both instead showing a pattern of overall colocalization (Fig. 3.2 A, middle and right panel, respectively). Next, to mark the endosomal region while visualizing EGFP-VAMP7 and VAMP2-pHuji, we introduced fluorescent-labeled FLAG-MOR post agonist-induced internalization (20 min treatment of 10 μM DAMGO at 37 ℃) as an endosomal marker. In this set of SRRF images, we observed that the internalized FLAG-MOR predominantly colocalized with VAMP2-pHuji (Fig. 3.2 B, orange region of interest, ROI) compared with EGFP-VAMP7 (Fig. 3.2 B, cyan ROI), and these two sets of ROIs were discrete even on intracellular compartments with continuous fluorescence. Finally, to confirm that the compartments we observed were indeed endosomes, we incubated the cells with fluorophore-conjugated Dextran for a limited period of time (20 min at 37 ℃ before fixation), so that through endocytosis Dextran would be loaded into endosomal lumen (but not yet reaching lysosomes) and therefore marking the outlines of the endosomes (see “Cell culture and reagents” in Materials and Methods section of this Chapter for details). SRRF images of HEK293 cells pulsed with Alexa Fluor 647 (AF647) -conjugated Dextran showed endosomal microdomains that exclusively contained either EGFP-VAMP7 or VAMP2-

pHuji (Fig. 3.2 C), providing additional evidence of the differential sub-endosomal localizations of these two v-SNAREs. Together, these results suggest that although VAMP7 and VAMP2 both resided on endosomes, they are associated with different microdomains potentially because of endosomal sorting.

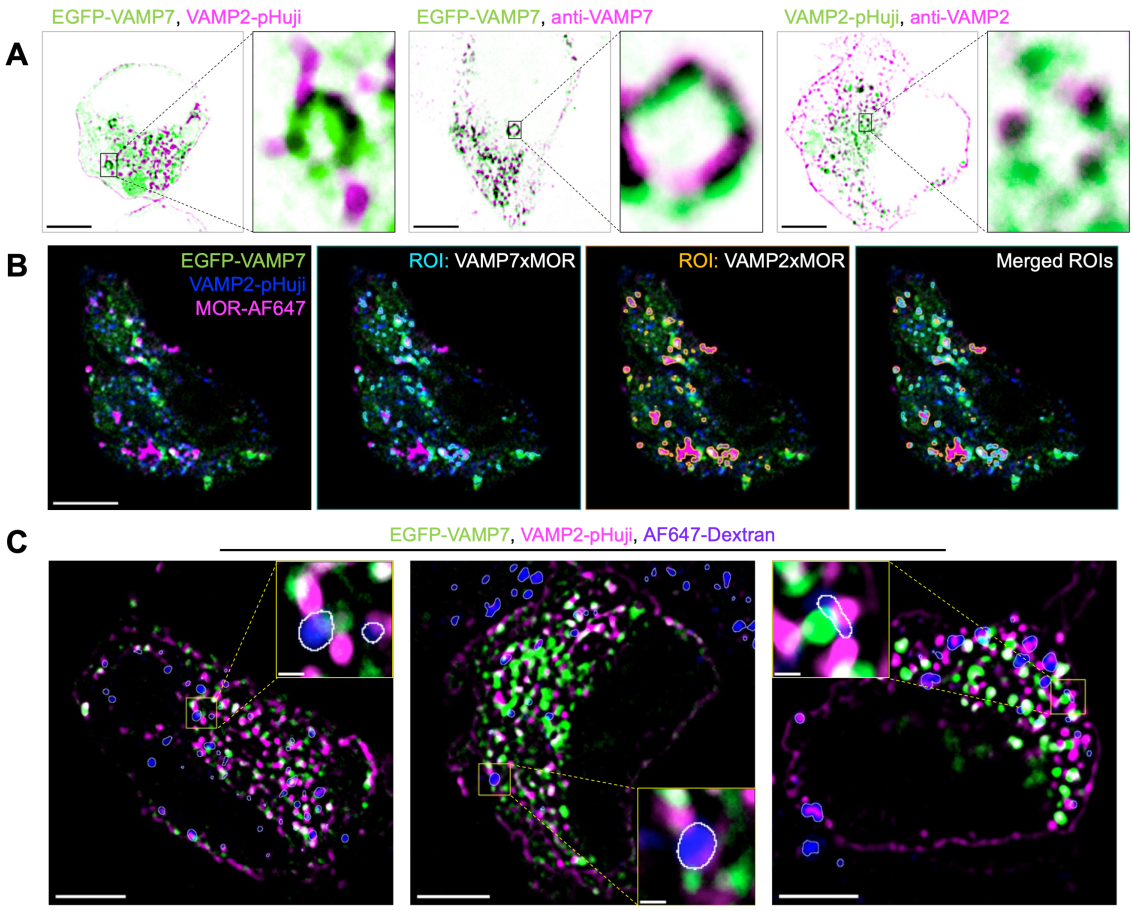

Figure 3.2. The sub-endosomal localization of VAMP2 is different from VAMP7's.
A. Representative super resolution radial fluctuation (SRRF)-deconvolved images of HEK293 cells of different expression and labeling conditions: left: a cell expressing EGFP-VAMP7 (green) and VAMP2-pHuji (magenta) showing different sub-endosomal localizations; middle: a cell expressing VAMP2-pHuji (green) immunostained with anti-VAMP2 antibody (magenta); right: a cell expressing EGFP-VAMP7 (green) immunostained with anti-VAMP7 antibody (magenta), with the latter two conditions not showing resolvable sub-endosomal localization differences. Scale bars = 10 µm. **B.** Representative SRRF image of a HEK293 cell expressing EGFP-VAMP7 (green), VAMP2-pHuji (blue), and FLAG-MOR (immunostained by Alexa Fluor 647-conjugated M1 antibody, called MOR-AF647; magenta) post-20 min 10 µM DAMGO treatment at 37 °C. Cyan-colored region of interest (ROI) marks the fluorescence overlap between EGFP-VAMP7 and internalized FLAG-MOR. Orange-colored ROI marks the fluorescence overlap between VAMP2-pHuji and internalized FLAG-MOR. Scale bar = 10 µm. **C.** Representative SRRF images of

HEK293 cells expressing EGFP-VAMP7 (green) and VAMP2-pHuji (magenta) with endosomal lumen marked by pulsing 1 mg/mL AF647-conjugated Dextran (blue with white outlines) into the cells for 20 min at 37 ℃. Scale bars = 10 μm, inset scale bars = 1 μm.

The N-terminus and SNARE motif of VAMP2 are both required for its preferential association with MOR fusion events

Next, we asked the question of whether the endosomal sorting of v-SNAREs onto different microdomains leads to their cargo-selectivity. We approached this question by examining two sets of VAMP2-pHuji truncation mutants in an experimental setting where wildtype VAMP2 (VAMP2 or VAMP2-WT, used interchangeably) would show preferential association with the fusion events of MOR-containing vesicles during recycling as thoroughly discussed in Chapter 2 (*30*). Briefly, we performed two-channel simultaneous acquisition total internal reflection fluorescence (TIRF) microscopy on HEK293 cells co-expressing SpH-MOR and VAMP2-pHuji. After treating the cells with saturating concentration of DAMGO (12.5 μM), we looked for agonist-induced recycling fusion events of SpH-MOR containing-vesicles and found a robust enrichment of VAMP2-pHuji in those fusion events (median enrichment score >1; enrichment was calculated as fold change of pHuji fluorescence at the peak of a fusion event over baseline fluorescence fluctuation).

Here, we performed the same microscopy assay with VAMP2-pHuji as a positive control alongside two sets of C-terminally pHuji-tagged VAMP2 truncation mutants: ① large motif truncation mutants (Fig. 3.3 A) without either N-terminus (amino acid, AA, 2-30; VAMP2-NtT), SNARE coiled-coil motif (AA 31-91; VAMP2-ScmT), or both (AA 1-91, only transmembrane domain and C-terminus were left intact; VAMP2-CtOnly); ② restricted N-terminal truncation mutants (Fig. 3.3 D) without either AA 2-10 (VAMP2-N2-10T), AA 11-20 (VAMP2-N11-20T), or AA 2-20 (VAMP2-N2-20T). We chose these two sets of truncation mutants to focus on the cytoplasmic protein region of VAMP2.

Right before the two-channel TIRF imaging for fusion events, we monitored the change of surface SpH-MOR fluorescence of cells on the same coverslips before and after the addition of 12.5 μM DAMGO. A continuous decrease in surface SpH fluorescence across time post-DAMGO treatment was observed in the VAMP2-pHuji co-expressing cells, and no significant differences in either rates or end-point magnitudes of decrease were noticed for the cells that co-expressed VAMP2 truncation mutants, including both the large and the restricted truncation mutants (Fig. 3.3 B and E, respectively). These data indicated that the expression of VAMP2 mutants did not alter the internalization of SpH-MOR. Moreover, no significant inhibition of SpH-MOR's recycling capacity was noticed across all conditions, as we obtained similar total count of fusion events from each condition out of similar sampling size and imaging duration (1 min acquisition per cell; Fig. 3.3 C and F). However, while the high enrichment of VAMP2-pHuji in SpH-MOR fusion events was consistent with that previously observed, neither of the truncation mutants maintained this phenotype, that their median enrichment was around or even below 0 (Fig. 3.3 C and F), indicating that both the SNARE motif and the full sequence of the N-terminus of VAMP2 were required for its association with MOR fusion events. Interestingly, different truncations seemed to cause different degrees of effect, that VAMP2-CtOnly (Fig. 3.3 C; median enrichment scores of VAMP2-WT, -NtT, -ScmT, and -CtOnly, respectively, = 2.645, 0.498, 0.402, and 0.153) and VAMP2-N2-10T (Fig. 3.3 F; median enrichment scores of VAMP2-WT, -N2-10T, -N11-20T, and -N2-20T, respectively, = 0.426, -0.559, -0.062, and -0.115) showed the smallest enrichment scores within their corresponding cohorts of mutants.

As discussed in Chapter 2, even though HEK293 cells lack endogenous expression of VAMP2, we could still observe SpH-MOR's agonist-induced fusion events without the exogenous introduction of VAMP2, indicating the presence of functional compensation of other v-SNARE(s).

Therefore, regardless of whether VAMP2 and the truncation mutants were functioning as part of the fusion machinery for SpH-MOR-containing vesicles or not, the VAMP2 truncation mutants' lack of enrichment, or their absence in vesicles, still suggested that they were not sorted into SpH-MOR-containing vesicles.

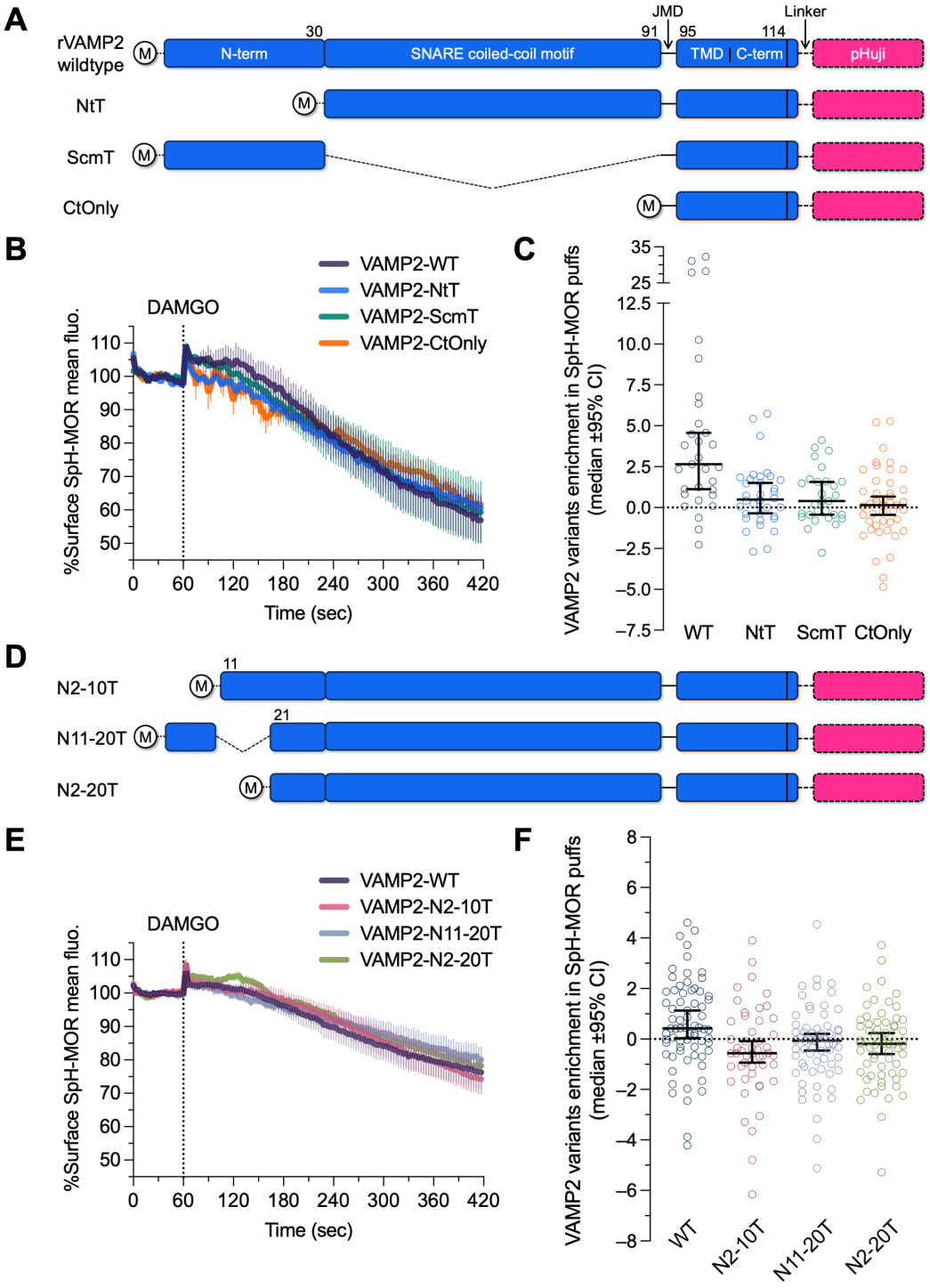

Figure 3.3. Truncation of VAMP2's N-terminus or/and SNARE motif disrupts its preferential association with MOR fusion events.

A. Schematics depicting the protein sequences of pHuji-tagged wildtype rVAMP2 and whole region truncated VAMP2 mutants. The wildtype VAMP2 protein sequence was segmented into N-terminus (amino acid, AA, 2-30; N-term/ Nt), SNARE coiled-coil motif (AA 31-91; Scm), juxta-membrane domain (AA 92-94; JMD), transmembrane domain and C-terminus (AA 95-114;

TMD and C-term/ Ct). pHuji tags were fused to the C-term (lumenal) of VAMP2 proteins via a 12 AA linker. **B.** Time course traces of baseline-normalized surface SpH-MOR mean fluorescence intensity prior to fusion event imaging. HEK293 cells stably expressing SpH-MOR and transiently expressing pHuji-tagged wildtype VAMP2 (VAMP2-WT)/ whole N-term truncated VAMP2 (VAMP2-NtT)/ whole SNARE motif truncated VAMP2 (VAMP2-ScmT)/ VAMP2 left with JMD, TMD, and C-term (VAMP2-CtOnly) were treated with 12.5 μM DAMGO at 37 ℃ after 60 seconds of baseline imaging under TIRF microscopy and tracked for additional 6 min before starting fusion event imaging on cells from the same coverslips (±SEM; 3, 4, 4, 4 cells for WT, NtT, ScmT, CtOnly, respectively; from 1 experiment). **C.** Enrichment quantification of the VAMP2 whole region truncation variants in SpH-MOR fusion events with VAMP2-WT as a positive control. Enrichment score of individual fusion event was calculated as the fold change of pHuji fluorescence at the peak of the event over baseline standard deviation (median ±95% CI; WT: 5 cells, 31 events; NtT: 7 cells, 34 events; ScmT: 6 cells, 30 events; CtOnly: 6 cells, 44 events; from 2 coverslips of 1 experiment). **D.** Schematics depicting the protein sequences of restricted N-term truncation VAMP2-pHuji variants. **E.** Similar time course traces as in **B** showing the baseline-normalized surface SpH-MOR mean fluorescence of HEK293 cells co-expressing SpH-MOR and AA 2-10 truncated VAMP2 (VAMP2-N2-10T), AA 11-20 truncated VAMP2 (VAMP2-N11-20T), or AA 2-20 truncated VAMP2 (VAMP2-N2-20T) following the same treatment and imaging schemes (±SEM; 9, 9, 8, 12 cells for WT, N2-10T, N11-20T, N2-20T, respectively; from 2 experiments). **F.** Similar enrichment quantification as in **C** but for VAMP2 restricted N-term truncation variants (median ±95% CI; WT: 19 cells, 69 events; N2-10T: 16 cells, 49 events; N11-20T: 16 cells, 63 events; N2-20T: 14 cells, 64 events; from 2 experiments).

VAMP7 gains VAMP2's sorting itinerary only after transplanted with both VAMP2's N-terminus and SNARE motif

Since we concluded that both the N-terminus and the SNARE motif were required for VAMP2's normal endosomal sorting, we then asked whether these two protein regions were sufficient to transform other v-SNAREs into a VAMP2-like phenotype. We chose VAMP7 as the major chimeric candidate because VAMP7 and VAMP2 showed different sub-endosomal localization (Fig. 3.1 D and F, Fig. 3.2) and association with MOR recycling fusion events (Fig. 3.4 A and Fig. 3.3 C and F; median enrichment score of VAMP7-pHuji in SpH-MOR fusion events = 0.109). Interestingly, VAMP7-pHuji exhibited a relative preference for transferrin receptor's (TfR) fusion events (Fig. 3.4 A; median enrichment score in TfR-SpH fusion events = 0.780), confirming the involvement of VAMP7 in exocytosis in our cell system.

We generated three C-terminally pHuji-tagged chimeric constructs by swapping VAMP7's protein regions with the ones from VAMP2 (Fig. 3.4 B): VAMP7 with VAMP2's N-terminus (VAMP2 AA 1-30 replacing VAMP7 AA 1-124, with the rest of the protein sequence from VAMP7, same applied to following chimeras; V2N-VAMP7); VAMP7 with VAMP2's SNARE motif (VAMP2 AA 31-91 replacing VAMP7 AA 125-185); VAMP7 with both VAMP2's N-terminus and SNARE motif (VAMP2 AA 1-91 replacing VAMP7 AA 1-185; V2NS-VAMP7). Next, we asked the question of whether these chimeras would display similar sub-endosomal localization as VAMP2. Using VAMP2-EGFP (C-terminally tagged) as a marker for normal VAMP2 localization, we co-expressed HEK293 cells with pHuji-tagged chimeras and analyzed for their colocalization levels, alongside the expression of VAMP2-WT as a positive control and VAMP7-WT as a negative control. SRRF-deconvolved confocal images of the co-expressing cells revealed high colocalization levels between VAMP2-EGFP and pHuji-tagged VAMP2-WT or V2NS-VAMP7, low levels with VAMP7-WT or V2S-VAMP7, and a moderate level with V2N-VAMP7 (Fig. 3.4 C). These observations were recapitulated by the quantification of $\bar{P}$ (Fig. 3.4 D; = 0.4543, -0.0074, 0.1655, -0.0058, 0.3005 for VAMP2-WT, VAMP7-WT, V2N-VAMP7, V2S-VAMP7, and V2NS-VAMP7, respectively), suggesting that VAMP2's N-terminus alone was sufficient to convert VAMP7 into VAMP2's sub-endosomal localization, potentially due to change in endosomal sorting. Moreover, VAMP7's sub-endosomal localization was further converted at the co-transplantation of VAMP2's SNARE motif, indicating the SNARE motif could facilitate the potential sorting process when the N-terminus was present (Fig. 3.4 E).

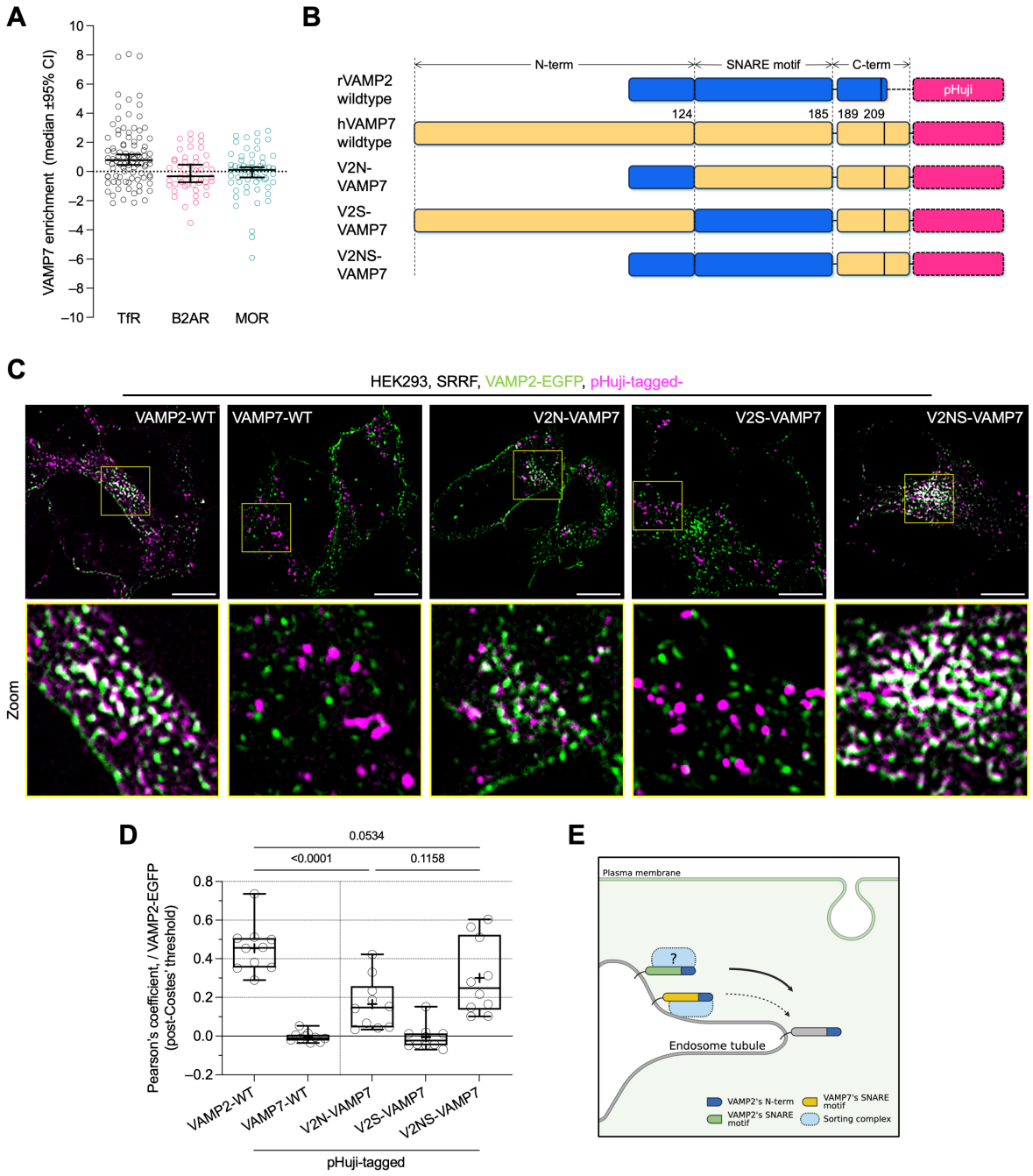

Figure 3.4. VAMP2's N-term is sufficient to mediate sorting, and the SNARE motif facilitates. **A.** Enrichment quantification of VAMP7-pHuji in fusion events of different receptor cargoes. Fusion events of SpH-tagged transferrin receptor (TfR) were recorded at baseline. Fusion events of SpH-tagged β2 adrenergic receptor (B2AR) or SpH-MOR were recorded after 6 min treatment of 12.5 µM isoproterenol or DAMGO, respectively, at 37 °C. All SpH-tagged receptor cargoes and VAMP7-pHuji were expressed in HEK293 cells transiently. Enrichment scores were calculated as described above. VAMP7-pHuji showed preferential association with TfR but not with B2AR or MOR (median ±95% CI; TfR: 3 cells, 91 events; B2AR: 12 cells, 46 events; MOR: 12 cells, 60 events; from 1 experiment). **B.** Schematics depicting the protein sequences of pHuji-tagged

VAMP2-WT, wildtype hVAMP7 (VAMP7-WT), and VAMP2-VAMP7 chimeras. Similar to VAMP2, wildtype VAMP7 protein sequence was segmented into N-term (AA 1-124), SNARE motif (AA 125-185), and the rest of the sequence in together referred as C-term. 3 chimeras were generated: VAMP7 with VAMP2's N-term (V2N-VAMP7), VAMP7 with VAMP2's SNARE motif (V2S-VAMP7), and VAMP7 with VAMP2's N-term and SNARE motif (V2NS-VAMP7). pHuji tags were fused to the C-term of VAMP proteins through a 12 AA linker. **C.** Representative SRRF-deconvolved confocal images of HEK293 cells transiently expressing VAMP2-EGFP (C-term EGFP) and pHuji-tagged VAMP proteins and chimeras as depicted in **B**. Enlarged views of the regions highlighted by yellow squares are shown in the bottom "Zoom" panels. Scale bars = 15 μm. **D.** Colocalization between VAMP2-EGFP and pHuji-tagged VAMP proteins and chimeras (indicated on the x-axis) from images of **C** quantified as Pearson's coefficient post-Costes' auto-threshold per field (10 fields for all conditions; from 1 experiment; One-way ANOVA, post-hoc Tukey test). "+" symbols indicate mean. **E.** Schematics of a proposed model on the sequence requirement of VAMP2's endosomal sorting. VAMP2's N-term is sufficient to partially drive VAMP7 into a VAMP2-like endosomal sorting itinerary. And this transformation is more prominent when VAMP2's SNARE motif is also present, indicating that VAMP2's SNARE motif can potentially facilitate the sorting process.

Since VAMP2 is an exocytosis-mediating v-SNARE and can be delivered to the plasma membrane following endosomal sorting, we then asked whether the chimeras could be delivered to the plasma membrane as well. Through confocal and TIRF imaging of HEK293 cells expressing pHuji-tagged VAMP proteins and chimeras at baseline equilibrium state, we found that while VAMP2-WT and V2NS-VAMP7 showed both intracellular and plasma membrane localization, VAMP7-WT, V2N-VAMP7, and V2S-VAMP7 showed exclusive intracellular localization (Fig. 3.5 A). Next, we chased the plasma membrane localized VAMP proteins through live-labeling the cells with AF647-conjugated anti-RFP antibody for 10 min at 37 ℃. This method allowed us to only label plasma membrane localized VAMP proteins with their C-terminal pHuji-tags exposed to the extracellular antibody. Consistent with our baseline data, confocal imaging of the live-labeled cells showed that VAMP2-WT and V2NS-VAMP7 were both abundantly labeled by the anti-RFP antibody, showcasing their exocytic activities (Fig. 3.5 B). On the other hand, VAMP7-WT and V2S-VAMP7 showed minimal anti-RFP labeling, despite the fact that the protein expression levels across variants were comparable, indicating their lack of constitutive exocytosis (Fig. 3.5 B). Surprisingly, V2N-VAMP7 expressing cells were also abundantly labeled, even

though most of the labeling appeared as intracellular puncta (Fig. 3.5 B). This result suggested that V2N-VAMP7 was delivered to the plasma membrane during the labeling period, but presumably due to rapid internalization it did not form a stable pool on the plasma membrane.

To confirm that the anti-RFP labeling of V2N-VAMP7 was due to its constitutive cycling between intracellular compartments and plasma membrane, in parallel to 37 ℃ we also performed the same labeling scheme but at 4 ℃ to achieve a condition where during the labeling period both the exocytic and endocytic activities of the cells were inhibited. Confocal imaging of HEK293 cells expressing pHuji-tagged VAMP proteins live-labeled by anti-RFP antibody for 15 min at 4 ℃ showed that the labeling of VAMP2-WT and V2NS-VAM7 were restricted to the stable plasma membrane pools and no intracellular puncta were observed, indicating the successful inhibition of trafficking (Fig. 3.5 B). We quantified the anti-RFP labeling levels across conditions using mean AF647 fluorescence and found that in comparison to 37 ℃, the labeling level of V2N-VAMP7 at 4 ℃ was significantly lower (Fig. 3.5 B and C; $p=0.0040$), indicating that the relatively high level of labeling we observed for V2N-VAMP7 at 37 ℃ was indeed due to its transient cycling. On the other hand, we found no significant difference in the labeling levels of V2NS-VAMP7 compared between labeling temperatures (Fig. 3.5 C; $p=0.8402$), indicating that the additional introduction of VAMP2's SNARE motif could stabilize VAMP proteins' plasma membrane localization. These data in together suggested that the sorting mediated by VAMP2's N-terminus was sufficient to target VAMP7 proteins for exocytosis, but without the presence of VAMP2's SNARE motif the VAMP7 proteins could not stably reside on the plasma membrane due to higher internalization rate (Fig. 3.5 D).

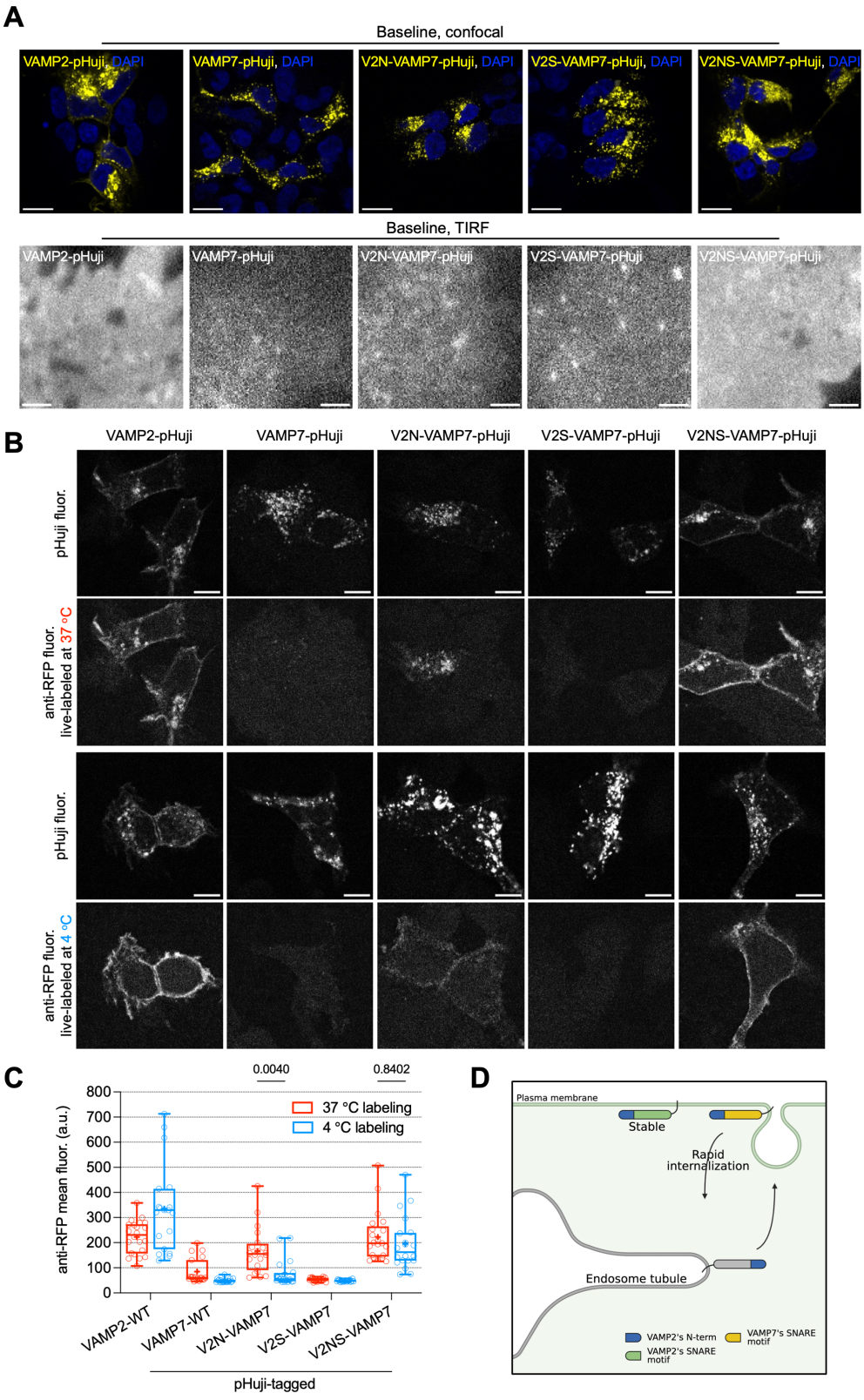

Figure 3.5. Chimeric VAMP7 with VAMP2's N-term and SNARE motif can stably localize on the plasma membrane.

A. Representative confocal (upper panels; fixed cells) and TIRF (bottom panels; live cells) images of HEK293 cells transiently expressing pHuji-tagged VAMP2-WT, VAMP7-WT, and VAMP2-VAMP7 chimeras acquired at baseline, showing that only VAMP2-WT and V2NS-VAMP7 were stably localized on the plasma membrane (PM). Scale bars = 30 μm for confocal images, and 5 μm for TIRF images. Images were background-subtracted and contrasted. **B.** Representative confocal images of HEK293 cells with the same expression conditions as in **A** but were incubated with AF647-conjugated anti-RFP antibody for either 10 min at 37 ℃ (top panels) or 15 min at 4 ℃ (bottom panels) to label pHuji-tags at the PM before fixation, showing that V2N-VAMP7 could only be labelled by anti-RFP antibody at 37 ℃ when trafficking was not inhibited. Images were background-subtracted, corresponding channels of same fluorescence were equally contrasted. Scale bars = 20 μm. **C.** PM levels of the pHuji-tagged VAMP proteins (indicated on the x-axis) from **B** quantified as mean anti-RFP fluorescence intensity per field (arbitrary unit, a.u.; for VAMP2-WT, VAMP7-WT, V2N-VAMP7, V2S-VAMP7, and V2NS-VAMP7, respectively: 37 ℃ labeling: 22, 19, 20, 19, 21 fields; 4 ℃ labeling: 19, 20, 20, 20, 20 fields; from 1 experiment), showing that the labeling temperature significantly impacted the anti-RFP labeling levels of V2N-VAMP7 but not V2NS-VAMP7 (Two-way ANOVA, post-hoc Šídák test, 37 vs 4 ℃: VAMP2-WT: $p<0.0001$, VAMP7-WT: $p=0.6275$, V2N-VAMP7: $p=0.0040$, V2S-VAMP7: $p>0.9999$, V2NS-VAMP7: $p=0.8402$). "+" symbols indicate mean. **D.** Schematics of a proposed model on VAMP2's PM localization. The endosomal sorting driven by VAMP2's N-term targets VAMP proteins to the PM. However, if the VAMP protein only has VAMP2's N-term, like the case of V2N-VAMP7, the delivered protein cannot stably localize on the PM due to rapid internalization. Only when VAMP2's SNARE motif is also present, like the case of VAMP2-WT or V2NS-VAMP7, the VAMP proteins can stably localize on the PM.

Discussion

In this Chapter, we have shown that the VAMP proteins not only show subcellular localization differences but also sub-endosomal localization differences. Further investigation using truncated and chimeric mutants reveals that the full sequence of N-terminus and SNARE motif of VAMP2 (AA 2-91) are not only required for its proper sorting, but also sufficient to transform VAMP7 into a similar sorting itinerary. Moreover, VAMP2's SNARE motif can both facilitate the N-terminus-mediated sorting and stabilize VAMP2 on the cell surface.

It is well-known that VAMP subtypes can display subcellular localization differences in correspondence to their functions (*30*, *32*, *33* and Fig. 3.1), and it is also known that VAMPs can mediate exocytic trafficking in a cargo-specific manner even when they share similar subcellular localization (*26*, *29*, *30*, *36*). We hypothesize that one of the mechanisms contributing to such

specificity is through spatial regulation, that VAMPs can be differentially sorted onto endosomal sub-structures of distinct biochemical compositions and properties (*11*, *13*, *37–39*). However, due to the technical difficulties of accurately imaging endosomal sub-structures, data regarding the sub-endosomal segregation of VAMPs are rarely found. We attempt to solve these challenges by enhancing microscopy resolution using SRRF and by marking endosomes using multiple methods. Our data provide evidence showing that the endosome-localized VAMP2 and VAMP7 (Fig. 3.1) indeed reside on different sub-structures (Fig. 3.2), proving truth to our hypothesis.

Previous studies have shown that through swapping the entire cytoplasmic domain between Golgi-localized VAMP4 and endosome- and plasma membrane-localized VAMP5 can bidirectionally interchange their subcellular localization (*33*), and the addition of VAMP2's cytoplasmic domain (AA 1-93) to TfR's N-terminal end can retarget the nonpolarized TfR to an axonal distribution in primary hippocampal neurons (*40*), indicating that the cytoplasmic domains of VAMPs possess subcellular-targeting functions. The question remains whether the cytoplasmic domains are also responsible for sub-endosomal sorting. Our results indicate that the full cytoplasmic domain of VAMP2, including the full range of N-terminus (AA 2-30) and the SNARE motif (AA 31-91), are both indispensable for VAMP2's proper sub-endosomal sorting.

Interestingly, although the truncation of either N-terminus or SNARE motif abolished VAMP2's preferential association with MOR fusion events (Fig. 3.3 C), transplantation of N-terminus alone was sufficient to induce a VAMP2-like endosomal sorting itinerary for VAMP7, while the transplantation of SNARE motif alone could not (Fig. 3.4 C and D). It is possible that the sub-endosomal sorting and vesicle-targeting are two separate processes, with the latter still requiring the presence of the SNARE motif. This means that even when VAMP2 has the right sub-endosomal localization, without the SNARE motif it is still not assured to be co-packaged into

vesicles alongside the cargoes. An early study on the sequence requirement for VAMP2's vesicle-targeting in PC12 cells identified two impactful sequences in the SNARE motif, AA 41-50 and 61-70, that the truncation of AA 41-50 significantly decreased VAMP2's vesicle-targeting, while the truncation of AA 61-70 elicited opposite effect of significant enhancement (*41*). This auto-inhibitory effect of AA 61-70 was also reported in hippocampal neurons (*40*). Nevertheless, due to technical limitations, these previous reports did not have the resolution to distinguish between endosomal sorting and vesicle biogenesis. Therefore, to confidently draw the conclusion on the hierarchical functionality of VAMP2's N-terminus and SNARE motif, future studies of careful design are required.

It was also interesting to observe that V2N-VAMP7 was also able to be labeled by the anti-RFP antibody (Fig. 3.5 B and C), given that at baseline it did not seem to localize to the plasma membrane to a similar degree as VAMP2-WT and V2NS-VAMP7 (Fig. 3.5 A and B). The fact that most of the anti-RFP labeling was inside the cells (Fig. 3.5 B) indicated V2N-VAMP7 was delivered to the plasma membrane at certain point during the labeling process but was rapidly internalized afterwards. It has been previously reported that VAMP2 might play a critical role in the exocytosis-coupled fast retrieval of vesicles at neuronal synapses for the cycling of fusion machinery, though the exact molecular mechanism of this process is still unknown (*42–44*). Our data support this model as we could also observe internalized anti-RFP labeling for VAMP2-WT and V2NS-VAMP2 (Fig. 3.5 B). However, there seemed to be major dynamic differences between the internalization rate of V2N-VAMP7 and VAMP2-WT or V2NS-VAMP7, as the latter two showed stable plasma membrane anti-RFP labeling which was absent for the former (Fig. 3.5 B). This difference can be explained if endocytosis mediation is a common property of v-SNAREs and can be regulated by their SNARE motifs. It is possible that the SNARE complex formed by

VAMP7 produces a weaker membrane clamping in comparison to the SNARE complex formed by VAMP2, leading to a lower retention burden and faster internalization rate.

It has been long proposed that the SNARE complex could only mediate fusion when forming the "correct" assemblies (*45–48*). Although it is not clear what the cognate t-SNAREs of VAMP7 are in HEK293 cells, the data of V2N-VAMP7 successfully being delivered to the plasma membrane at least indicated the overexpression of v-SNARE protein containing VAMP7's SNARE motif was not inhibiting membrane fusion. These data, together with the positive association VAMP7-pHuji exhibited with TfR-SpH fusion events (Fig. 3.4 A), showcased the fusion capability of VAMP7 in HEK293 cells. Accordingly, the absence of plasma membrane localization of VAMP7-WT and V2S-VAMP7 (Fig. 3.5 A and B) could only be explained as they were not sorted onto a releasable pathway. Therefore, we propose that the N-terminus of VAMP2 is the primary sorting sequence governing its endosomal sorting. As to how VAMP2's SNARE motif could seemingly facilitate the transformation of VAMP7's sorting itinerary, (Fig. 3.4 C and D) we provide three potential explanations: ① based on the hierarchical functionality model, with the presence of VAMP2's SNARE motif, the chimeric v-SNARE was packaged into a distinct pool of exocytic vesicles characteristically closer to the pool VAMP2-WT are packaged into, thus providing additional vesicular colocalization; ② based on the stronger plasma membrane retention model, the increased colocalization was due to additional plasma membrane localization; ③ the SNARE motif is an auxiliary sorting sequence that it was also able to interact with the unknown sorting complex, and by providing structural integrity to facilitate sorting. Unfortunately, our current knowledge cannot exclude any of the possibilities and this question is open for future investigations.

Materials and Methods

Plasmid cloning

Wildtype VAMP2-pHuji, SpH-MOR, FLAG-SpH-MOR, TfR-SpH, and SpH-B2AR plasmids are described in "Plasmid cloning and lentivirus production" in Materials and Methods section of Chapter 2. EGFP-VAMP7 plasmid expressing human VAMP7 was a gift from Thierry Galli (Addgene, #42316). VAMP7-pHuji plasmid was cloned by ligating a VAMP7-pHuji DNA fragment (synthesized by Twist Bioscience) with pmCherry-N1 backbone of VAMP2-pHuji between NheI and NotI sites. All plasmids encoding pHuji-tagged VAMP2 truncation mutants (including both the whole motif truncations and N-terminal restricted sequence truncations) were cloned by site-directed mutagenesis on the VAMP2-pHuji plasmid using Q5 DNA polymerase (M0492, NEB). Primer pairs used to generate these plasmids are summarized in Table 3.1. All plasmids encoding pHuji-tagged VAMP2-VAMP7 chimeric mutants were cloned by ligating the chimeric DNA fragments (synthesized by GenScript) with the VAMP2-pHuji backbone between SacI and AgeI sites. VAMP2-EGFP plasmid was cloned by swapping pHuji from the VAMP2-pHuji plasmid with EGFP from the EGFP-VAMP7 plasmid between AgeI and NotI sites, where the NotI site was introduced to EGFP via PCR reaction.

Table 3.1. Primers used to generate plasmids encoding VAMP2 truncation mutants.

Plasmid	Forward primer (5'-3')	Reverse primer (5'-3')
VAMP2-NtT	AGACTGCAGCAGACC	CATGGTGGCAAGCTTG
VAMP2-ScmT	AACCTCAAGATGATGATC	CCTGTTACTGGTAAGATTTG
VAMP2-CtOnly	AACCTCAAGATGATGATCATC	CATGGTGGCAAGCTTG
VAMP2-N2-10T	GCCGCCCCGGCCGG	CATGGTGGCAAGCTTGAGCTC GAGATCTG
VAMP2-N11-20T	GCACCTCCTCCAAATCTTACC	AGGCGGGACGGTGG
VAMP2-N2-20T	GCACCTCCTCCAAATC	CATGGTGGCAAGCTTG

Cell culture and reagents

The culture of HEK293, PC12, and SpH-cargoes stably expressing HEK293 cells are the same as described in "Cell culture and reagents" in Materials and Methods section of Chapter 2.

EGFP-VAMP7, VAMP2-EGFP, and all VAMP-pHuji plasmids were transiently transfected into HEK293 cells using Effectene transfection reagent (301425, Qiagen) following manufacturer's protocol. To trigger internalization and subcellular re-localization of SpH-MOR and FLAG-SpH-MOR for confocal imaging, the cells were treated with 10 μM of [D-Ala^2, *N*-Me-Phe^4, Gly^5-ol]-enkephalin (DAMGO; E7384, Sigma-Aldrich) for 20 min at 37 ℃. To trigger internalization and subsequent recycling of SpH-MOR or SpH-B2AR for fusion event imaging, the cells were treated with 12.5 μM of DAMGO or Isoproterenol (I5627, Sigma-Aldrich), respectively, for 6 min at 37 ℃ before the onset of imaging. To label endosomal lumen, Alexa Fluor 647-conjugated Dextran (AF647-Dextran; D22914, Invitrogen) was used at 1 mg/mL and was pulsed into cells for 20 min at 37 ℃ before fixation following a previously published protocol (*49*).

Sample preparation for confocal microscopy

The procedures to prepare fixed cell samples for confocal microscopy, including samples subjected to super resolution radio fluctuation (SRRF) deconvolution, were essentially the same as described in "Sample preparation for immunofluorescence microscopy" in Materials and Methods section of Chapter 2. Note that sample coverslips from Fig. 3.2, 3.4, and 3.5 with cells expressing pH-sensitive fluorophores of SpH or pHuji and did not require post-fixation antibody labeling were washed thrice with phosphate buffered saline (PBS) after 4% formaldehyde (FB002, Invitrogen) fixation (20 min at room temperature) prior to mounting. AF647-conjugated FluoTag-X4 anti-RFP nanobody (N0404, NanoTag Biotechnologies) was used to live-label surface VAMP-pHujis at 1:200 for 10 min at 37 ℃ or 15 min at 4 ℃ before fixation. In contrast, sample coverslips from Fig. 3.1 and 3.2 that were labeled by antibodies post-fixation were blocked and washed using specialized blocking (with 1.25 ‰ Triton X-100) and washing buffers as described in Chapter 2. Primary antibodies used: anti-TGN38 mouse monoclonal antibody (MmAb, sc-166594, Santa Cruz Biotechnology) was used at 1:50; anti-VAMP2 MmAb (104211, Synaptic Systems) was used at 1:1000; anti-VAMP4 rabbit polyclonal antibody (136002, Synaptic Systems) was used 1:100; anti-VAMP7 MmAb (232011, Synaptic Systems) was used at 1:200. All fluorophore-conjugated secondary antibodies were used at 1:1000. AF647-conjugated M1 anti-FLAG antibody (F3040, Sigma-Aldrich) was used to label FLAG-SpH-MOR at 1:1000. All post-fixation antibody labeling was done in blocking buffer for at least 1 hour.

Confocal microscopy and SRRF deconvolution

Confocal microscopy was performed using an Andor Dragonfly multimodal microscopy system equipped with a Nikon Eclipse Ti2 inverted microscope outfitted with a 37 ℃ temperature-controlling chamber. Specifically, images of Fig. 3.1 A and B and Fig. 3.5 A and B were acquired through a 60× 1.49 NA Apochromat TIRF objective (Nikon), while images of Fig. 3.1 C and D, Fig. 3.2, and Fig. 3.4 C were acquired through a 100× 1.49 NA Apochromat TIRF objective (Nikon). Excitation was conducted using direct modulation lasers (Andor ILE) at the indicated wavelength passing through a 405/ 488/ 561/ 640 quad excitation dichroic. Fluorophores including DAPI and Cascade Blue were excited using 405 nm laser, and the emission was collected through a 450/50 emission filter. Fluorophores including AF488 (secondary antibody), SpH, and EGFP were excited using 488 nm laser, and the emission was collected through a 540/30 emission filter. Fluorophores including AF561 (secondary antibody) and pHuji were excited using 561 nm laser, and the emission was collected through a 600/50 emission filter. AF647 was excited using 640 nm laser, and the emission was collected through a 700/75 emission filter. Dichroic and emission filters were purchased from Semrock. Multi-channel images were collected using an iXon Life 888 electron-multiplying charge-coupled device (EMCCD) camera (Andor) in sequential manner.

Super resolution radial fluctuation (SRRF)-deconvolved confocal images were acquired using the same Andor Dragonfly microscopy system but in SRRF-Stream mode. Detailed SRRF settings used are as following: 100 frame count, 4× radiality magnification, 2-pixel ring radius, temporal analysis using mean, and 100 frame count for fixed pattern noise correction.

TIRF microscopy for fusion events imaging

The experimental procedures and settings for two-channel simultaneous acquisition total internal reflection fluorescence (TIRF) microscopy to visualize fusion events of SpH-cargoes and VAMP-pHujis as for Fig. 3.3 C and F and Fig. 3.4 A were the same as described in "TIRF microscopy for fusion events imaging" in Materials and Methods section of Chapter 2.

Image registration and data processing

All images are processed using Fiji, an ImageJ derivative software (*50*). Representative images were made using Fiji integrated functions and plugins.

For Fig. 3.1 F and Fig. 3.4 D, colocalization was analyzed using ImageJ plugin JACoP (*51*). Briefly, Pearson's coefficient of image fields were calculated on single slice confocal images applied with Costes' automatic threshold. For Fig. 3.5 C, the mean anti-RFP fluorescence of image

fields that were background-subtracted (rolling ball radius = 20 pixels) were quantified over automatic thresholds (method = triangle).

Methods to analyze VAMP-pHujis' enrichment in MOR fusion events were the same as described in Chapter 2: the image pre-processing procedures were described in "Image registration and data processing" in Materials and Methods section; and the quantification metrics was described in "*VAMP2 is detected preferentially in fusion events that mediate MOR recycling*" in Results section. Note that for Fig. 3.3 C and F and Fig. 3.4 A, the representative frame used for analyzing VAMP enrichment was the same as previously described as the second frame (fr2) of the onset of SpH-MOR fusion events.

Raw data were processed using Excel (Microsoft). Graphs were generated using Prism10 (GraphPad Software). Model schematics were made using BioRender.

References

1. M. Gallon, P. J. Cullen, Retromer and sorting nexins in endosomal sorting. *Biochem. Soc. Trans.* **43**, 33–47 (2015).

2. N. Naslavsky, S. Caplan, The enigmatic endosome – sorting the ins and outs of endocytic trafficking. *J. Cell Sci.* **131**, jcs216499 (2018).

3. A. N. Vagnozzi, D. Praticò, Endosomal sorting and trafficking, the retromer complex and neurodegeneration. *Mol. Psychiatry* **24**, 857–868 (2019).

4. K. L. Pierce, R. T. Premont, R. J. Lefkowitz, Seven-transmembrane receptors. *Nat. Rev. Mol. Cell Biol.* **3**, 639–650 (2002).

5. N. J. Pavlos, P. A. Friedman, GPCR signaling and trafficking: the long and short of it. *Trends Endocrinol. Metab.* **28**, 213–226 (2017).

6. M. von Zastrow, A. Sorkin, Mechanisms for regulating and organizing receptor signaling by endocytosis. *Annu. Rev. Biochem.* **90**, 1–29 (2021).

7. G. A. Kumar, M. A. Puthenveedu, Diversity and specificity in location-based signaling outputs of neuronal GPCRs. *Curr. Opin. Neurobiol.* **76**, 102601 (2022).

8. R. Vistein, M. A. Puthenveedu, Reprogramming of G protein-coupled receptor recycling and signaling by a kinase switch. *Proc. Natl. Acad. Sci.* **110**, 15289–15294 (2013).

9. S. L. Bowman, D. J. Shiwarski, M. A. Puthenveedu, Distinct G protein–coupled receptor recycling pathways allow spatial control of downstream G protein signaling. *J. Cell Biol.* **214**, 797–806 (2016).

10. T. T. Cao, H. W. Deacon, D. Reczek, A. Bretscher, M. von Zastrow, A kinase-regulated PDZ-domain interaction controls endocytic sorting of the beta2-adrenergic receptor. *Nature* **401**, 286–90 (1999).

11. M. A. Puthenveedu, B. Lauffer, P. Temkin, R. Vistein, P. Carlton, K. Thorn, J. Taunton, O. D. Weiner, R. G. Parton, M. von Zastrow, Sequence-dependent sorting of recycling proteins by actin-stabilized endosomal microdomains. *Cell* **143**, 761–773 (2010).

12. B. E. L. Lauffer, C. Melero, P. Temkin, C. Lei, W. Hong, T. Kortemme, M. von Zastrow, SNX27 mediates PDZ-directed sorting from endosomes to the plasma membrane. *J. Cell Biol.* **190**, 565–574 (2010).

13. P. Temkin, B. Lauffer, S. Jäger, P. Cimermancic, N. J. Krogan, M. von Zastrow, SNX27 mediates retromer tubule entry and endosome-to-plasma membrane trafficking of signaling receptors. *Nat. Cell Biol.* **13**, 715–721 (2011).

14. M. Tanowitz, M. von Zastrow, A novel endocytic recycling signal that distinguishes the membrane trafficking of naturally occurring opioid receptors. *J. Biol. Chem.* **278**, 45978–45986 (2003).

15. J. L. Seachrist, P. H. Anborgh, S. S. G. Ferguson, β2-adrenergic receptor internalization, endosomal sorting, and plasma membrane recycling are regulated by Rab GTPases. *J. Biol. Chem.* **275**, 27221–27228 (2000).

16. F. Wang, X. Chen, X. Zhang, L. Ma, Phosphorylation state of mu-opioid receptor determines the alternative recycling of receptor via Rab4 or Rab11 pathway. *Mol. Endocrinol.* **22**, 1881–92 (2008).

17. F. R. Maxfield, T. E. McGraw, Endocytic recycling. *Nat. Rev. Mol. Cell Biol.* **5**, 121–132 (2004).

18. B. D. Grant, J. G. Donaldson, Pathways and mechanisms of endocytic recycling. *Nat. Rev. Mol. Cell Biol.* **10**, nrm2755 (2009).

19. M. Bakr, D. Jullié, J. Krapivkina, V. Paget-Blanc, L. Bouit, J. D. Petersen, N. Retailleau, C. Breillat, E. Herzog, D. Choquet, D. Perrais, The vSNAREs VAMP2 and VAMP4 control recycling and intracellular sorting of post-synaptic receptors in neuronal dendrites. *Cell Reports* **36**, 109678 (2021).

20. D. M. O. Ramirez, E. T. Kavalali, The role of non-canonical SNAREs in synaptic vesicle recycling. *Cell Logist.* **2**, 20–27 (2012).

21. R. Jahn, D. C. Cafiso, L. K. Tamm, Mechanisms of SNARE proteins in membrane fusion. *Nat. Rev. Mol. Cell Biol.*, 1–18 (2023).

22. C. Imig, S.-W. Min, S. Krinner, M. Arancillo, C. Rosenmund, T. C. Südhof, J. Rhee, N. Brose, B. H. Cooper, The morphological and molecular nature of synaptic vesicle priming at presynaptic active zones. *Neuron* **84**, 882 (2014).

23. G. F. Kusick, M. Chin, S. Raychaudhuri, K. Lippmann, K. P. Adula, E. J. Hujber, T. Vu, M. W. Davis, E. M. Jorgensen, S. Watanabe, Synaptic vesicles transiently dock to refill release sites. *Nat. Neurosci.* **23**, 1329–1338 (2020).

24. J. Raingo, M. Khvotchev, P. Liu, F. Darios, Y. C. Li, D. M. O. Ramirez, M. Adachi, P. Lemieux, K. Toth, B. Davletov, E. T. Kavalali, VAMP4 directs synaptic vesicles to a pool that selectively maintains asynchronous neurotransmission. *Nat. Neurosci.* **15**, 738–745 (2012).

25. T. C. Südhof, Neurotransmitter release: the last millisecond in the life of a synaptic vesicle. *Neuron* **80**, 675–690 (2013).

26. S. Jurado, D. Goswami, Y. Zhang, A. J. M. Molina, T. C. Südhof, R. C. Malenka, LTP requires a unique postsynaptic SNARE fusion machinery. *Neuron* **77**, 542–558 (2013).

27. F. Finetti, L. Patrussi, D. Galgano, C. Cassioli, G. Perinetti, G. J. Pazour, C. T. Baldari, The small GTPase Rab8 interacts with VAMP-3 to regulate the delivery of recycling T-cell receptors to the immune synapse. *J. Cell Sci.* **128**, 2541–2552 (2015).

28. E. T. Kavalali, The mechanisms and functions of spontaneous neurotransmitter release. *Nat. Rev. Neurosci.* **16**, 5–16 (2015).

29. Y. Gu, R. L. Huganir, Identification of the SNARE complex mediating the exocytosis of NMDA receptors. *Proc. Natl. Acad. Sci.* **113**, 12280–12285 (2016).

30. H. Chen, Z. Y. Weinberg, G. A. Kumar, M. A. Puthenveedu, Vesicle-associated membrane protein 2 is a cargo-selective v-SNARE for a subset of GPCRs. *J. Cell Biol.* **222**, e202207070 (2023).

31. S. Coco, G. Raposo, S. Martinez, J.-J. Fontaine, S. Takamori, A. Zahraoui, R. Jahn, M. Matteoli, D. Louvard, T. Galli, Subcellular localization of tetanus neurotoxin-insensitive vesicle-associated membrane protein (VAMP)/VAMP7 in neuronal cells: evidence for a novel membrane compartment. *J. Neurosci.* **19**, 9803–9812 (1999).

32. M. Steegmaier, J. Klumperman, D. L. Foletti, J.-S. Yoo, R. H. Scheller, Vesicle-associated membrane protein 4 is implicated in trans-Golgi network vesicle trafficking. *Mol. Biol. Cell* **10**, 1957–1972 (1999).

33. Q. Zeng, T. T. H. Tran, H.-X. Tan, W. Hong, The cytoplasmic domain of Vamp4 and Vamp5 is responsible for their correct subcellular targeting. *J. Biol. Chem.* **278**, 23046–23054 (2003).

34. N. Gustafsson, S. Culley, G. Ashdown, D. M. Owen, P. M. Pereira, R. Henriques, Fast live-cell conventional fluorophore nanoscopy with ImageJ through super-resolution radial fluctuations. *Nat. Commun.* **7**, 12471 (2016).

35. S. Culley, K. L. Tosheva, P. M. Pereira, R. Henriques, SRRF: universal live-cell super-resolution microscopy. *Int. J. Biochem. Cell Biol.* **101**, 74–79 (2018).

36. T. Galli, T. Chilcote, O. Mundigl, T. Binz, H. Niemann, P. D. Camilli, Tetanus toxin-mediated cleavage of cellubrevin impairs exocytosis of transferrin receptor-containing vesicles in CHO cells. *J. Cell Biol.* **125**, 1015–1024 (1994).

37. C. J. Traer, A. C. Rutherford, K. J. Palmer, T. Wassmer, J. Oakley, N. Attar, J. G. Carlton, J. Kremerskothen, D. J. Stephens, P. J. Cullen, SNX4 coordinates endosomal sorting of TfnR with dynein-mediated transport into the endocytic recycling compartment. *Nat. Cell Biol.* **9**, 1370–1380 (2007).

38. C. Burd, P. J. Cullen, Retromer: a master conductor of endosome sorting. *CSH Perspect. Biol.* **6**, a016774 (2014).

39. B. Simonetti, B. Paul, K. Chaudhari, S. Weeratunga, F. Steinberg, M. Gorla, K. J. Heesom, G. J. Bashaw, B. M. Collins, P. J. Cullen, Molecular identification of a BAR domain-containing coat complex for endosomal recycling of transmembrane proteins. *Nat. Cell Biol.* **21**, 1219–1233 (2019).

40. A. E. West, R. L. Neve, K. M. Buckley, Targeting of the synaptic vesicle protein synaptobrevin in the axon of cultured hippocampal neurons: evidence for two distinct sorting steps. *J. Cell Biol.* **139**, 917–927 (1997).

41. E. Grote, J. C. Hao, M. K. Bennett, R. B. Kelly, A targeting signal in VAMP regulating transport to synaptic vesicles. *Cell* **81**, 581–589 (1995).

42. F. Deák, S. Schoch, X. Liu, T. C. Südhof, E. T. Kavalali, Synaptobrevin is essential for fast synaptic-vesicle endocytosis. *Nat. Cell Biol.* **6**, 1102–1108 (2004).

43. J. Xu, F. Luo, Z. Zhang, L. Xue, X.-S. Wu, H.-C. Chiang, W. Shin, L.-G. Wu, SNARE proteins synaptobrevin, SNAP-25, and syntaxin are involved in rapid and slow endocytosis at synapses. *Cell Rep.* **3**, 1414–1421 (2013).

44. N. L. Chanaday, E. T. Kavalali, Synaptobrevin-2 dependent regulation of single synaptic vesicle endocytosis. *Mol. Biol. Cell*, mbc.E21-04-0213 (2021).

45. R. Fukuda, J. A. McNew, T. Weber, F. Parlati, T. Engel, W. Nickel, J. E. Rothman, T. H. Söllner, Functional architecture of an intracellular membrane t-SNARE. *Nature* **407**, 198–202 (2000).

46. J. A. McNew, F. Parlati, R. Fukuda, R. J. Johnston, K. Paz, F. Paumet, T. H. Söllner, J. E. Rothman, Compartmental specificity of cellular membrane fusion encoded in SNARE proteins. *Nature* **407**, 153–159 (2000).

47. F. Parlati, J. A. McNew, R. Fukuda, R. Miller, T. H. Söllner, J. E. Rothman, Topological restriction of SNARE-dependent membrane fusion. *Nature* **407**, 194–198 (2000).

48. F. Parlati, O. Varlamov, K. Paz, J. A. McNew, D. Hurtado, T. H. Söllner, J. E. Rothman, Distinct SNARE complexes mediating membrane fusion in Golgi transport based on combinatorial specificity. *Proc. Natl. Acad. Sci.* **99**, 5424–5429 (2002).

49. M. Podinovskaia, C. Prescianotto-Baschong, D. P. Buser, A. Spang, A novel live-cell imaging assay reveals regulation of endosome maturation. *eLife* **10**, e70982 (2021).

50. J. Schindelin, I. Arganda-Carreras, E. Frise, V. Kaynig, M. Longair, T. Pietzsch, S. Preibisch, C. Rueden, S. Saalfeld, B. Schmid, J.-Y. Tinevez, D. J. White, V. Hartenstein, K. Eliceiri, P. Tomancak, A. Cardona, Fiji: an open-source platform for biological-image analysis. *Nat. Methods* **9**, 676 (2012).

51. S. Bolte, F. P. Cordelières, A guided tour into subcellular colocalization analysis in light microscopy. *J. Microsc.* **224**, 213–232 (2006).

Chapter 4: Overall Discussion and Future Directions

The work presented in this dissertation contributes to an improved understanding of the mechanism of G protein-coupled receptor (GPCR) trafficking by unveiling the involvement and the specificity of the soluble NSF attachment receptor proteins (SNARE)-mediated fusion machinery. Through studying the recycling of μ opioid receptor (MOR) and β2 adrenergic receptor (B2AR), two clinically relevant prototypical GPCRs that are evidenced to undergo distinct trafficking regulation (*1–10*), we find that vesicle-associated membrane protein 2 (VAMP2), a canonical vesicular-SNARE (v/R-SNARE) that primarily mediates vesicle to plasma membrane fusion (*11–16*), functions in a cargo-selective manner and is specifically required for the recycling of MOR (Chapter 2). And with further studies, we find that the cargo-selectivity of VAMP2 is encoded in its cytoplasmic domain (Chapter 3).

The phenotype of VAMP2-exclusivity in MOR recycling did not seem to be cell type-dependent since we had successfully reproduced the same conclusion in multiple different cell lines. However, this mechanistic connection between VAMP2 and MOR might not be generalizable to other receptor cargoes such as B2AR. In PC12 cells and primary rat striatal neurons, depletion of endogenous VAMP2 decreased the degree of MOR recycling in response to the full agonist DAMGO ([D-Ala^2, *N*-Me-Phe^4, Gly^5-ol]-enkephalin; Fig. 2.5 F and J for PC12 cells and Fig. 2.7 H for neurons), but depletion of endogenous VAMP4 in PC12 cells showed no significant impact (Fig. 2.5 G). However, in HEK293 cells where endogenous VAMP2 expression was undetectable (Fig. 2.4 A and B), MOR still displayed normal recycling activity (Fig. 2.1 and

2.2; *9*, *17*), indicating a potential mechanism of functional compensation by other v-SNAREs presenting at baseline. Nevertheless, VAMP2 still showed a preferential correlation with MOR recycling fusion events in HEK293 cells when it was ectopically expressed (Fig. 2.2 E-H), indicating the sorting hierarchy leading to VAMP2's preference for MOR was somehow conserved in HEK293 cells. These results make us wonder: To what extent is this hierarchy conserved across cell types? Among the five VAMP subtypes we have tested for B2AR recycling in baseline PC12 cells, VAMP1 and 3 were not endogenously expressed (Fig. 2.10 C-E). However, we could robustly observe B2AR recycling fusion events in these cells (Fig. 2.5 E). Therefore, VAMP1 and 3 were not exclusively required for B2AR recycling. On the other hand, although VAMP2, 4, and 7 were endogenously expressed in baseline PC12 cells (Fig. 2.4 B and Fig. 3.1 D), none of them were correlating with or required for B2AR recycling (Fig. 2.2 E-H and Fig. 2.5 E for VAMP2, Fig. 2.10 A and B for VAMP4, and Fig. 2.10 I and J for VAMP7). Based on these results, we conclude that B2AR either exclusively utilizes an untested v-SNARE for recycling or has a promiscuous v-SNARE selectivity. However, could this be a biased view resulted from the limited cell models we tested? And is there an unidentified biological system where B2AR's recycling would also be exclusively dependent on a particular v-SNARE? We can approach this question by testing B2AR's v-SNARE requirement in a cell model where B2AR is endogenously expressed.

Nevertheless, the finding of fusion machinery specificity in GPCR recycling showcases another level of complexity coded in the endosomal trafficking network. As discussed in previous Chapters, the specificity of v-SNAREs likely originated from their co-sorting with receptor cargoes on the endosomes. However, given that the molecular mechanism underlying endosomal sorting of v-SNAREs and most of the GPCRs, including MOR, are both still largely unknown, it is a field open for novel discoveries. Whether the sorting of GPCR cargoes and v-SNAREs are

correlated or independent is one of the questions worth future investigations. Although it has been reported that the Gβγ subunit of heterotrimeric Gαi/o complex could interact with target-SNAREs (t/Q-SNAREs) to inhibit neurotransmitter release (*18–20*), there is yet any evidence of a direct interaction between any receptor cargoes and v-SNAREs. Therefore, if the endosomal sorting of MOR and VAMP2 are correlated they are likely mediated by a common sorting machinery such as the Retromer or Retriever sorting complexes which have promiscuous protein-binding capability (*21–25*). However, even though the co-sorting is spatially correlated it can still be temporally two separate processes since MOR's sorting into recycling pathways only happens after agonist-induced internalization, but VAMP2's sorting would presumably happen at any given time to accommodate its wide range of client cargoes (Table 1.1). How do these two seemingly temporally distinct processes reconcile to produce vesicles that contain the right protein content? Hopefully studying the underlying sorting mechanism of MOR and VAMP2 will help to set a starting point to further look into this question.

We initiated the investigation into VAMP2's sorting mechanism by first confirming the endosomal tubule hypothesis we proposed in Chapter 2 (Fig. 2.9 E), that through sorting VAMP2 would localize on specific endosomal tubules of distinct biochemical compositions. A series of immunofluorescence studies showed that VAMP2 primarily localized on EEA1-marked early endosomes and Rab11-marked recycling endosomes (Fig. 2.8; *26*), but not on TGN38 or GM130-marked Golgi apparatus (Fig. 2.3 E and F). On the other hand, VAMP4 showed primary Golgi-localization (Fig. 3.1 A, B, and F), which was apparently different from VAMP7's (Fig. 3.1 D and F), suggesting that VAMP7 shared similar endosomal localization like VAMP2. Simultaneous SRRF (super-resolution radial fluctuation) imaging of VAMP2 and 7 on endosomes labeled using different strategies provided evidence supporting their sub-endosomal segregation onto distinct

tubular structures (Fig. 3.2). However, this set of SRRF imaging still bore two limitations: (i). the resolution of SRRF (~90 nm) was not high enough to resolve endosomes of below-average sizes (<100 nm); (ii). the endosomal labeling was ambiguous and was not optimal to cover the whole membrane area and all endosomal structures. We propose two advanced imaging methods to resolve these limitations for future attempts to image endosomal tubules. The resource-friendly method is expansion microscopy (*27*, *28*), where the fluorescently labeled proteins in fixed cell samples are crosslinked to polyacrylamide gels that can be isotropically expanded, so that after physical expansion the relative distance between proteins is multiple times larger (3-10×), making the imaging of sub-endosomal ultrastructures using conventional light microscopy feasible (~200 nm with NA=1.49 objectives). A more sophisticated but technically demanding method is super-resolution correlative light and electron microscopy (CLEM; *29*), where the super-resolution images of fluorescently labeled proteins can be overlapped with EM images revealing membrane ultrastructures so that every endosome and their tubules can be precisely marked, allowing for an accurate interpretation on proteins' sub-endosomal localization.

It is important to note that there is still a long way ahead to uncover the whole picture of the fusion machinery associated with GPCR exocytosis. As discussed in Chapter 1: "*Molecular mechanism of vesicle fusion at the plasma membrane*", vesicle fusion is mediated by a collective of proteins from different families. From this perspective, the most intuitive question to follow-up on might be what the cognate t-SNAREs from VAMP2-mediated MOR recycling are? And would the t-SNAREs also exhibit specificity? However, in comparison to the relatively small number of v-SNARE proteins, one of the t-SNARE, syntaxin, has twice the number of subtypes. If we are to implement the same shRNA knockdown strategy as for studying v-SNAREs to study t-SNAREs, it would be unreasonably tedious. Additionally, is the fusion of vesicles that carry receptor cargoes

also calcium-dependent similar to neurotransmitter release (*15*)? Intuitively the answer should be no since, unlike neurotransmitter release, the exocytosis of receptors is not always paired with an excitatory membrane potential to activate the voltage-gated calcium channels that causes calcium influx. Previous *in vitro* studies had shown that although the SNARE complex on its own was capable of mediating membrane fusion, the incorporation of calcium-sensing synaptotagmin-1 could increase fusion kinetics even in the absence of calcium, indicating that synaptotagmins might still play critical roles in fusion events that were calcium-independent (*30*, *31*). Moreover, is the plasma membrane tethering complex exocyst also involved in receptor exocytosis (*32*, *33*)? And does the exocyst complex have any functions beyond tethering in this context? These questions leave us more candidates-of-interest to look at in future studies.

The ultimate goal of this work is to determine the trafficking regulation of GPCRs in the hope of classifying them into different trafficking subclasses. Through searching for the common ground underlying different GPCRs' trafficking pathways, we would be able to understand their biological properties further, explain their cellular and physiological behaviors better, and eventually utilize their pharmacological potentials in a more precise manner. Studying fusion machinery using prototype GPCRs as demonstrated in this dissertation is merely a starting point toward the goal. To move forward efficiently, we need to develop a reliable high-throughput screen that can cover most of the trafficking-related proteins while maintaining the ability to adapt to various of receptors. In the future, we can design and perform a ratiometric recycling assay-based CRISPR (clustered regularly interspaced short palindromic repeats) knock-out screen that, instead of targeting the whole genome, only focuses on a concentrated pool of trafficking proteins (Table 4.1). The ratiometric recycling assay has been proven to work robustly across multiple cell lines and receptors (Fig. 2.7 C for MOR in PC12 cells, H for MOR in rat striatal neurons; Fig. 2.10 J

for B2AR in PC12 cells) and can be used to analyze both endocytosis and recycling in a single set of experiments. Compared to a genome-wide screen, using a concentrated pool of CRISPR targets can have multiple benefits: (i). fewer non-specific effects caused by knock-out of housekeeping genes; (ii). greater time-efficiency due to the significantly shorter cell culture cycle to reach an adequate representation; (iii). higher confidence compared to expenditure since, for a given number of oligonucleotides, more copies of single guide RNAs can be allocated to each individual gene-of-interest. Nonetheless, the obvious drawback of this method is that valuable targets with undiscovered function in trafficking might be left untested, and this caveat should be taken into consideration when designing and performing the assay.

Table 4.1. Major protein targets for customized library CRISPR knock-out screen to study GPCR trafficking classified by function and complex ascription.

Function	Protein complex	Examples
Membrane fusion	SNARE complex	VAMPs, SNAPs, Syntaxins
Calcium sensing		Synaptotagmins
Calcium influx		Voltage-gated calcium channels
Calcium channel recruitment and scaffolding	Active zone protein complex	RIM, RIM-BP, Munc13, etc.
Plasma membrane tethering	Exocyst complex	Exo70, Exo84, Sec8, etc.
Miscellaneous		Rab small GTPases
		Phosphoinositide-related enzymes
Endosomal sorting for cargo recycling	Retromer complex	VPS35, VPS26, VPS29, etc.
	Retriever complex	C16orf62, DSCR3, etc.
	CCC complex	CCDC22, CCDC93, COMMDs
		Sorting nexins
		PDZ proteins
Actin polymerization	WASH complex	WASHC1, Fam21, CCDC53, etc.
Actin-associated proteins		Arp2/3, Coronin, Cortactin, etc.
Endosomal sorting for cargo degradation	ESCRT complex	ESCRT-I/II/III complexes, etc.
Lysosomal tethering and fusion	CORVET complex	VPS3, VPS8, etc.
	HOPS complex	VPS39, VPS41, etc.
Vesicle transport	Adaptor protein complexes	AP2/3 complexes, etc.
Vesicle movement		Kinesins and Dyneins
Golgi transport		COPI/II complexes, etc.

Note: different protein groups might have overlapped members. Notable abbreviations: WASH: WASP (Wiskott-Aldrich syndrome protein) and SCAR (suppressor of cAR) homologue; ESCRT: endosomal sorting complexes required for transport; CORVET: class C core endosomal vacuole tethering; HOPS: homotypic fusion and vacuole protein sorting.

We believe that through dedication we shall solve every unknown noted in this Chapter. And with the answers we shall build a heathier and brighter future.

References

1. T. T. Cao, H. W. Deacon, D. Reczek, A. Bretscher, M. von Zastrow, A kinase-regulated PDZ-domain interaction controls endocytic sorting of the beta2-adrenergic receptor. *Nature* **401**, 286–90 (1999).

2. M. Tanowitz, M. von Zastrow, A novel endocytic recycling signal that distinguishes the membrane trafficking of naturally occurring opioid receptors. *J. Biol. Chem.* **278**, 45978–45986 (2003).

3. F. Wang, X. Chen, X. Zhang, L. Ma, Phosphorylation state of mu-opioid receptor determines the alternative recycling of receptor via Rab4 or Rab11 pathway. *Mol. Endocrinol.* **22**, 1881–92 (2008).

4. B. E. L. Lauffer, C. Melero, P. Temkin, C. Lei, W. Hong, T. Kortemme, M. von Zastrow, SNX27 mediates PDZ-directed sorting from endosomes to the plasma membrane. *J. Cell Biol.* **190**, 565–574 (2010).

5. M. A. Puthenveedu, B. Lauffer, P. Temkin, R. Vistein, P. Carlton, K. Thorn, J. Taunton, O. D. Weiner, R. G. Parton, M. von Zastrow, Sequence-dependent sorting of recycling proteins by actin-stabilized endosomal microdomains. *Cell* **143**, 761–773 (2010).

6. P. Temkin, B. Lauffer, S. Jäger, P. Cimermancic, N. J. Krogan, M. von Zastrow, SNX27 mediates retromer tubule entry and endosome-to-plasma membrane trafficking of signaling receptors. *Nat. Cell Biol.* **13**, 715–721 (2011).

7. R. Vistein, M. A. Puthenveedu, Reprogramming of G protein-coupled receptor recycling and signaling by a kinase switch. *Proc. Natl. Acad. Sci.* **110**, 15289–15294 (2013).

8. S. L. Bowman, D. J. Shiwarski, M. A. Puthenveedu, Distinct G protein–coupled receptor recycling pathways allow spatial control of downstream G protein signaling. *J. Cell Biol.* **214**, 797–806 (2016).

9. J. M. Kunselman, A. S. Zajac, Z. Y. Weinberg, M. A. Puthenveedu, Homologous regulation of mu opioid receptor recycling by Gβγ, protein kinase C, and receptor phosphorylation. *Mol. Pharmacol.* **96**, 702–710 (2019).

10. J. M. Kunselman, J. Lott, M. A. Puthenveedu, Mechanisms of selective G protein–coupled receptor localization and trafficking. *Curr. Opin. Cell Biol.* **71**, 158–165 (2021).

11. T. Söllner, S. W. Whiteheart, M. Brunner, H. Erdjument-Bromage, S. Geromanos, P. Tempst, J. E. Rothman, SNAP receptors implicated in vesicle targeting and fusion. *Nature* **362**, 318–324 (1993).

12. T. Söllner, M. K. Bennett, S. W. Whiteheart, R. H. Scheller, J. E. Rothman, A protein assembly-disassembly pathway in vitro that may correspond to sequential steps of synaptic vesicle docking, activation, and fusion. *Cell* **75**, 409–418 (1993).

13. S. Schoch, F. Deák, A. Königstorfer, M. Mozhayeva, Y. Sara, T. C. Südhof, E. T. Kavalali, SNARE function analyzed in synaptobrevin/VAMP knockout mice. *Science* **294**, 1117–1122 (2001).

14. R. Jahn, R. H. Scheller, SNAREs — engines for membrane fusion. *Nat. Rev. Mol. Cell Biol.* **7**, 631–643 (2006).

15. T. C. Südhof, Neurotransmitter release: the last millisecond in the life of a synaptic vesicle. *Neuron* **80**, 675–690 (2013).

16. R. Jahn, D. C. Cafiso, L. K. Tamm, Mechanisms of SNARE proteins in membrane fusion. *Nat. Rev. Mol. Cell Biol.*, 1–18 (2023).

17. S. L. Bowman, A. L. Soohoo, D. J. Shiwarski, S. Schulz, A. A. Pradhan, M. A. Puthenveedu, Cell-autonomous regulation of mu-opioid receptor recycling by substance P. *Cell Reports* **10**, 1925–1936 (2015).

18. Z. Zurawski, B. Page, M. C. Chicka, R. L. Brindley, C. A. Wells, A. M. Preininger, K. Hyde, J. A. Gilbert, O. Cruz-Rodriguez, K. P. M. Currie, E. R. Chapman, S. Alford, H. E. Hamm, Gβγ directly modulates vesicle fusion by competing with synaptotagmin for binding to neuronal SNARE proteins embedded in membranes. *J. Biol. Chem.* **292**, 12165–12177 (2017).

19. Z. Zurawski, A. D. T. Gray, L. J. Brady, B. Page, E. Church, N. A. Harris, M. R. Dohn, Y. Y. Yim, K. Hyde, D. P. Mortlock, C. K. Jones, D. G. Winder, S. Alford, H. E. Hamm, Disabling the Gβγ-SNARE interaction disrupts GPCR-mediated presynaptic inhibition, leading to physiological and behavioral phenotypes. *Sci. Signal.* **12**, eaat8595 (2019).

20. Y. Y. Yim, W. H. McDonald, K. M. Betke, A. Kaya, K. Hyde, K. Erreger, R. Gilsbach, L. Hein, H. E. Hamm, Specificities of Gβγ subunits for the SNARE complex before and after stimulation of α2a-adrenergic receptors. *Sci. Signal.* **14**, eabc4970 (2021).

21. M. N. J. Seaman, The retromer complex – endosomal protein recycling and beyond. *J. Cell Sci.* **125**, 4693–4702 (2012).

22. C. Burd, P. J. Cullen, Retromer: a master conductor of endosome sorting. *CSH Perspect. Biol.* **6**, a016774 (2014).

23. M. Lucas, D. C. Gershlick, A. Vidaurrazaga, A. L. Rojas, J. S. Bonifacino, A. Hierro, Structural mechanism for cargo recognition by the retromer complex. *Cell* **167**, 1623-1635.e14 (2016).

24. K. E. McNally, R. Faulkner, F. Steinberg, M. Gallon, R. Ghai, D. Pim, P. Langton, N. Pearson, C. M. Danson, H. Nägele, L. L. Morris, A. Singla, B. L. Overlee, K. J. Heesom, R. Sessions, L. Banks, B. M. Collins, I. Berger, D. D. Billadeau, E. Burstein, P. J. Cullen, Retriever is a multiprotein complex for retromer-independent endosomal cargo recycling. *Nat. Cell Biol.* **19**, 1214–1225 (2017).

25. K. Chen, M. D. Healy, B. M. Collins, Towards a molecular understanding of endosomal trafficking by Retromer and Retriever. *Traffic* **20**, 465–478 (2019).

26. B. D. Grant, J. G. Donaldson, Pathways and mechanisms of endocytic recycling. *Nat. Rev. Mol. Cell Biol.* **10**, nrm2755 (2009).

27. F. Chen, P. W. Tillberg, E. S. Boyden, Expansion microscopy. *Science* **347**, 543–548 (2015).

28. G. Wen, V. Leen, T. Rohand, M. Sauer, J. Hofkens, Current progress in expansion microscopy: chemical strategies and applications. *Chem. Rev.* **123**, 3299–3323 (2023).

29. P. de Boer, J. P. Hoogenboom, B. N. G. Giepmans, Correlated light and electron microscopy: ultrastructure lights up! *Nat. Methods* **12**, 503–513 (2015).

30. T. Weber, B. V. Zemelman, J. A. McNew, B. Westermann, M. Gmachl, F. Parlati, T. H. Söllner, J. E. Rothman, SNAREpins: minimal machinery for membrane fusion. *Cell* **92**, 759–772 (1998).

31. L. K. Mahal, S. M. Sequeira, J. M. Gureasko, T. H. Söllner, Calcium-independent stimulation of membrane fusion and SNAREpin formation by synaptotagmin I. *J. Cell Biol.* **158**, 273–282 (2002).

32. B. Wu, W. Guo, The exocyst at a glance. *J. Cell Sci.* **128**, 2957–2964 (2015).

33. S. M. Ahmed, H. Nishida-Fukuda, Y. Li, W. H. McDonald, C. C. Gradinaru, I. G. Macara, Exocyst dynamics during vesicle tethering and fusion. *Nat. Commun.* **9**, 5140 (2018).